DISS. ETH NO. 24354

Imaging HIF activity and pyruvate metabolism in colon carcinoma xenografts in the context of cancer-driving mutations

A thesis submitted to obtain the degree of

DOCTOR OF SCIENCES of ETH ZURICH

(Dr. sc. ETH Zurich)

presented by

CATHERINE GERMANIER

MSc ETH Biomedical Engineering

born on 05.11.1985

from Conthey (Valais)

accepted on the recommendation of

Prof. Dr. Markus Rudin, examiner

Prof. Dr. Wilhelm Krek, co-examiner

Prof. Dr. Ian Frew, co-examiner

2017

Contents

Abbreviations

HIF	Hypoxia Inducible Factor
ATP	Adenosine triphosphate
ARNT	Aryl hydrocarbon receptor nuclear translocator protein
PAS	Per-ARNT-Simhomology
PHD	Prolyl-4-hydroxylase
ODDD	Oxygen-dependent degradation domain
2-OG or α-KG	2-oxoglutarate, also referred as α-ketoglutarate
pVHL	Von Hippel-Lindau tumor suppressor
HBS	HIF binding site
HRE	Hypoxia responsive element
FIH	Factor inhibiting HIF-1
VEGF	Vascular endothelial growth factor
PDGF	Platelet-derived growth factor
MMP	Matrix metalloproteinase
BNIP3	Bcl-2/adenovirus EIB interacting protein 3
NIX	Nip-3-like protein
Mcl-1	Myeloid cell factor-1
EMT	Epithelial to mesenchymal transition
CA9	Carbonic anhydrase 9
PI3K	Phosphoinositide-3-kinase
MAPK	Mitogen-activated protein kinase

RTK	Receptor tyrosine kinase
nRTK	Nonreceptor tyrosine kinase
mTOR	Mechanistic target of rapamycin
ERK	Extracellular signal-regulated kinase
TPZ	Tirapazamine
CPT	Camptothecin
RCC	Renal cell carcinoma
Hsp90	Heat shock protein 90
GA	Geldanamycin
TCA	Tricarboxylic acid cycle
18F-FDG	^{18}F-fluorodeoxyglucose
NADPH	Nicotinamide adenine dinucleotide phosphate
NADH	Nicotinamide adenine dinucleotide
$FADH_2$	Flavin adenine dinucleotide
PPP	Pentose phosphate pathway
R5P	Ribose-5-phosphate
FASN	Fatty acid synthase
ACC	Acethyl-CoA carboxylase
ROS	Reactive oxygen species
SREBP	Sterol regulatory element-binding protein
CAD	Carbamoyl-phosphate synthetase 2, aspartate transcarbamoylase, dihydroorotase
GLUT1	Glucose transporter 1
G6P	Glucose-6-phosphate

LDHA	Lactate dehydrogenase A
MCT4	Monocarboxylate transporter 4
PDH	Pyruvate dehydrogenase
PDK	Pyruvate dehydrogenase kinase
TFAM	Transcription factor A
IDH	Isocitrate dihydrogenase
PEP	Phosphoenolpyruvate
ADP	Adenosine diphosphate
PK	Pyruvate kinase
D-2HG	D-2-hydroxyglutarate
FH	Fumarate hydratase
US	Ultrasound
MRI	Magnetic resonance imaging
MRS	Magnetic resonance spectroscopy
CT	Computed tomography
PET	Positron emission tomography
NIR	Near infrared
CCD	Charge-coupled device
SBR	Signal-to-background ratio
FMT	Fluorescent molecular tomography
DOT	Diffuse optical tomography
MSOT	Multispectral optoacoustic tomography
NMR	Nuclear magnetic resonance
RF	Radio-frequency

FID	Free induction decay
DNP	Dynamic nuclear polarization
FMISO	^{18}F-fluoromisonidazole
GFP	Green fluorescent protein
RFP	Red fluorescent protein
FBS	Fetal bovine serum
DMEM	Dulbecco's Modified Eagle's Medium
RPMI	Roswell Park Memorial Institute medium
CMV	Cytomegalovirus
SV40	Simian virus 40
HEK	Human embryonic kidney cells
DMOG	Dimethyloxalylglycine
iRFP	Infrared fluorescent protein
G13D	Glycine to aspartic acid mutation on position 13
V600E	Valine to glutamic acid mutation on position 600
HUVECs	Human umbilical vein endothelial cells
EGM	Endothelial growth medium
CD31	Cluster of differentiation 31

Summary

Tumor hypoxia, i.e. the reduced access to oxygen within the tumor mass, is an adverse prognostic for survival of cancer patients. Moreover, it is associated with resistance to chemo- and radiotherapy. Tumor hypoxia arises in developing tumors when the proliferating cells outgrow the supply of oxygen by the vascular system of the tumor microenvironment. In addition, limited diffusion of nutrients also creates a state of metabolic stress for the deprived tumor cells. The cellular response to hypoxic conditions is orchestrated by the Hypoxia Inducible Factor (HIF), a transcription factor formed by an α and a β subunit, the levels of the α subunit being regulated by an oxygen-dependent mechanism. Under normoxic conditions, the HIF-α subunit is hydroxylated by a prolyl-4-hydroxylase domain (PHD), the activity of which depends on the availability of molecular oxygen and cofactors such as α-ketoglutarate. Hydroxylated HIF-α is recognized by the Von Hippel-Lindau (pVHL) complex, and subsequently degraded via the proteasome 26S. However, under conditions of reduced tissue oxygen levels, the activity of PHD is reduced and HIF-α therefore stabilized, which enables its dimerization with HIF-β. The HIF complex then enters the nucleus, binds a Hypoxia Responsive Element (HRE) site on the DNA and initiates gene transcription. Downstream genes of HRE elements are associated with angiogenesis, metastasis, cell survival and metabolism. HIF expression typically modulates the upregulation of metabolic enzymes found in the glycolytic pathway.

Recent studies have shown that in addition to hypoxia, factors such as oncogenes and metabolites are capable of stabilizing HIF-α and enhance HIF-dependent gene transcription. The most striking example is the activation of HIF signaling in glioblastoma multiformae as a consequence of a loss-of-function mutation on isocitrate dehydrogenase 1 (IDH1), an enzyme converting isocitrate into α-ketoglutarate. The resulting reduction of α-ketoglutarate levels leads to inactivation of PHD and hence to the stabilization of HIF-α, even under normoxic conditions (so-called “pseudo-hypoxia”). The fact that HIF modulates some parts of the metabolism, but is on its own influenced by altered levels of metabolite suggests the existence of a feed-forward loop regarding HIF signaling.

In this thesis, we aimed at understanding the influence of specific cancer-driving mutations on HIF signaling and on metabolism of pyruvate, a gatekeeper molecule for the tricarboxylic acid cycle (TCA cycle). For this purpose, we developed a fluorescent imaging assay and employed a pre-established ^{13}C-pyruvate spectroscopic assay for *in vivo* longitudinal imaging studies.

Two tumor models of human colon carcinoma exhibiting an activating mutation in the MAPK pathway were used: DLD-1 cells with a KRAS mutation and RKO cells with a BRAF mutation. Both mutations were active and driving the constitutive activation of KRAS or BRAF and their respective downstream effectors within the MAPK pathway. To monitor HIF activity *in vivo,* DLD-1 and RKO cells were modified to express an infrared fluorescent protein (iRFP) under the control of two HREs. Transfected tumor cells were extensively characterized *in vitro* by monitoring HRE-dependent iRFP expression under hypoxic conditions and upon pharmacological inhibition of PHD. The characterized cells were then injected subcutaneously in mice, and the xenografts expressing fluorescence were measured longitudinally using spectrally resolved 2D planar fluorescence. Metabolic measurements were performed using the same animal models. To examine whether the cancer-driving mutations had an influence on the metabolism of pyruvate, we monitored the fate of [1-^{13}C]-pyruvate in mutated and wild-type DLD-1 and RKO tumors. The sensitivity of the ^{13}C-magnetic resonance spectroscopy (^{13}C-MRS) experiments was enhanced by hyperpolarization via dynamic nuclear polarization (DNP). A solution of hyperpolarized [1-^{13}C]-pyruvate was injected intravenously in the mice, and the subsequent conversion of [1-^{13}C]-pyruvate to [1-^{13}C]-lactate followed within the tumor mass in a longitudinal manner. Upon termination of the studies, the tumors were extracted for *ex vivo* stainings with different hypoxia-related markers: pimonidazole as marker of hypoxic areas, carbonic anhydrase 9 (CA9) as downstream product of HIF signaling, and cluster of differentiation 31 (CD31) as marker of vascular vessels.

In vivo imaging of iRFP in the different tumor types revealed a significant increase of fluorescence intensity in the KRAS- and BRAF-mutated cells. Interestingly, these differences were more pronounced in the early tumor development stage, when the tumor volume was below 100mm^3, compared to later development stages where those intensities tended to equalize. Based on both the optical results and the *ex vivo* stainings, we concluded that the increased HIF activity in small mutant tumors was the result of hypoxia-independent factors, while HIF activity in larger tumors was dominated by tumor hypoxia. Surprisingly, the results of the metabolic studies did not expose any significant differences between wild-type and mutated tumors regarding the pyruvate metabolism. This can be explained by the fact that the method may not be sensitive enough, particularly when the tumors are small, but also by the fact that pyruvate may not be the metabolite whose level is imbalanced between mutated and wild-type tumors.

In conclusion, we have demonstrated that cancer-driving mutations in the MAPK pathway do have an impact of the activity of HIF in xenograft tumors, but do not influence the pyruvate metabolism. For the purpose of this thesis we have developed a robust fluorescent reporter gene for the activity of HIF: the optical properties of iRFP reducing scattering and absorption by the tissues make it an attractive imaging probe for *in vivo* studies. Despite the fact that we did not observe significant changes in metabolic readouts for the various tumor cell lines studied, ^{13}C-MRS providing robust information on metabolic fluxes in tumors constitutes an attractive approach for investigating the link between tumor metabolism and HIF signaling *in vivo*.

Résumé

L'hypoxie tumorale, l'accès restreint à l'oxygène dans la masse cancéreuse, a prouvé être un facteur défavorable pour le pronostic de survie des patients. De plus, elle joue un rôle important dans l'issue d'une radiothérapie. L'hypoxie tumorale émerge dans les tumeurs en développement quand les cellules qui prolifèrent dépassent l'approvisionnement en oxygène et nutriments par le réseau vasculaire du microenvironnement tumoral. D'autre part, la diffusion limitée des nutriments crée un état de stress métabolique pour les cellules tumorales auxquels l'accès est limité. La réponse cellulaire à des conditions hypoxiques est modulée par le Hypoxia Inducible Factor (HIF), un facteur de transcription formé d'une sous-unité β stable et d'une sous-unité α qui est, elle, labile. Durant une phase de normoxie, la sous-unité α de HIF est hydroxylée par l'enzyme proline dioxygénase (PHD), en une réaction qui marque HIF-α pour être reconnue par le complexe von Hippel-Lindau (pVHL), et conséquemment dégradée dans le protéasome 26S. En période de réduction d'oxygène, PHD est inactivé et HIF-α stabilisée, ce qui permet sa dimérization avec HIF-β. Le complexe HIF peut ainsi entrer dans le noyau cellulaire, se lier à un élément d'ADN appelé Hypoxia Responsive Element (HRE) et déclencher la transcription génétique. Les gènes en aval d'un élément HRE sont associés à l'angiogenèse, la métastase, la survie cellulaire et le métabolisme. De façon plus particulière, l'expression de HIF régule positivement l'expression d'enzymes métaboliques impliquées dans la glycolyse.

De récentes études ont montré qu'en plus de l'hypoxie, des facteurs tels que des oncogènes ou des métabolites étaient capables de stabiliser HIF-α et d'augmenter la transcription de gènes dépendant de HIF. L'exemple le plus frappant est l'accumulation du complexe HIF dans les glioblastomes comportant une mutation sur l'enzyme isocitrate déshydrogénase 1 (IDH1). IDH1 convertit l'isocitrate en α-kétoglutarate, cependant la mutation empêche le bon fonctionnement de cette réaction, conduisant à une réduction du niveau d'α-kétoglutarate. α-kétoglutarate étant un cofacteur nécessaire pour l'hydroxylation de HIF, sa diminution marquée cause une stabilisation de HIF-α, et cela même en période de normoxie (un phénomène appelé « pseudo-hypoxie »). Le fait que HIF module certaines parties du métabolisme et puisse être modulé par des niveaux de métabolites déséquilibrés suggère l'existence d'un circuit de régulation positive autour de la voie de signalisation de HIF. De plus,

la combinaison génétique propre à une tumeur peut promouvoir certains comportements métaboliques.

Dans cette thèse, nous avons eu pour but de comprendre l'influence d'une mutation active sur la voie de signalisation HIF ainsi que sur le métabolisme du pyruvate, « le portier » du cycle de l'acide citrique (TCA). Dans ce but, nous avons développé un test d'imagerie fluorescente et employé un test préétabli pour l'étude du pyruvate ^{13}C *in vivo*. Deux modèles de cancer du colon humain possédant une mutation active dans la voie de signalisation MAPK ont été utilisés : une lignée cellulaire DLD-1 avec une mutation au niveau de KRAS, et une lignée cellulaire RKO avec une mutation au niveau de BRAF. Les deux mutations étant actives, elle déclenchent de façon ininterrompue la voie de signalisation MAPK. Pour mesurer l'activité de HIF, nous avons modifié les cellules DLD-1 et RKO pour qu'elles expriment une protéine fluorescente infrarouge (iRFP) sous le contrôle de deux éléments de liaison de HIF. Les cellules tumorales ont ensuite été injectées de façon sous-cutanée dans des souris, et les xénogreffes exprimant de la fluorescence ont été mesurées longitudinalement durant des expériences de fluorescence en plan 2D. Au cours de ces expériences, des mesures additionnelles du métabolisme ont été pratiquées sur les mêmes animaux. Pour examiner le métabolisme du pyruvate, nous avons utilisé du pyruvate [1-^{13}C] et l'avons hyperpolarisé via un processus de polarisation nucléaire dynamique (DNP) pour augmenter sa sensibilité durant les expériences de spectroscopie de résonnance magnétique (^{13}C-MRS). Une solution contenant du pyruvate [1-^{13}C] hyperpolarisé a été injectée par intraveineuse dans les souris de manière à suivre la conversion du pyruvate [1-^{13}C] en lactate [1-^{13}C] dans les tumeurs. À la fin des expérimentations animales, les tumeurs ont été extraites pour la détection *ex vivo* de différents marqueurs liés à l'hypoxie : le marqueur de régions hypoxiques pimonidazole, le produit de la transcription par HIF appelé anhydrase carbonique 9 (CA9) et enfin le marquer de vaisseaux sanguins « cluster of differentiation 31 » (CD31).

L'imagerie *in vivo* de iRFP dans les différents types de tumeurs a révélé une augmentation significative de fluorescence dans les tumeurs mutées pour KRAS ou BRAF. De façon intéressante, ces différences étaient plus prononcées dans les tumeurs en phase de développement initial, c'est-à-dire d'un volume inférieur à 100mm^3, en comparaison avec l'état de développement avancé des tumeurs où les intensités de fluorescence ont tendance à s'égaliser. À partir de résultats obtenus *ex vivo,* nous concluons que l'activité augmentée de

HIF dans les petites tumeurs avec une mutation est la conséquence de facteurs indépendants de l'hypoxie cellulaire. Cependant, l'activité de HIF dans les tumeurs plus développées découle plutôt de l'hypoxie. Étonnamment, les résultats des études métaboliques n'ont pas montré de différences significatives entre les tumeurs mutées et non-mutées au niveau du métabolisme du pyruvate. Ces résultats pourraient être dûs à un manque de sensibilité de la méthode DNP, particulièrement envers les tumeurs de petit volume, mais aussi au fait que les mutations KRAS et BRAF aient un impact sur un métabolite autre que le pyruvate et que cette différence passe donc inaperçue lors des expériences de DNP.

En conclusion, nous avons démontré qu'une mutation active dans la voie de signalisation MAPK possède un impact sur l'activité de HIF dans des xénogreffes, mais qu'elles n'influencent en rien le métabolisme du pyruvate dans ces tumeurs. Pour arriver à cette conclusion, nous avons développé un test pour détecter l'activité de HIF de façon indirecte, en mesurant la fluorescence. L'utilisation d'un fluorochrome infrarouge nous a permis de diminuer l'absorption et la diffusion de photons par les tissus et d'augmenter ainsi la qualité d'imagerie optique. De plus, nous avons démontré les bénéfices liés à l'utilisation de métabolites contenant du carbone 13 pour suivre des réactions métaboliques *in vivo* dans des tumeurs.

1. Introduction

1 Impact of tumor hypoxia on clinical outcome

In the beginning of the 20th century, studies by Schwarz[1] and Müller[2] revealed that a patient response to radiation was raised when blood flow in the tumor was increased. This dependency of the radiation treatment outcome on blood flow led Thomlinson and Gray[3] to investigate the tumor oxygenation status and to later demonstrate that it constituted, in fact, a determinant factor for the outcome of radiation therapy. Oxygen acts as a powerful radiosensitizer by accepting electrons produced by DNA and other molecules after radiation, yielding reactive particles prone to chemical bond breakage. Therefore, radiosensitivity increases with increased oxygen tension within the tumor. Following these findings, efforts were invested in researches aiming at answering three major questions: what is the biological cellular response to the lack of oxygen, how to precisely and non-invasively measure the oxygenation status of a tumor and finally, what strategies can be applied to counterbalance hypoxia during radiation treatment. Hypoxia has been shown to regulate the expression of genes involved in cell survival and proliferation via the expression of the transcription factor Hypoxia Inducible Factor (HIF) and a high level of HIF has been associated with poor patient prognosis in various tumor type[4]. Based on those conclusions, imaging techniques depending on the tumor oxygen level or HIF expression as well as its downstream genes expression have been developed. Nowadays, imaging tumor hypoxia can be achieved to a certain extent, but the challenge still remains to detect regions of transient hypoxia and regions with oxygen levels considered hypoxic but not recognized as such by the probes available. To complete this triad, attempts have been made to improve radiation outcome by oxygen delivery or by

sensitizing hypoxic cells. Conclusions regarding such studies are mixed and many unknowns still persist.

Tumor hypoxia is a very complex and dynamic process leading to important intra- and inter-tumor variations. Additionally, lack of standardized methods to identify and quantify it participates to this variability. Therefore, there is a need to develop better tools to understand and image tumor hypoxia precisely and homogenously in order to establish better treatment strategies to fight hypoxia-dependent effects on tumor response to radiation therapy and tumor malignancy.

2 Cellular response to hypoxia

2.1 Oxygen regulation of HIF

All metazoans need oxygen (O_2) to maintain their intracellular level of adenosine triphosphate (ATP) through aerobic metabolism. Furthermore, O_2 also participates as an electron acceptor to various organic and inorganic chemical reactions. In addition to sustaining bioenergetics levels, O_2 availability contributes to the regulation of a wide diversity of physiological and pathophysiological events such as adaptation to high altitude, wound healing, inflammation and the growth of solid tumors [5,6]. Air contains usually 21% of O_2 (corresponding to a partial pressure pO2=150mm Hg) while partial oxygen pressure in tissues ranges between 2% to 9% (pO_2=40mm Hg). Hypoxia is defined as a lack of O_2 or a reduced O_2 availability, which corresponds, for human tissues and tumors, to an oxygenation level equal or below 2% of O_2. When tissue oxygenation falls below 0.02% of O_2 the condition is termed sever hypoxia, also referred to as anoxia. Hypoxia is a critical component of the tumor microenvironment. It is a consequence of the tumor initial avascular growth consuming nutrients and molecular oxygen via molecular diffusion. Once the diffusion becomes insufficient in supplying the neoplastic tissue, a molecular program triggering the development of the tumor vasculature is initiated. Yet, the tumor vascular system is poorly organized and the blood flow and delivery of substrates very inefficient, leading to hypoxic tumor domains. Two different types of hypoxia can be identified: acute and chronic hypoxia. Acute hypoxia is linked to perfusion and occurs whenever there is a reduction in blood supply. Chronic hypoxia on the other hand is linked to diffusion and occurs when vascularization is insufficient and fails to deliver O_2 to a tumor subregion[7]. The physiological responses to hypoxia such as the development of a vascular

system indicate that low oxygen levels within tissues initiate cellular responses enabling the adaptation and potentially the survival under hypoxic conditions. The specific molecular regulation will depend on both the nature and the duration of the stressful conditions, e.g. it might differ when considering acute and chronic hypoxia.

The main modulator of the cellular response and adaptation to hypoxia is the Hypoxia Inducible Factor (HIF), a heterodimeric transcription factor. HIF is constituted by the assembly of two subunits, HIF-α and HIF-β. HIF-α was first identified by Semenza and Wang in 1992[8], whereas the HIF-β subunit was already known as a member of the aryl hydrocarbon receptor nuclear translocator protein (ARNT) family. In both subunits, the amino terminal belongs to the basic-helix-loop-helix polypeptide family and contain a Per-ARNT-Simhomology (PAS) domain, which is necessary for heterodimerization and DNA binding. On the carboxyl terminal, the α and β subunits contain domains necessary to the transcriptional activity of the protein and, in the case of the α subunit the O_2-sensitive regulatory domains. HIF-α subunit comprises three isoforms, HIF-1α, HIF-2α and HIF-3α, whereas HIF-β occurs in the form of three paralogues (ARNT1, ARNT2, ARNT3). HIF-1α was found to be expressed ubiquitously in all metazoans, while HIF-2α expression is restricted to vertebrates and to certain types of cells such as endothelial cells, hepatocytes, macrophages, muscle cells and astrocytes[9]. HIF-3α expression is also specific to a subset of cells, but still little is known about its expression and function.

For a long time, the process, by which HIF-α was being stabilized, under hypoxic conditions remained a mystery. It is only in 2001 that the groups of Ratcliffe[10] and Kaelin[11] shed light on the O_2-dependent cascade leading to the activation of the HIF complex. Both groups identified a prolyl-4-hydroxylase domain (PHD) protein, an enzyme, which catalyzes the hydroxylation of one of the two prolines (Pro-403 or Pro-564 in human HIF-α) found within a specific oxygen-dependent degradation (ODD) domain on the HIF-α subunit. There are three homologues of this enzyme, designated PHD1, PHD2, PHD3. All three dioxygenases require oxygen and 2-oxoglutarate (2-OG, also referred to as α-ketoglutarate) as co-substrates, and iron and ascorbate as co-factors. The first step in the cascade is binding of 2-OG and HIF-α by the PHD-Fe^{2+}, a step that is reversible. The binding of HIF-α to the enzyme displaces a water molecule coordinated to Fe^{2+}, allowing O_2 to bind to the PHD and react with iron. This step leads to the oxidative decarboxylation of 2-OG and production of succinate, CO_2 and a ferryl complex

(Fe^{IV}=O). This Fe^{IV}=O intermediate can now reacts with HIF-α and oxidize a C-H bond on the proline residues of the subunit yielding C-OH. In this reaction, ascorbate is required to maintain Fe^{2+} in its ferrous state[12].

In normoxic conditions, the hydroxylation of one of the two prolines in the ODD domain of HIF-α is sufficient to trigger the recognition and binding of the subunit by the Von Hippel-Lindau tumor suppressor protein (pVHL) (Fig 1A). The role of pVHL in HIF-α degradation was identified when studying the VHL syndrome, an autosomal dominant disease characterized by tumor formation in the brain, kidney and other organs, due to a loss-of-function germline mutation on the *VHL* gene. Once bound to the HIF-α subunit, pVHL interacts with Elongin C to recruit an E3 ubiquitin-protein ligase. Following ubiquitination, the HIF-α-pVHL complex is directed towards the 26S proteasome, a multiprotein proteolytic system, which degrades HIF-α.

In hypoxic conditions, insufficient O_2 level prevents the hydroxylation of HIF-α by the PHDs, leading to a stabilization of this subunit (Fig 1C). Following this step, HIF-α is translocated to the nucleus where it dimerizes with HIF-β. However, the HIF complex is not fully active yet. It recognizes and binds to a HIF binding site (HBS) on the DNA, which is a CGTG consensus sequence contained in the Hypoxia Responsive Element (HRE) region of many oxygen-regulated genes. In order to start the transcription of such genes, the HIF complex recruits two coactivators, namely the CBP and p300. Those two molecules are necessary to initiate transcription by binding and stabilizing the transcription initiation complex containing RNA polymerase II. Moreover, their histone acetyltransferase activity provides access of the polymerase to DNA. Interaction of HIF with the CBP/p300 complex can however still be disturbed by the Factor Inhibiting HIF-1 (FIH), an enzyme capable of hydroxylating an asparagine residue in the C-terminal domain of HIF-1α (Fig 1B). This reaction prevents the binding of CBP/p300 to the C-terminal domain of HIF-1, impairing the transcription of C-transactivation domain-dependent genes. Similarly to the PHDs, FIH is a hydroxylase which requires O_2, Fe^{2+} and 2-OG to function. Interestingly, PHDs have a lower oxygen affinity than FIH, leading to the activation of FIH at O_2-levels at which PHDs are inactive. This adds a new dimension to the oxygen-dependent control of HIF stability and activity, as FIH allows the N-terminal-regulated genes and represses the C-terminal-dependent ones or the genes requiring both C- and N-terminal regulation.

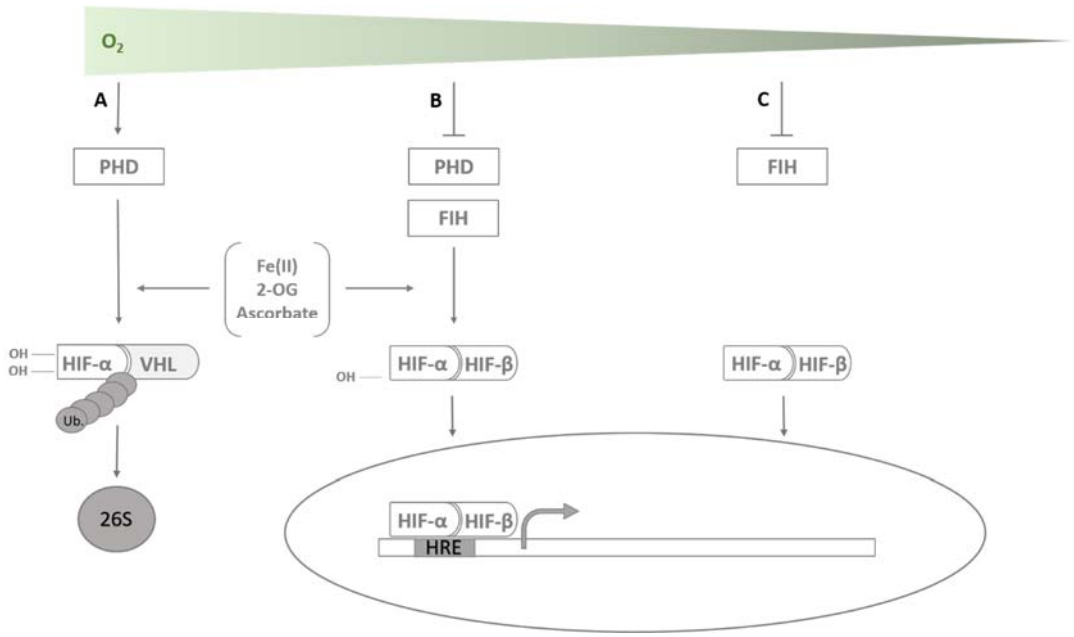

Figure 1 *Oxygen-dependent stabilisation of the Hypoxia Inducible Factor (HIF)* ***A*** *In normoxic conditions, the prolyl-4-hydroxylase domain (PHD) hydroxylates the HIF-α subunit in a reaction using O_2 and 2-oxo-glutarate (2-OG or α-ketoglutarate) as co-substrates and iron (FeII) and ascorbate as cofactors. The hydroxylated subunit is recognized by the Von Hippel-Lindau (VHL) tumor suppressor which recruits an E3-ubiquitin protein ligase complex to ubiquitinate the α subunit, a labeling step which direct the HIF-α to be degraded in the 26S proteasome.* ***B*** *In mild hypoxia, PHD is inactive, however the Factor-Inhibiting HIF (FIH), due to its higher affinity for O_2, is active and hydroxylates an asparagine residue on the C-terminal transactivation domain of HIF-α. This reaction inhibits the interaction between the C-terminal domain of HIF-α and the transcriptional co-activator CBP/p300, therefore participating to the modulation of HIF transcriptional activity.* ***C*** *In hypoxic conditions, both PHD and FIH are inactive. This prevents the hydroxylation of HIF-α and leads to its stabilization and dimerization with the HIF-β subunit. Upon entry in the nucleus, the dimer recognizes and binds to a Hypoxia Responsive Element (HRE) sequence on the DNA and activates the transcription of downstream genes.*

2.2 Implication of hypoxia and HIF in tumor progression

The development of a tumor mass is characterized by cellular proliferation, invasion of the microenvironment and, in a later stage, of tissues located remotely from the primary tumor. As a tumor reaches a diameter of about 400µm, it needs to start developing its own vasculature in order to feed the tumor subregions furthest from the local blood vessels with O_2 and nutrients. The newly formed vasculature varies greatly from the physiological vasculature as it displays many structural and functional abnormalities. Vessels are leaky, tortuous and often lack vascular tone. This results in an inefficient delivery of O_2 to some areas of the tumor, leading to the development of hypoxic or anoxic regions. Hypoxia, via the activation of HIF, is capable of inducing cellular changes to allow the tumor cells to adapt to

harsh conditions and survive. Target genes of HIF have been identified to be involved in three important steps causing tumor progression: angiogenesis, cellular proliferation and survival, metastasis.

Angiogenesis: To feed tumor cells beyond the O_2 diffusion limit (70µm), the tumor mass initiates the development of a new vasculature penetrating the tumor tissue and supplying proliferating cells with O_2 and nutrients. The formation of new blood vessels branching from pre-existing ones is termed angiogenesis. The angiogenic process is achieved by the tumor mass by producing pro-angiogenic factors capable of competitively overcoming the effect of anti-angiogenic factors. This step is referred to as the angiogenic switch[13]. Angiogenesis is regulated by HIF as some of its target genes are involved in the different steps of the process. HIF triggers the primitive vascular network formation by regulating the transcription of the vascular endothelial growth factors (VEGFs) and stimulating the production of VEGF receptors, fibroblast growth factors (FGF), and platelet-derived growth factors (PDGF). The splitting and sprouting of new vessels from pre-existing ones is achieved by HIF-induced enzymes such as matrix metalloproteinases (MMPs). Eventually HIF activates Ang-1 and PDGF to support the maturation of newly-formed vessels, and TGF-β to recruit smooth muscle cells and pericytes necessary for the tone and stability of the vessel[14].

Proliferation and apoptosis: HIF activates a panel of genes among which some are involved in cell proliferation and some in cellular apoptosis. The outcome of their simultaneous activation is highly determined by external factors such as degree and duration of hypoxia, cell type, tumor microenvironment and genetic alterations. HIF-1 is involved in cellular apoptosis by either stabilizing the tumor suppressor p53[15], leading to an increase in p53-mediated cell cycle arrest and apoptosis, or by upregulating the pro-apoptotic Bcl-2/adenovirus EIB interacting protein 3 (BNIP3) and its homologue Nip-3-like protein X (NIX)[16]. On the other hand, various anti-apoptotic agents are upregulated via HIF under hypoxia. BCL-xL, a member of the anti-apoptotic protein family Bcl-2, was recently identified as a HIF target. In addition to that, increase in myeloid cell factor-1 (Mcl-1) and gene expression of survivin were also linked to HIF. Numerous modulators of cell proliferation and apoptosis have been identified to be linked to HIF-1. However, it is now established that HIF-2 might have additional effects in the cellular fate, although its precise mechanism still remains blurry. HIF-2 target genes and their positive

or negative effects on the cell cycle come additionally in the balance between HIF-1 effects, tumor type and microenvironment to decide on the ultimate cell finality.

Metastasis: In various studies, cell exposure to hypoxia has been shown to positively influence the metastatic potential of those cells[17]. In fact, many of the HIF target genes are involved in the different steps leading to metastasis. In order to escape the primary tumor site, cells have to undergo an epithelial to mesenchymal transition (EMT), a process in which the cell decreases the expression of epithelial-associated genes such as E-cadherin and β-catenin and acquires more plastic and mobile abilities by increasing the expression of mesenchymal-like genes such as N-cadherin and vimentin. HIF impacts on EMT by inducing the transcription of TWIST, a transcription factor involved in the repression of E-cadherins[18]. Following EMT, tumor cells can invade the microenvironment thanks to the expression of HIF-dependent matrix remodeling enzymes (MMPs and lysyl oxidase) which disrupt cell-cell and cell-matrix connections. Recently, it was shown that hypoxia also promotes epithelial-to-amoeboid transition via MMP-independent mechanisms, extending the scope of HIF-dependent influence on tumor cell dissemination[19]. Another event promoting metastasis is the acidification of the microenvironment and the consequent degradation of the extracellular matrix. Regulation of the intra- and extracellular pH is mainly directed by carbonic anhydrase, among which the carbonic anhydrase 9 (CA9) is a downstream gene of HIF. Finally, a leaky and heterogeneous tumor vasculature resulting from a chaotic angiogenesis also drastically enhances cellular escape, circulation and relocation.

2.3 Genetic influence on HIF transcription regulation

The stability and activity of the HIF-1α protein is modulated by hypoxia, however, its translation and synthesis are mediated by oxygen-independent processes (Fig 2). Two main pathways are responsible for activating HIF translation: the phosphoinositide-3-kinase (PI3K) and the mitogen-activated protein kinase (MAPK) pathways. Both of them are responding to receptor and nonreceptor protein tyrosine kinase (RTKs and nRTKs) activation, which, in turn, respond to growth factors, oncogenes activation and suppression of tumor suppressor activity. Contrary to hypoxia inducing HIF stability in all cell types, HIF expression is cell specific. HIF-1α translation is activated via Akt and the mechanistic target of rapamycin (mTOR) on the PI3K pathway, and via the activation of the extracellular signal-regulated kinase

(ERK) in the MAPK pathway. Interestingly both HIF-1α and HIF-2α enhance the transcription of growth factors activating RTKs and their subsequent pathways, leading to a potential positive autocrine feedback loop.

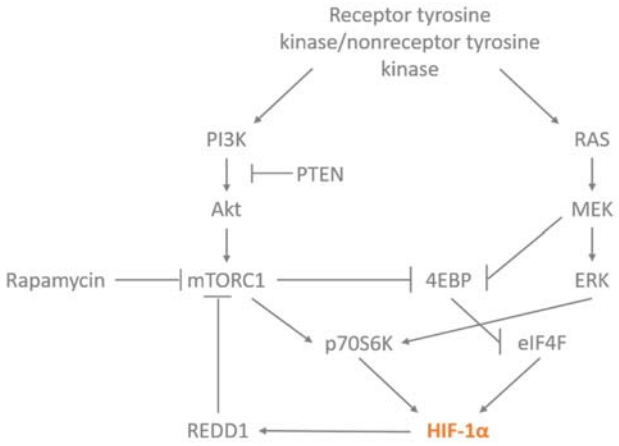

Figure 2 *Pathways influencing HIF-1α protein synthesis. Activation of the receptor and nonreceptor tyrosine kinase activates in turn the phosphoinositide3-kinase (PI3K) pathway and RAS in the mitogen-activated protein kinase (MAPK) pathway. HIF-1α translation is upregulated on one hand through the PI3K pathway via the protein kinase B (Akt) and the mechanistic target of rapamycin complex 1 (mTORC1), and on the other hand through the MAPK pathway via the activation of the extracellular signal-regulated kinase (ERK). The specific translation of mRNA is activated by mTORC1 through the ribosomal protein 6S kinase (p70S6K) activation, and by MEK through the inactivation of the translational repressor eukaryotic initiation factor 4E-binding protein (4EBP), which leads to the assembly of the multisubunit eIF4F complex. The eIF4F formation facilitates the cap-dependent translation and increases translation of mRNAs possessing a regulatory element in the 5'-untranslated terminal region, such as HIF-1α mRNA.*

During prolonged hypoxia, protein synthesis is reduced or completely shut down to spare energy via the inhibition of mTORC1 by REDD1, a direct target of HIF-1α. However, hypoxic cells still exhibit a continuous translation of HIF-1α mRNA, which allow them to transcribe genes essential for cell survival. The process by which a HIF-specific mRNA translation is achieved is still not fully understood[20].

2.4 Hypoxia and HIF as therapeutic targets

Hypoxia and the subsequent stabilization of HIF-1 and HIF-2 complexes are involved in many aspects of the cellular proliferation and survival, as well as tumor progression and metastasis. Taken together the effects of HIF activity are capable of promoting resistance to treatment,

compromising to a large extent the outcome of cancer treatment. Therefore, great efforts are being invested in developing therapies targeting either hypoxia or the different steps leading to HIF activation.

Targeting hypoxic cells is mostly achieved by using bioreductive prodrugs. Bioreductive prodrugs are first chemically reduced within the cell, a step that is followed by re-oxidization of the drug in normoxic cells, or by the generation of active drugs in the case of hypoxic cells. The development of effective prodrugs is based on five chemical ingredients (nitro groups, quinones, aromatic *N*-oxides, aliphatic *N*-oxides and transition metals), providing the capacity of being reduced enzymatically under hypoxic conditions. The redox cycling between prodrug and the reduced, potentially active prodrug radical, prevents the hazardous activation of the compound within normoxic cells and results in hypoxia-specific cell destruction. The cytotoxicity of bioreductive prodrugs is achieved by generating DNA-reactive cytotoxins capable of inducing cytotoxic DNA strand breaks. So far the most promising prodrugs developed are the aromatic *N*-oxide tirapazamine (TPZ)[21] and apaziquone[22], both of them currently in Phase III clinical trials. The 2-nitroimidazole-based nitrogen mustard prodrug TH-302 is also showing promising results in Phase I clinical trials and is undergoing evaluation in Phase II clinical trials. Besides achieving specificity towards hypoxic cells, prodrugs need to overcome two additional challenges: tissue penetration and drug affinity. Drugs have a limited extravascular penetration within tumor tissue, as it is typically characterized by an elevated interstitial pressure, and even more within hypoxic tissue where the vasculature is very limited. To circumvent this problem, emphasis has been put on optimizing physicochemical properties of the compound such as lipophilicity, molecular weight and hydrogen bonds donors and acceptors to enhance the prodrugs penetration within cancerous tissues. Regarding the affinity of the prodrugs it is preferable to target cells exhibiting a moderate hypoxia (~1-10μM O_2) rather than highly hypoxic or anoxic cells, as the latter are less likely to participate in tumor growth after therapy. This is achieved by either producing drugs with a high K_{O2} (~1μM), which get activated under moderate hypoxia, or by designing drugs with a much lower K_{O2} (~0.1μM), therefore restraining their activation to pathologically hypoxic cells only[23].

HIF-1 and HIF-2 participate in the modulation of tumor cell survival, therefore the different steps leading to HIF activation constitute interesting targets for the development of inhibitory

drugs. At the messenger RNA level, *EZN-2698*, an anti-sense oligonucleotide, inhibits the expression of HIF-1α mRNA and its target genes[24]. HIF-1α protein synthesis is mainly prevented via the inhibition of topoisomerases I and II, receptor tyrosine kinase, and oncogenic pathways. Camptothecins *(*CPTs*)* analogues inhibit the topoisomerase I and prevent HIF-1α protein accumulation by inducing the formation of Top 1-DNA complexes capable of forming double strands DNA breaks. Another important route for HIF translation downregulation is by inhibiting the PI3K/Akt/mTOR signaling pathway, which is active in over 70% of human cancer cell lines[25]. Temsirolimus (Torisel®-CCI-779) is an mTOR inhibitor successfully approved for treatment of metastatic renal cell carcinoma (RCC) and which, additionally, is being investigated for its antiangiogenic properties in breast cancer[26].

Inhibition of HIF-1α stabilization is modulated by targeting the Heat Shock Protein 90 (Hsp90), a molecule promoting HIF-1α activity by blocking VHL-independent proteasomal degradation and by providing help to the HIF dimer to find the appropriate configuration to recruit p300 and initiate transcription. Various molecules have been developed to inhibit Hsp90, among which Geldanamycins (GAs)[27] which are under clinical trials now. The next step in the HIF pathway which can be prevented is HIF-1 dimerization. Recently a new molecule, Acriflavin, has been shown to efficiently inhibit HIF dimerization by binding to the PAS-B domain of HIF-1α and HIF-2α[28]. Lastly, a potential way of inhibiting HIF activity is by disrupting the formation of an active transcription complex formed by HIF dimer and p300. *Bortezomib* is a proteasome inhibitor preventing this step at very low dose (~nM). However it has been shown recently that *Bortezomib* was also active in downregulating the PI3K/Akt/mTOR pathway in prostate cancer[29] and therefore it is now under study to assess the spectrum of its anticancer activity.

3 Tumor metabolism

Almost 100 years ago, long before the discovery and description of oncogenes and tumor suppressors and their function, scientists in cancer biology established that tumor cells possess a very different metabolism than normal quiescent cells. More precisely, cancerous cells exhibit an altered metabolism that is necessary to face unique tumor mass physiological stresses made up by hypoxia, scarcity of nutrients, acidosis, and to foster the acquisition and maintenance of malignant properties. A modified metabolism is not a specificity of a single type of cancer; on the contrary, it has been shown to appear in various tumor types. Therefore an altered or reprogrammed metabolism has become one the hallmark displayed by tumor cells, together with maintaining proliferative signaling, evading growth suppressors, avoiding immune destruction, enabling replicative immortality, activating invasion and metastasis, inducing angiogenesis and escaping apoptotic signals[30]. The alterations generated in the cellular metabolism concern all the steps in the cell-metabolite interactions. They affect the influx of metabolites through an increased capability to import necessary nutrients, they direct the way metabolites are preferentially assigned to metabolic pathways contributing to the tumorigenesis, and finally they have long-lasting effects on the tumor cells differentiation as well as on the tumor microenvironment. Metabolic reprogramming, defined as the enhancement or suppression of conventional metabolic routes by oncogenes or other factors, has to be differentiated from the term “oncometabolite”[31], which defines a metabolite whose level is drastically increased in tumor cell. Reprogramming of tumor metabolism is achieved through different pathways, among which HIF plays an important role, as it will be described later on in this chapter.

3.1 The Warburg effect

In 1920s, Otto Warburg used tumor slices *ex vivo* to demonstrate that even when incubated in glucose-enriched medium and in the presence of oxygen, tumor sections preferentially convert pyruvate into lactate at the end-point of glycolysis rather than fully oxidizing glucose in the tricarboxylic acid cycle (TCA) and produce more ATP molecules[32]. This newly described phenomenon of aerobic phosphorylation was later identified in various types of cancer including breast, lung, colorectal cancer, glioblastoma and termed the Warburg effect. Based on the fact that energy production is much more efficient via the TCA in the mitochondrion

rather than through glycolysis, it was assumed that tumorigenesis provided by aerobic phosphorylation was in fact an alternative to non-functioning mitochondria. Years later, Warburg's theory of the tumor mitochondria malfunction was rejected when new studies showed that the mitochondria of cancer cells were actually fully active and functional[33]. In fact it was even established that within a tumor subpopulation, some tumor cells can be rather oxidative whereas others are preferentially glycolytic[34].

An increased glucose uptake is commonly associated with the Warburg effect in tumor cells and has been used extensively in ^{18}F-fluorodeoxyglucose (18F-FDG) PET imaging to detect tumors and metastasis in human. However not all tumors can be detected by PET, and sometimes a strong PET signal does not correlate with malignant tissue. Misleading PET results can be due to other physiological events such as inflammation or to the glucose uptake by the tumor microenvironment, a process called the reverse Warburg effect[35]. It is also important to note that not all cancer types exhibit Warburg or reverse Warburg effects. Tumor metabolism depends mostly on the tumor microenvironment and on the activity of oncogenes, tumor suppressors and other factors, leading to a very heterogeneous reprogrammation of metabolic pathways, even within the tumor mass itself [36].

3.2 Metabolic pathways reprogrammed during tumor development

Glucose and glutamine metabolism: In order to sustain proliferation and provide building blocks for the formation of new cells, tumor cells rely on the increased uptake of two essential nutrients: glucose and glutamine. The catabolism of those two molecules produces carbon intermediates used in the assembly of macromolecules. In addition to that, the oxidation of glucose and glutamine serves the cell to re-establish its reducing power either in the form of NADH and $FADH_2$, or in the form of the cofactor NADPH. In addition to providing a carbon skeleton, glutamine acts as a nitrogen donor and therefore plays an important role in the biosynthesis of the nucleotides purine and pyrimidine as well as in the synthesis of proteins, glucose-6-phosphate and non-essential amino acids.

The pentose phosphate pathway: The pentose phosphate pathway (PPP) is highly increased during tumor cell proliferation to support DNA replication and RNA formation by modulating the flux of carbons between nucleic acids synthesis and lipogenesis. The PPP is composed of

two branches: the oxidative branch partially and irreversibly oxidizes glucose-6-phosphate (G6P), yielding NADPH and ribose-5-phosphate (R5P), a structural component of nucleotides, whereas the non-oxidative branch reversibly interconverts R5P with glycolytic intermediates.

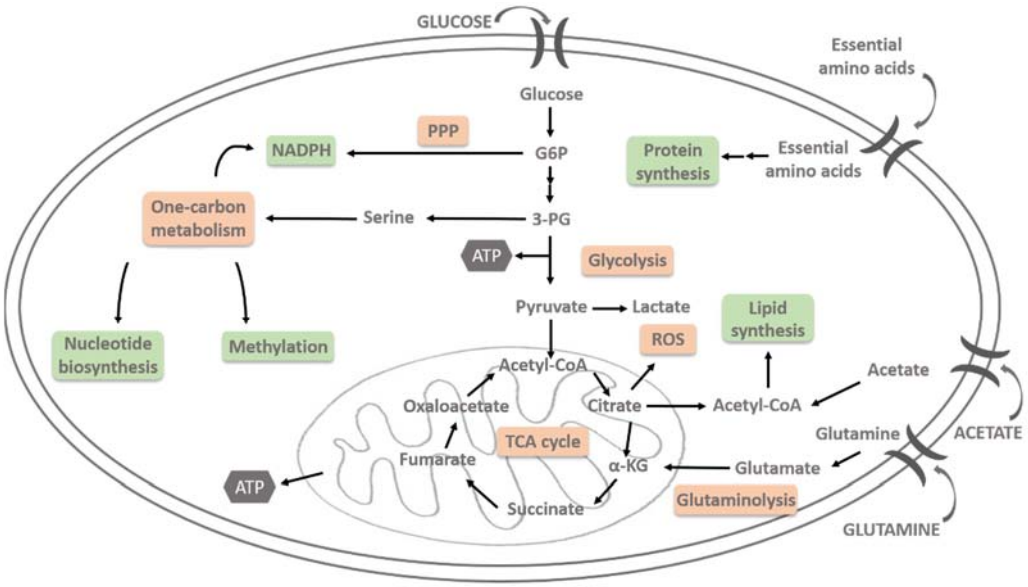

Figure 3 *Principal metabolic pathways involved in tumor macromolecule production. Glycolysis metabolizes glucose into pyruvate, a process yielding ATP and glycolytic intermediates which can also be diverted into other pathways. For example, glucose 6-phosphate (G6P) is oxidized through the pentose phosphate pathway (PPP) to maintain the level of the reducing agent nicotinamide adenine dinucleotide phosphate (NADPH) and to provide structural components for nucleotide formation. Additionally, 3-phosphoglyceric acid (3-PG) can be converted into serine, a non-essential amino acid contributing to nucleotide biosynthesis, methylation and NADPH balance as a one-carbon donor for the folate cycle. The tricarboxylic acid cycle (TCA) support tumor metabolism by oxidizing acetyl-CoA, a process producing energy molecules ATP, the reducing agents nicotinamide adenine dinucleotide (NADH) and flavin adenine dinucleotide ($FADH_2$), reactive oxygen species (ROS) and intermediates necessary for lipid synthesis. Similar to glucose, glutamine uptake is increased in tumors. Glutaminolysis converts glutamine into glutamate and α-ketoglutarate (α-KG), an intermediate of the TCA which oxidation yields ATP, NADH and $FADH_2$. Also, glutamine serves as a precursor for protein and lipid synthesis.*

<u>Lipid metabolism:</u> Normal dividing cells mainly use extracellular lipids as building blocks for the formation of new membranes. Unlike non-transformed cells, tumor cells rely on *de novo* lipid biosynthesis to sustain cell proliferation. The synthesis of fatty acids, the primary components of lipids, is achieved by condensing acetyl and malonyl groups through cyclic reaction of the fatty acid synthase (FASN). The acetyl group is obtained by exporting citrate from the mitochondria and converting it into acetyl-CoA and oxaloacetate, whereas the

malonyl group is produced by the conversion of acetyl-CoA into malonyl-CoA by the acetyl-CoA carboxylase (ACC).

Amino acids metabolism: Another group of molecules vital for cellular proliferative metabolism and for cell survival is amino acids. It is therefore not surprising that cells developed an elaborated amino acid sensing system via mTOR to detect levels of amino acids and decide whether or not to proceed with protein synthesis[37]. Amino acids are an important source of carbon and nitrogen for biosynthesis as they contain a carboxyl and an amino group. Among the 20 amino acids, 11 can be produced endogenously, while the remaining ones, the essential amino acids, need to be obtained from external sources. Production of non-essential amino acids is reached by using either glycolytic intermediates, such as 3-phosphoglycerate and pyruvate, or intermediates of the TCA, such as oxaloacetate and α-KG, as precursors for serine, alanine, aspartate and glutamate respectively. Interestingly, proliferating tumor cells display an imbalance between the consumption of some amino acids and the quantity required for protein synthesis, which suggest an alternative use of it[38]. For example, serine and glycine participate in the one-carbon metabolism and generate precursors for the biosynthesis of lipids, nucleotides and proteins. Additionally, they are being used in the redox balance of the cell as well as in the methylation of protein and nucleic acids[39].

Mitochondrial metabolism: The mitochondria contributes to tumor growth and proliferation by providing tumor cells with various crucial processes. It generates energy, signals to different pathways via the production of reactive oxygen species (ROS), regulates apoptosis and modulates cytosolic calcium levels and the trafficking of small metabolites[40]. The most important metabolic pathway occurring in the mitochondria is the TCA cycle. TCA intermediates are important precursors for lipids, proteins and nucleic acids synthesis, and provide the tumor cell with the reducing agents NADH and $FADH_2$ used in ATP generation.

3.3 Role of oncogenes in tumor metabolism reprogramming

Reprogramming of tumor metabolism occurs by redirecting intracellular metabolic pathways under the influence of mutated oncogenes and tumor suppressors regulating important cellular pathways. Most of the tumor types display an activating mutation on oncogenes and/or an inactivating mutation on tumor suppressors. This tumor specific genetic

composition is responsible for providing the tumor mass with a particular metabolic phenotype and malignant capabilities over non-transformed cells. The most common oncogenes and pathways involved in the tumor metabolic reprogramming comprise MYC, the PI3K pathway, Akt and mTOR. HIF also does have a very important influence on metabolism and will be described in the following section.

MYC: MYC is a transcription factor governing cell proliferation, cell-cycle progression, cell growth, cellular growth, metabolism, apoptosis, differentiation and response to stress stimuli. In several cancers, MYC is deregulated and overexpressed due to insertional mutagenesis, chromosomal translocation or gene amplification. MYC upregulates glycolysis by promoting the expression of various glycolytic enzymes as well as by inducing the expression of glucose transporters[41]. In addition to supporting glucose intake and catabolism, MYC is responsible for the tumor cell addiction to glutamine and glutaminolysis. Elevated levels of MYC enhance the expression of the glutamine transporters ASCT2 and SN2 and of various enzymes utilizing glutamine and converting it into glutamate[42]. Glutamate accumulation in the cytoplasm leads to the replenishment of the TCA cycle therefore stimulating mitochondrial biogenesis and function, which promotes oxygen consumption and energy production. Besides producing crucial precursors for the TCA cycle, glutaminolysis reaction results in NADPH production, a cofactor needed in many important metabolic reactions.

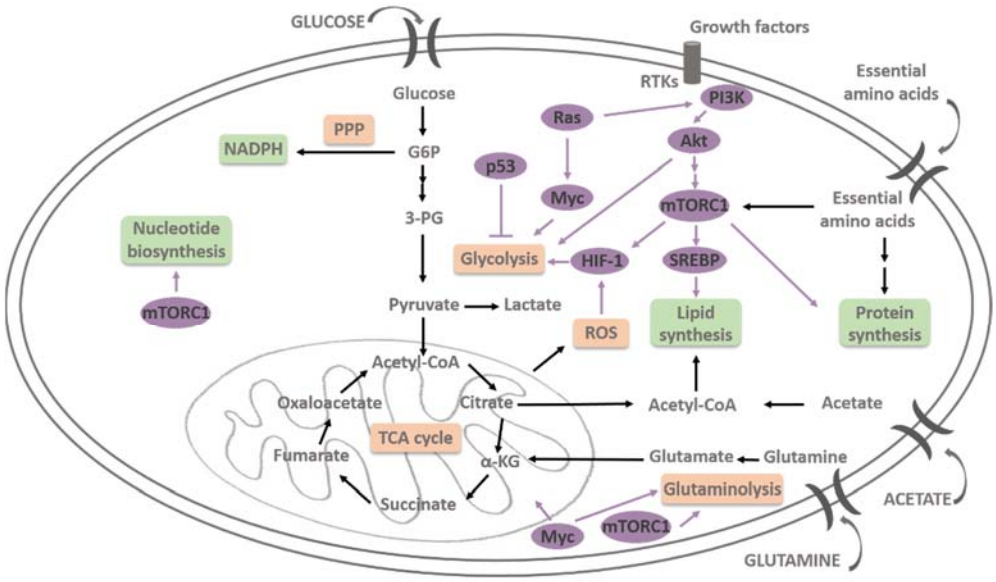

Figure 4 *Principle oncogenes and pathways involved in tumor metabolic reprogramming. The transcription factor Myc enhances glutaminolysis by upregulating glutamine transporters and enzymes converting glutamine into glutamate and α-KG. It also participates to the increase in glycolysis by upregulating glucose transporters and glycolytic enzymes. mTORC1 raises glutaminolysis rate in a similar way as Myc. Additionally, it regulates lipid synthesis by inducing the sterol regulatory element-binding protein (SREBP), a transcription factor targeting genes involved in fatty acids, triglycerides, phospholipids and cholesterol synthesis. Finally, mTORC1 is associated with nucleotide synthesis and more specifically with pyrimidine synthesis via the activation of CAD, an enzyme catalyzing the first three steps of pyrimidine construction. The PI3K pathway is involved, via the activation of Akt, in glycolysis and de novo lipid synthesis through the upregulation of glycolytic enzyme driving irreversible steps in the glycolysis and through the increase of cytosolic pool of acetyl-CoA, a precursor for lipid synthesis. As a result of its effect on Myc and the PI3K pathway, the MAPK pathway, mainly through Ras, in involved in glycolysis, glutaminolysis, nucleotide and lipid synthesis. Lastly, the hypoxia inducible factor (HIF) mainly target glycolysis and upregulates it by increasing the levels of glucose transporters and glycolytic enzymes.*

<u>mTOR:</u> In normal cells, growth factors stimulate the PI3K pathway which in turns activates Akt and mTOR. mTOR is a cytoplasmic serine-threonine protein kinase involved in the regulation of several cellular processes such as protein synthesis, ribosome biogenesis, autophagy and metabolism, which together lead to cell growth and survival. Various oncogenes and tumor suppressors are associated with the PI3K-AKT-mTOR signaling; hence, a common mechanism of tumorigenesis in different cancer types results from the aberrant activation of the PI3K-AKT-mTOR pathway. mTOR is separated into two structurally and functionally different complexes, mTOR complex 1 (mTORC1) and mTOR complex 2 (mTORC2). The role of mTORC2 in tumor metabolism is not yet fully unraveled. On the other hand, mTORC1 has been shown to interfere in diverse ways in the tumor metabolic reprogramming to sustain cell replenishment in amino acids, lipids and nucleic acids. Non-essential amino acids in

proliferative cells are produced by transferring an amino group from glutamate onto a ketoacid. Glutamate is formed by successive deamidation and transamidation of glutamine by glutaminases. mTORC1 is involved in both the uptake of glutamine and the glutaminase activity, providing the cell with a glutamate pool for transamination reaction and maintenance of the TCA cycle. In addition to amino acids and proteins, mTORC1 regulates the synthesis of lipids by activating the sterol regulatory element-binding protein (SREBP), a transcription factor controlling the expression of different genes responsible for the synthesis of fatty acids, triglycerides, phospholipids and cholesterol. Finally, mTORC1 drives the activation of the CAD (carbamoyl-phosphate synthetase 2, aspartate transcarbamoylase, dihydroorotase) an enzyme catalyzing the first three steps of pyrimidine synthesis and therefore regulates the biogenesis of pyrimidine in response to intracellular level of glutamine.

PI3K/Akt: A common facet of many cancer types is the overactivation of the phosphoinositide-3-kinase(PI3K)/Akt pathway, a signaling route sustaining cell proliferation and growth as well as cell survival and metabolic reprogramming. In addition to participating in the activation of mTOR and MYC and their subsequent metabolic interference, PI3K/Akt plays a direct role in the tumor metabolic program. It starts by enhancing glucose uptake through the expression of the glucose transporter *GLUT1* mRNA and the translocation of GLUT1 from the endomembrane to the cell surface. Akt also prevents the expulsion of glucose from the cell by upregulating the enzyme hexokinase which phosphorylates glucose molecules, and by enhancing expression of the phosphofructokinase, an enzyme driving irreversible steps of the glycolysis. Besides glycolysis, PI3K/Akt is implicated in the *de novo* synthesis of fatty acids by increasing the cytosolic pool of Acetyl-CoA. Akt activates the enzyme ATP-citrate lyase which catalyzes the cleavage of the TCA-derived citrate into Acetyl-CoA and oxaloacetate. During phases of metabolic stress, tumor cells may face difficulties to supply sufficient building blocks required by the oncogene-driven demands. In the case of the fatty acids and lipids, cells are capable of acquiring both from the extracellular space via PI3K signaling; fatty acid uptake is enhanced whereas fatty acids oxidation is repressed to maximize lipogenesis in growth-factors controlled proliferative cells[43].

3.4 Role of hypoxia and HIF in tumor metabolic reprogramming

As described earlier in this chapter, HIF is involved in tumor progression by modulating angiogenesis, cell proliferation, apoptosis and metastasis. The last component of tumor malignancy that is influenced by HIF is the reprogramming of tumor metabolism. HIFs play various roles in modulating the metabolic response of cancer cells to limited O_2 and nutrients access and increased accumulation of waste in the extracellular space.

In many cancer types, HIF targets a large group of genes involved in glycolysis. The first step to increase glycolytic rate consists in increasing glucose uptake, which is achieved through an increase in the levels of the glucose transporters GLUT1 and GLUT3, both HIF target genes. Once glucose is taken up by the cell, it is rapidly converted into glucose-6-phosphate (G6P) by hexokinase (HK), an enzyme induced by HIF-1. G6P is negatively charged and cannot cross the cellular membrane. It is trapped in the cell and therefore available for metabolism through glycolysis or the pentose phosphate pathway. As glycolysis increases, the cell accumulates pyruvate, the glycolytic end-product. In normoxic cells pyruvate is converted into Acetyl-CoA and enters the TCA to be oxidized to CO_2 thereby generating nicotinamide adenine dinucleotide (NADH) and Flavin adenine dinucleotide ($FADH_2$), two important reducing equivalents used in ATP synthesis. However, in hypoxic cells, pyruvate is shunted away from the TCA cycle by the HIF-1-induced lactate dehydrogenase A (LDHA), an enzyme converting pyruvate and NADH into lactate and NAD^+. Lactate is ejected from the cytoplasm via the HIF-inducible membrane monocarboxylate transporter 4 (MCT4) and NAD^+ is recycled into the glycolysis.

Using HIF-1 knockout and knockdown cells and VHL-negative renal cancer cells, Papandreou et al.[44] demonstrated that HIF is both necessary and sufficient to downregulate mitochondrial functions under hypoxia. Two mechanisms were found responsible for the modulation of the mitochondrial activity. The first consists of diminishing oxidative phosphorylation, total cellular O_2 consumption and ROS generation by directing pyruvate away from the mitochondria. After pyruvate entry in the mitochondria, pyruvate dehydrogenase (PDH) catalyzes the irreversible conversion of pyruvate into Acetyl-CoA and CO_2 while generating NADH. Under hypoxia this chemical reaction is prevented by the HIF-1 target pyruvate dehydrogenase kinase (PDK), a protein kinase phosphorylating PDH, which is thereby inactivated. As a consequence, the entry of pyruvate into the TCA cycle is prevented, which

reduces the production of the reducing agents necessary to power the electron transport chain.

Expression of the mitochondrial genome and of the genes needed for mitochondrial DNA replication is activated by the transcription factor A (TFAM). Transactivation of the TFAM gene expression is directly induced by the transcription factor MYC and its activating partner MAX. In particular cases of chronic HIF activation, O_2 demand is reduced via a reduction of the mitochondrial biogenesis by HIF-mediated activation of MXI1. MXI1 belongs to the Myc family and is capable of inactivating MYC by displacing MAX, therefore decreasing mitochondrial mass and mitochondrial O_2 consumption.

Under hypoxia, reduction of Acetyl-CoA by redirection of pyruvate represents a challenge for proliferating cells, which need Acetyl-CoA as primary source for fatty acids synthesis. To substitute for that loss, hypoxic cells use glutamine to produce α-KG in the cytoplasm and subsequently convert it into citrate by the enzymes isocitrate dehydrogenase (IDH) and aconitase. This transfer from glycolysis to glutaminolysis as a source of Acetyl-CoA is mainly due to reallocation of pyruvate away from the mitochondria by PDK.

3.5 Altered metabolite levels in cancer: role in tumor biology and HIF signaling

Cancer cells rewire their metabolic pathways to sustain proliferation and survival. Transforming the normal cellular metabolism into a tumor- or cell-specific metabolism can be achieved by altering nutrients uptake, allocating nutrients to more biomass-generating pathways and by excreting waste products. In addition to the reprogramming of cancer cell metabolism, genetic mutations affecting metabolism are also capable of supporting tumorigenesis. Modifications of enzymatic activity by gain or loss of function, as well as through neomorphic activity are modulating the steady-state level of metabolites, which can influence different metabolic and cellular aspects.

Metabolic reactions are tightly regulated and an increase in flux along one metabolic route might modulate the flux along other metabolic pathways. This is seen in cancer, where redirecting the flux of metabolic substrates from energy production to synthesis of macromolecules is used to stimulate tumorigenesis. One interesting example is the activity of the pyruvate kinase (PK) enzyme. PK catalyzes the final step of glycolysis by transferring a

phosphate group from phosphoenolpyruvate (PEP) to adenosine diphosphate (ADP), producing pyruvate and ATP. Most tissues express two of the four isoforms of PK, PKM1 and PKM2. However, PKM2 is predominant in most cancer types where its activity is controlled by allosteric modulators. PKM2 is thought to be selected in cancer because its inhibition promotes the accumulation of upstream glycolytic intermediates such as G6P, which can be re-directed into the PPP. To this day, it is however not fully proven that redirection of glycolytic metabolites to other pathways originates primarily from a reduced PKM2 enzymatic activity.

In particular types of cancer, loss of enzymatic activity or neomorphic enzymatic activity result in an accumulation of metabolites which are capable of competing with other metabolites and affect specific enzyme activity. A well-known case is the stabilization of HIF by an increased level of succinate, fumarate or even D-2-hydroxyglutarate (D-2HG). In subtypes of gliomas and in acute myeloid leukaemia, D-2HG is produced by the mutated IDH1 and IDH2, which normally catalyze the conversion of isocitrate into α-KG and CO_2[45]. Succinate and fumarate can accumulate in the cell due to a loss of function of succinate dehydrogenase (SDH) and fumarate hydratase (FH). Like 2-HG, succinate and fumarate are structurally similar to α-KG and can therefore compete with it, in particular for the α-KG-dependent dioxygenase PHD[46,47]. As already discussed, under normoxic conditions the hydroxylation of HIF-α subunit is catalyzed by PHD and driven by O_2 and α-KG, and marks HIF-α to be recognized by pVHL and degraded in the proteasome. Increased levels of α-KG analogs 2-HG, succinate and/or fumarate contribute to the competitive inhibition of PHD, leading to the stabilization of HIF-α under normoxic conditions and the development of HIF-driven tumorigenesis.

4 Molecular imaging

"Indeed we often mark our progress in science by improvement in imaging" *Martin Chalfie, winner of a Nobel prize together with Osamu Shimomura and Roger Y. Tsien for the discovery and development of the green fluorescent protein GFP.*

The latest progresses in molecular diagnostic and therapy development has been brought by the use of molecular imaging to question molecular and cellular processes in diseases and physiology. The ability to visualize non-invasively the distribution of endogenous or exogenous molecules has emerged as a powerful tool to evaluate biological systems. Among the great variety of imaging techniques, the most commonly used in pre-clinical and clinical studies are radiotracer imaging/nuclear medicine (PET), magnetic resonance imaging (MRI) and spectroscopy (MRS), optical imaging and ultrasound (US). Molecular imaging represents an interesting tool to address all aspects of various physiological disorders, from the detection of a disease, diagnosis and staging, up to the personalized treatment, treatment monitoring and follow-up.

In oncology, molecular imaging is used to describe and measure important biomolecules and molecular events crucial to tumorigenesis by investigating the presence of abnormal molecules together with their aberrant interactions within a tissue. In the clinics, the most widely used imaging modalities in oncology at the moment are Computed Tomography (CT), Positron Emission Tomography (PET)/CT and MRI, whereas in preclinical research fluorescence and bioluminescence imaging is extensively used. PET/CT is a very versatile technology due to the range of molecular probes, which have been developed for this technique. However, most of them are still at the stage of clinical evaluation and only ^{18}F-fluorodeoxyglucose (^{18}F-FDG) is routinely used in the clinics. MRI on the other hand provides better spatial and temporal resolution than PET and a wider scope of application than CT, and is used in the clinics to obtain functional (blood flow, vascular permeability, cell infiltration) and metabolic information. The use of target specific therapies requires molecular diagnostic, demonstrating that the target is actually present under pathological conditions. Hence, the development of a therapeutic drug will require the parallel development of a companion

diagnostic drug, a concept termed theranostics. Today theranostic approaches generally consist in *in vitro* testing of tissue specimen followed by specific therapy provided that the target is expressed. This approach is currently used in breast cancer, where biopsy specimen of tissues are tested for their growth factor receptors status including HER-2 mutations; only if HER-2 overexpression is confirmed treatment with trastuzumab, an anti-HER2 drug, will be initiated. Yet, collecting tissue biopsies is prone to artifacts given the heterogeneity of the typical tumors. Molecular imaging approaches that allow sampling the whole 3D volume of the tumor might constitute an attractive alternative. In addition, this would avoid the invasive procedure of tissue sampling.

4.1 Fluorescence imaging

4.1.1 Basics

From the use of microscopy with tissue sections for diagnosis, to macroscopic imaging in pre-clinical research and clinical application, optical imaging is the most varied tool among the molecular imaging technologies mentioned in the previous section. It offers a variety of contrast methods based on the physical properties of light and the wide range of light-tissue interactions allow for the detection of processes occurring at the molecular level. In the last decade, fluorescence microscopy and imaging has emerged as an extremely powerful technique to investigate gene and protein expression, protein-protein interaction and many more cellular episodes based on the use of more and more versatile fluorescent proteins, dyes and probes.

Fluorescence is a type of luminescence arising when a substance or fluorophore absorbs a photon and spontaneously re-emits light. This phenomenon is caused by transferring the fluorescent molecule to an excited electronic state due to the absorbed photon energy, and the rapid return to the electronic ground state through the emission of a photon at a longer wavelength, and therefore lower energy, than the absorbed light, a paradox called the Stoke shift. In fluorescent experiments, a photon travels through biological tissues and excites a fluorophore, which in turn emits a fluorescent light traveling back to be detected at the surface of the sample or the animal. However, the path of the absorbed and emitted photon is not a straight line from the light source to the target and back. The tissue absorption and scattering properties as well as its refractive index make the photon path highly scattered,

such that it appears as a diffusive wave. In living tissue, the main absorbers are water, lipids, oxy- and deoxyhemoglobin. In order to gain maximum signal intensity and therefore information from the emitted light it is primordial to ensure a minimal absorption of the excitation photons by the sample. Consequently the optimal excitation wavelength, referred to as the "optical window", lies in the near-infrared (NIR) spectral range between 650 and 900nm (Fig 5), where absorption coefficient of the main absorbers are at their lowest value.

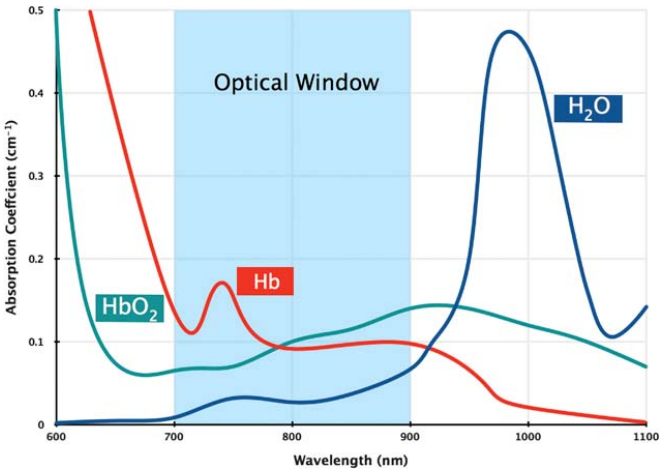

Figure 5 *The optical window is defined as the range of wavelengths between 650nm and 950nm at which light absorption coefficients of water, melanin, fat, oxy- and deoxyhemoglobin are at their lowest. Imaging within those wavelengths permits a better penetration of light in the tissue and is adequate for small animal whole-body imaging. Picture adapted from Phan et al. (2010)*[48].

Advantages of fluorescence over bioluminescence, a type of luminescence in which light energy is released after the chemical oxidation of a substrate (e.g. luciferin) by the enzymes called luciferases, are numerous. Fluorescence is more flexible than bioluminescence as it offers a wider range of probes, and specifically near-infrared fluorophores allowing for the excitation of deep tissue. It can be multiplexed via the use of targeting agents labeled with distinct fluorophores to disentangle complex biological properties. Compared to CT, MRI and PET it is a relatively inexpensive technology and provides a higher throughput for animal imaging. The spatial scale covered by fluorescence technology is rather extended; it can be

used either for *in vivo* imaging with spatial resolution of the order of 1mm or *ex vivo* examination of biopsies at microscopic resolution.

4.1.2 Planar fluorescence imaging

In planar imaging, a fluorescent imaging method frequently used to reach deeper tissues, the sample is illuminated with an expanded light beam and the emitted light collected at the same side of the tissue (Fig 6A). If the wavelength of the excited light is appropriate, it can excite not only fluorophores at the surface but also a few millimeter underneath. Using an adequate filter, the emitted light is directed onto a sensitive charge-coupled device (CCD) camera for quantification. The instrumental setup for planar imaging is simple. Throughput can be enhanced by imaging multiple mice simultaneously as the field-of-view can be made rather large. On the other hand, there are significant disadvantages to this technique. Planar imaging is incapable of resolving depth and does not take into account the nonlinear dependencies of the detected signal on light propagation and on the optical properties of the surrounding tissue. In addition, planar fluorescence faces a problem not encountered in bioluminescence: autofluorescence. Generally speaking, fluorescence produces a higher number of photons than bioluminescence, but the presence of autofluorescence impedes the signal-to-background ratio (SBR). In small animal imaging experiment, sources of autofluorescence originate from components of the skin like collagen, and from food, mainly from the products of chlorophyll breakdown. A solution to increase SBR, i.e. to improve the distinction between imaging probe specific fluorescence and autofluorescence, is to disentangle the two signals by multispectral imaging. Based on the use of Liquid Crystals Tunable filters, complete images can be acquired at each wavelength in the wavelength band defined by the filters. Subsequently the stack of images obtained is used to discriminate different fluorescent signals, which may overlap spatially and spectrally.

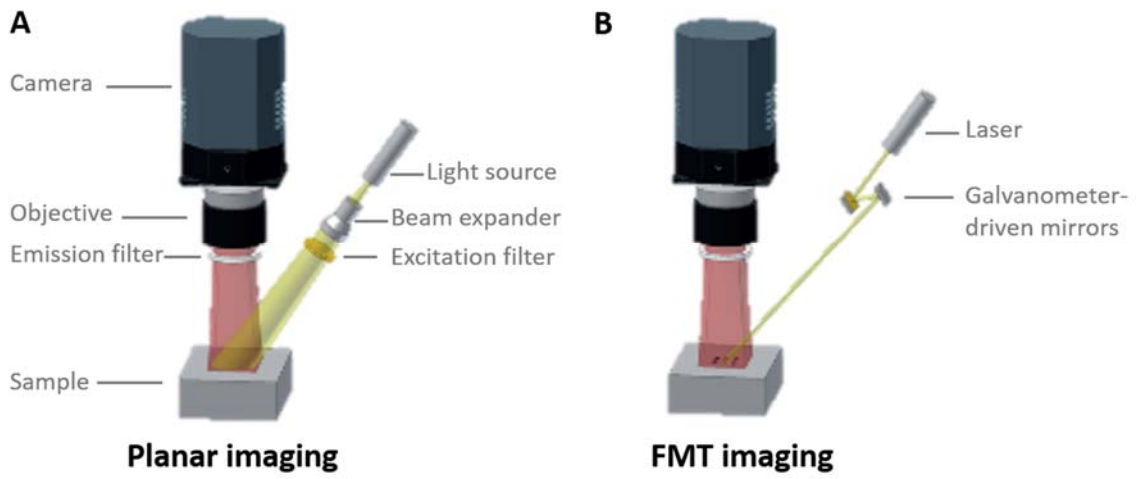

Figure 6 *Planar and Fluorescent Tomography imaging systems.* ***A*** *In planar imaging, a beam of light passes through a filter which selects the excitation wavelength corresponding to the fluorophore used in the experiment. The wide field excitation light is shone on the sample and the fluorescent emission wavelength corresponding to the emission spectra of the fluorophore is selected by an emission filter prior to being detected by a CCD camera. Due to the lack of depth information, planar imaging is a rather qualitative imaging technique.* ***B*** *In fluorescence molecular tomography (FMT), the sample is imaged with a laser of appropriate wavelength on an array of points or sources, and for each sources the emitted light distribution on the sample is collected. Based on all the sources emission information, a 3D reconstruction of the fluorophore localization within the sample can be achieved and used for quantitative analysis. Picture adapted from Stuker et al. (2011)*[49].

4.1.3 Fluorescent Molecular Tomography (FMT)

A recent development in the field of fluorescence imaging is the use of optical tomography to reconstruct three-dimensionally the distribution of fluorescent dye within a whole-animal and tissues. In a similar way than CT, a fluorescence tomographic image is reconstructed based on the projection of light at different location on the sample and the collection of the corresponding light emitted at the tissue boundary (Fig 6B). However, the excitation light, in the visible range and even in the NIR range, is highly scattered by the tissues and a mathematical model describing the propagation of photons within scattering materials is required. The main advantage of using physical models to represent photon propagation is that the reconstructed image not only provides a 3D distribution of the signal in structures as deep as a few millimeters below the surface, but also offers quantification of the fluorescent signal[50]. Fluorescent Molecular Tomography (FMT) has evolved from diffuse optical tomography (DOT) and provides advantages over planar imaging regarding reflectance and transillumination. Additionally, FMT constitutes a reliable modality for quantification of the fluorescent reporters used *in vivo*. However, this last part is highly criticized. Concerns have

raised based on the fact that the recorded fluorescent signal at the surface of the tissue results from the combined effect of the fluorochrome distribution, tissue scattering and absorbing properties, as well as tissue heterogeneity. A fluorescent probe targeting a highly vascularized tumor may produce misleading results due the absorbing properties of the blood found in the surrounding of the probe. Combining FMT with other imaging modalities such as CT or MRI appears to be a very interesting strategy to complement FMT and overcome certain drawbacks of the method. The co-registration of a fluorescent tomogram with anatomical images obtained with CT or MRI provides useful information as to where the source of contrast is localized within the animal, but more importantly, anatomical scans yield prior knowledge useful for the more accurate reconstruction of the fluorescent tomogram.

4.1.4 Multispectral Optoacoustic Tomography (MSOT)

As described earlier, two- and three-dimensional fluorescent imaging represent an attractive modality as it is versatile, easy to implement and cheap. However, the low tissue penetration by the photons and the loss of signal by absorption and scattering limit the use of this technology and confine it to remain semi-quantitative and suitable only for detection of probes very close to the surface of the skin. Recently, Multispectral Optoacoustic Tomography (MSOT) has emerged as a new promising non-invasive technology able to provide better spatial resolution and deeper penetration of tissues. A pulsed-NIR light illuminates the sample and triggers the thermoelastic expansion of the molecules absorbing the incident photons. In response to this fast absorption, acoustic waves are produced via the photoacoustic effect and propagate to reach ultrasonic transducers on the surface. To generate an image, models of photon and acoustic wave propagation are used in combination with an inverse model. The excitation of the sample with light of different wavelength provides contrast based on the absorption properties of the different tissues and molecules within the sample. Intrinsic chromophores such as melanin, oxy- and deoxyhaemoglobin represent the main source of optical absorption in the body. It has been shown that MSOT is capable of resolving anatomical structures as deep as 4.7mm below the skin and with a spatial resolution of 60µm[51]. MSOT technology is still an infant field of optical imaging but it holds great potential of development in pre-clinical research but also in clinical settings. Lately, MSOT was used clinically to reconstruct skin tumor geometry and guide the surgical excision of the mass[52].

4.2 MRI

4.2.1 Basics

In the previous section, we looked at different techniques of fluorescence imaging and optical imaging technology based on the interaction of a sample with electromagnetic waves located around the visible light window. On the same electromagnetic spectrum, we find another window, which can be used to look through our body: the radio-frequency window. Magnetic resonance imaging (MRI) makes use of the interaction between those low energy waves together with the magnetic nuclei of a sample and allow us to obtain macroscopic pictures of the soft tissues in a human body. MRI proves to be a very versatile technology used in pre-clinical research, but more importantly in clinics in fields such as neuroimaging, cardiovascular imaging, and oncology.

MRI is based on principles of Nuclear Magnetic Resonance (NMR). When a nucleus carries an odd number of protons and/or neutrons, it displays an intrinsic magnetic moment and a nuclear angular momentum. As a result of the non-zero nuclear spin, an associated magnetic dipole is created. When placed in an external static magnetic field B_0, the nucleus will tend to align its nuclear magnetic moment with the direction of the magnetic field, leading to a change in energy state and to the precession of the nuclear magnetic moment about the axis of the external magnetic field. Based on the quantum mechanics description of this phenomenon, only discrete values of energy state and angular momentum are allowed. A proton with spin I=1/2 for example possesses two energy eigenstates, with the nuclear magnet pointing either parallel or antiparallel to the static magnetic field. The energy difference between the two states is directly proportional to the magnitude of the magnetic field B_0, therefore the energy needed to induce a transition between the two states is

$$E = h \cdot \gamma \cdot B_0$$

where h is the Planck's constant ($h = 6.626 \cdot 10^{-34}\ J \cdot s$) and ɣ the gyromagnetic ratio of the particle which is a characteristic of the particle studied (for hydrogen ɣ = 42.58MHz/T).

A tissue placed in a magnetic field B_0 will see an excess of spins pointing along the field as compared to the spins pointing in the opposite direction, generating a macroscopic net magnetization vector M_0 pointing along the magnetic field B_0. When the net magnetization is brought away from its equilibrium orientation by exposing it to a radio frequency wave, it

produces a torque inducing the orientation of the magnetization M_0 to change in time and to precess around the static magnetic field. The magnetization has now both a transverse magnetization component M_{xy} and a longitudinal component M_z. The frequency at which the magnetization vector rotated about the z-axis is called the Larmor frequency and depends on both the strength of the external field B_0 and on the gyromagnetic ratio ɣ.

$$\omega_0 = \gamma \cdot B_0$$

If the sample is placed next to a coil, a voltage will be induced by the time-dependent transverse magnetization. After some time, the magnetization vector will return to its initial equilibrium state M_0 along the axis of the magnetic field. To describe this phenomenon, two relaxation constants are employed. The relaxation of the longitudinal component of the magnetization vector is described by T_1 and the relaxation of the transverse component by T_2. More precisely, T_1 describes the return of the system to equilibrium by exchange of energy with the environment, an event called spin-lattice relaxation, whereas T_2 describes the spin-spin interactions, or the time needed by the in-phase spins to influence each other and to dephase with respect to one another.

$$M_Z = M_0 \cdot \left(1 - e^{-t/T_1}\right)$$

$$M_{XY} = M_{XY_0} \cdot e^{-t/T_2}$$

Tissue relaxation rates depends on the protons interaction with their neighbors and on the consistency of the sample. Therefore, by selecting a specific MR sequence and parameters one can measure preferentially one or the other constant and control the contrast of the resulting image.

In a simple NMR experiment, a short radio-frequency (RF) pulse is applied to the system at the resonant frequency, inducing the rotation of the net magnetization vector away from the z-axis. The subsequent rotation of the perturbed magnetization vector generates an oscillating signal picked-up by the receiver coil and which decreases with time. This signal is referred to as the free induction decay (FID). The FID is detected in the time domain but its Fourier Transform provide spectral information, i.e. the amplitude of the observed signal as a function of frequency (Fig 7).

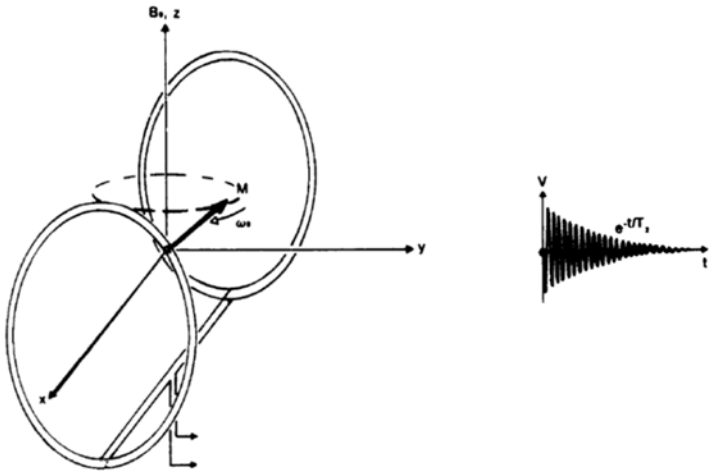

Figure 7 *The net magnetization vector M_0 is flipped towards the XY plane by a radio frequency at the resonance frequency and start precessing about the z-axis at the Larmor frequency. The precession of the magnetization vector creates a small voltage that can be picked up by coils placed close to the sample. After termination of the radio frequency pulse, the magnetization vector starts coming back to equilibrium, which leads to an oscillating voltage whose amplitude decreases exponentially: this phenomenn is termed free induction decay (FID). Picture adapted from Fullerton et al. (1982)*[53]

In order to produce an image of the sample, the location of each NMR signal needs to be spatially encoded. This can be achieved by applying additional magnetic field gradients along the x- and y-axis, which makes the Larmor frequency of each resonant nucleus depends on its position within the sample. By varying the orientation of the magnetic field gradients in a sufficient number of projections, the three-dimensional distribution of the spins can be determined and used to create an image. An MRI sequence is conducted in the Fourier space. However, the data are collected in the time domain. For each position, the transverse magnetization evolves as a function of t_1 and t_2, which are dependent on the magnetic field gradients G_1 and G_2, which span the image plane. For each excitation, t_1 is being incremented and the signal is detected in the t_2 domain (frequency domain) as the evolution of the signal in the t_1-domain (phase domain) modulates the signal phase at t_2=0. To obtain the image in the frequency domain, a two-dimensional Fourier transform is applied to the data collected in the time-domain.

An elegant way to rationalize MRI is a concept called the k-space. The k-space is basically the two- or three-dimensional Fourier transform of the measured image. In one dimension, an object can be represented in image space by its proton density in that dimension. After turning

on the frequency-encoding gradient, the individual Larmor frequencies of the spins become proportional to their location, and the signal collected by the receiver is the sum of all the Larmor frequencies weighted by the proton density. The signal received can be seen as the Fourier Transform of the proton density of the image. It is then no longer described as a signal time course but rather as a function of the coordinate k_{read}. Based on this definition, we can then add a coordinate for the phase-encoding. Therefore, each point in the k space corresponds to a specific spatial oscillation in the image space with a weight given by the k intensity at that particular point in the k space. The reconstruction of an image is achieved by taking the two- or three-dimensional Fourier transform of the k space and adding the resulting oscillation images together.

4.2.2 Dynamic Nuclear Polarization (DNP)

As explained in the previous section, an MR signal is based on the density of water molecules in the tissues and the ability to detect them during NMR experiments. Metabolites other than water, however, are found in a much lower concentration in the body and are much less sensitive to NMR detection. Therefore, it is not feasible to detect them with the clinical settings used currently except when using a low spatial and temporal resolution. Proton spectroscopy provides information about the steady-state concentration of some metabolites within the tissue but does not reveal anything regarding metabolic flux. Also, the method suffers from low specificity due to the small spectral range associated with ^{1}H-MRS, leading to strongly overlapping signals. The specificity towards those molecules can be enhanced by introducing ^{13}C-labeled metabolites in the system. Incorporation of the label into metabolites linked to the labeled substrate can be monitored yielding information on metabolic pathways and fluxes. Yet, the method suffers from low sensitivity, which is not adequate for generating images reflecting metabolic fluxes. The solution to this problem was provided by introducing so-called hyperpolarization techniques, including Dynamic Nuclear Polarization (DNP)[54,55].

At the beginning of a DNP experiment, a solution containing the sample to be polarized, a stable radical and a solvent are mixed and placed in a high magnetic field (3T), where they are rapidly frozen to a very low temperature (~1K). The high magnetic field and low temperature are required to achieve a quasi full polarization of the unpaired electrons of the stable free radical. Polarization of the protons cannot be achieved as successfully as their magnetic

moment is much smaller than that of the electrons. However, the energy of the electron spin polarization can be transferred to the protons through a microwave irradiation applied at the resonance frequency of the electron spins. To use the hyperpolarized sample in a biological experiment, it should be available in soluble form at body temperature. This is achieved by flushing the sample out of the polarizer using a high temperature pressurized buffer. Through polarization, the sensitivity of a ^{13}C compound can be enhanced up to 10^4 folds, making it now possible to detect them in an NMR experiment with high temporal and decent spatial resolution[56]. This new and very promising technology however contains disadvantages. First, the chosen compound to be ^{13}C-labeled must hold the ability to be soluble at high concentration during the dissolution step. In addition to that, the compound must convey a polarization lifetime long enough to dissolve, inject and study metabolic pathway. This is typically achieved by labeling quaternary carbon atoms, as the absence of directly bound ^{1}H nuclei significantly enhances the lifetime of the polarized state.

So far, ^{13}C-pyruvate is the most widely used substrate in DNP experiments, but polarization of fumarate[57], glucose and ascorbate have also be achieved. In oncology, pre-clinical results obtained with ^{13}C-pyruvate appear to be very promising for clinical application. For example, the assessment of the early response to treatment was investigated in mice bearing lymphoma and injected with hyperpolarized ^{13}C-pyruvate. It was found that decreased pyruvate to lactate conversion corresponded well with cellular death[58]. In clinical settings, such results would be an invaluable asset to evaluate the patient response to treatment and switch treatment early enough in case of absence of effects. Additionally, another study presented to potential of ^{13}C-pyruvate to identify and grade prostate cancer in a model of mouse prostate cancer[59] based on the production of lactate. These results have been transferred to humans and the first clinical trial also demonstrated an elevated concentration of lactate in a region where a biopsy had revealed prostate cancer[60].

5 Aims of the PhD project

As explained in the section 3.5 of this chapter, it has been shown that particular tumor types exhibited mutations on specific metabolic enzymes, which perturbed drastically the level of some metabolites intervening in the degradation process of HIF, leading to a pseudo-hypoxia stabilization and activation of HIF. Therefore, it was asked whether tumors with a distinct cancer-driving mutation would also be associated with a specific metabolic fingerprint influencing in some ways the activity of HIF. Particularly we chose to investigate this hypothesis in two models of human colon carcinoma possessing an activating mutation in the MAPK pathway. To address this question, two different tools were developed and applied to the study of both aspects longitudinally and non-invasively *in vivo*: A fluorescent HIF activity reporter assay and a metabolic assay for the probing of pyruvate metabolism.

Development of a fluorescent reporter gene for the transcriptional activity of the Hypoxia Inducible Factor (HIF) In a previous study in our group by Lehmann et al.[61], the efficiency of a bioluminescent reporter gene for HIF activity was reported in murine colon carcinoma. To study the activity of HIF in DLD-1 and RKO cells we chose the fluorescent version of the above-mentioned plasmid. Unfortunately, this plasmid failed to be transfected efficiently in our human cell lines. Therefore, a new strategy was implemented with the use of a lentiviral vector to insert an infrared fluorescent protein sequence under the control of two hypoxia-responsive elements in the different cell lines under study.

Study of the activity of HIF in the context of a cancer-driving mutation The transduced DLD-1 and RKO cell lines were investigated *in vitro* and *in vivo* for the HIF signaling activity. The DLD-1 set of cells was used to understand the effect of an activating mutation on KRAS, whereas the RKO set of cells was dedicated to understanding the effect of a BRAF cancer-driving mutation. *In vivo* tumor cells were inoculated to nude mice and imaged longitudinally for the detection of iRFP in both mutated and non-mutated tumors. Results were confirmed *ex vivo* with histological sections.

Application of Dynamic Nuclear Polarization (DNP) for the magnetic resonance spectroscopic detection of ^{13}C-labeled pyruvate metabolism A new spectroscopic technique termed Dynamic Nuclear Polarization (DNP) has been established to increase magnetic resonance sensitivity towards ^{13}C-labeled compound. Applying this to [1-^{13}C]-pyruvate, we

aimed to follow the pyruvate metabolism *in vivo* in tumors exhibiting a cancer-driving mutation and compare it to metabolism in non-mutated cells.

6 References

1. Schwarz, G. Über Desensibiliserung gegen Röntgen- und Radiumstrahlen. *Münchener Medizinische Wochenschrift* **24,** (1909).

2. Müller, C. Eine neue Behandlungsmethode bösartiger Geschwülste. *Münchener Medizinische Wochenschrift* **28,** (1910).

3. Thomlinson, R. H. & Gray, L. H. The histological structure of some human lung cancers and the possible implications for radiotherapy. *Br. J. Cancer* **9,** 539–49 (1955).

4. Bos, R. *et al.* Levels of hypoxia-inducible factor-1a independently predict prognosis in patients with lymph node negative breast carcinoma. *Cancer* **97,** 1573–1581 (2003).

5. Bertout, J. A., Patel, S. A. & Simon, M. C. The impact of O2 availability on human cancer. *Nat. Rev. Cancer* **8,** 967–975 (2008).

6. Wenger, R. H. Cellular adaptation to hypoxia: O2-sensing protein hydroxylases, hypoxia-inducible transcription factors, and O2-regulated gene expression. *FASEB J.* **16,** 1151–62 (2002).

7. Walsh, J. C. *et al.* The clinical importance of assessing tumor hypoxia: relationship of tumor hypoxia to prognosis and therapeutic opportunities. *Antioxid. Redox Signal.* **21,** 1516–54 (2014).

8. Semenza, G. L. & Wang, G. L. A nuclear factor induced by hypoxia via de novo protein synthesis binds to the human erythropoietin gene enhancer at a site required for transcriptional activation. *Mol. Cell. Biol.* **12,** 5447–5454 (1992).

9. Wiesener, M. S. *et al.* Widespread, hypoxia-inducible expression of HIF-2α in distinct cell populations of different organs. *FASEB J.* **17,** 271–273 (2003).

10. Jaakkola, P. *et al.* Targeting of HIF-alpha to the von Hippel-Lindau ubiquitylation complex by O2-regulated prolyl hydroxylation. *Science (80-.).* **292,** 468–472 (2001).

11. Ivan, M. *et al.* HIFa targeted for VHL-mediated destruction by proline hydroxylation: implications for O2 sensing. *Science* **292,** 464–468 (2001).

12. Myllyla, R., Majamaa, K., Giinzler, V., Hanauske-abel, H. M. & Kivirikko, K. I. Ascorbate is consumed stoichiometrically in the uncoupled reactions catalyzed by prolyl 4-

hydroxylase and lysyl hydroxylase. *J. Biol. Chem.* **259,** 5403–5405 (1984).

13. Hansen, A. E., Kristensen, A. T., Law, I., Jørgensen, J. T. & Engelholm, S. A. Hypoxia-inducible factors - regulation, role and comparative aspects in tumourigenesis. *Vet. Comp. Oncol.* **9,** 16–37 (2010).

14. Muz, B., Puente, P. de la, Azab, F. & Azab, A. K. The role of hypoxia in cancer progression, angiogenesis, metastasis, and resistance to therapy. *Hypoxia* **3,** 83–92 (2015).

15. Delin Chen, Muyang Li, Jianyuan Luo, W. G. Direct Interactions between HIF-1a and Mdm2 Modulate p53 function. *J. Biol. Chem.* **278,** 4597–4600 (2003).

16. Sowter, H. M., Ratcliffe, P. J., Watson, P., Greenberg, A. H. & Harris, A. L. HIF-1-dependent Regulation of Hypoxic Induction of the Cell Death Factors BNIP3 and NIX in Human Tumors. *Cancer Res.* **61,** 6669–6673 (2001).

17. Cairns, R. A. & Hill, R. P. Acute hypoxia enhances spontaneous lymph node metastasis in an orthotopic murine model of human cervical carcinoma. *Cancer Res.* **64,** 2054–61 (2004).

18. Yang, M.-H. *et al.* Direct regulation of TWIST by HIF-1a promotes metastasis. *Nat. Cell Biol.* **10,** 295–305 (2008).

19. Lehmann, S. *et al.* Hypoxia Induces a HIF-1-Dependent Transition from Collective-to-Amoeboid Dissemination in Epithelial Cancer Cells. *Curr. Biol.* **27,** 392–400 (2017).

20. Young, R. M. *et al.* Hypoxia-mediated Selective mRNA Translation by an Internal Ribosome Entry Site-independent Mechanism. *J. Biol. Chem.* **283,** 16309–16319 (2008).

21. Brown, J. M. SR 4233 (Tirapazamine): a new anticancer drug exploiting hypoxia in solid tumours. *Br. J. Cancer* **67,** 1163–1170 (1993).

22. Jain, A. *et al.* Response of Multiple Recurrent TaT1 Bladder Cancer to Intravesical Apaziquone (EO9): Comparative Analysis of Tumor Recurrence Rates. *Urology* **73,** 1083–1086 (2009).

23. Hicks, K. O. *et al.* Oxygen Dependence and Extravascular Transport of Hypoxia-Activated Prodrugs: Comparison of the Dinitrobenzamide Mustard PR-104A and Tirapazamine. *Int. J. Radiat. Oncol. Biol. Phys.* **69,** 560–571 (2007).

24. Greenberger, L. M. *et al.* A RNA antagonist of hypoxia-inducible factor-1a , EZN-2968, inhibits tumor cell growth. *Mol. Cancer Ther.* **7,** 3598–3608 (2008).

25. Xia, Y., Choi, H. K. & Lee, K. Recent advances in hypoxia-inducible factor (HIF)-1 inhibitors. *Eur. J. Med. Chem.* **49,** 24–40 (2012).

26. Zhang, H. *et al.* Digoxin and other cardiac glycosides inhibit HIF-1a synthesis and block tumor growth. *Proc. Natl. Acad. Sci. U. S. A.* **105,** 19579–19586 (2008).

27. Bohen, S. P. Genetic and Biochemical Analysis of p23 and Ansamycin Antibiotics in the Function of Hsp90-Dependent Signaling Proteins. *Mol. Cell. Biol.* **18,** 3330–3339 (1998).

28. Lee, K. *et al.* Acriflavine inhibits HIF-1 dimerization, tumor growth, and vascularization. *Proc. Natl. Acad. Sci. U. S. A.* **106,** 17910–5 (2009).

29. Befani, C. D. *et al.* Bortezomib represses HIF-1a protein expression and nuclear accumulation by inhibiting both PI3K/Akt/TOR and MAPK pathways in prostate cancer cells. *J. Mol. Med.* **90,** 45–54 (2012).

30. Hanahan, D. & Weinberg, R. A. Hallmarks of cancer: The Next Generation. *Cell* **144,** 646–674 (2011).

31. Ward, P. S. & Thompson, C. B. Metabolic Reprogramming: A Cancer Hallmark Even Warburg Did Not Anticipate. *Cancer Cell* **21,** 297–308 (2012).

32. Warburg, B. Y. O., Wind, F. & Negelein, E. The Metabolism of Tumors in the Body. *J. Gen. Physiol.* (1926).

33. Ju, Y. S. *et al.* Origins and functional consequences of somatic mitochondrial DNA mutations in human cancer. *Elife* **3,** 1–28 (2014).

34. Weinhouse, S. Glycolysis, Respiration, and Enzyme Alterations in Rat Liver Neoplasia. *Science (80-.).* **158,** (1967).

35. Pavlides, S. *et al.* The reverse Warburg effect: Aerobic glycolysis in cancer associated fibroblasts and the tumor stroma. *Cell Cycle* **8,** 3984–4001 (2009).

36. Lee, M. & Yoon, J.-H. Metabolic interplay between glycolysis and mitochondrial oxidation: The reverse Warburg effect and its therapeutic implication. *World J. Biol. Chem.* **6,** 148–61 (2015).

37. Nicklin, P. *et al.* Bidirectional Transport of Amino Acids Regulates mTOR and Autophagy. *Cell* **136,** 521–534 (2009).

38. Tsun, Z.-Y. & Possemato, R. Amino acid management in cancer. *Semin. Cell Dev. Biol.* **43,** 22–32 (2015).

39. Tedeschi, P. M. *et al.* Contribution of serine, folate and glycine metabolism to the ATP, NADPH and purine requirements of cancer cells. *Cell Death Dis.* **4,** (2013).

40. Weinberg, F. *et al.* Mitochondrial metabolism and ROS generation are essential for Kras-mediated tumorigenicity. *Proc. Natl. Acad. Sci. U. S. A.* **107,** 8788–93 (2010).

41. Osthus, R. C. *et al.* Deregulation of glucose transporter 1 and glycolytic gene expression by c-Myc. *J. Biol. Chem.* **275,** 21797–21800 (2000).

42. Gao, P. *et al.* c-Myc suppression of miR-23a/b enhances mitochondrial glutaminase expression and glutamine metabolism. *Nature* **458,** 762–765 (2009).

43. DeBerardinis, R. J., Lum, J. J. & Thompson, C. B. Phosphatidylinositol 3-Kinase-dependent Modulation of Carnitine Palmitoyltransferase 1A Expression Regulates Lipid Metabolism during Hematopoietic Cell Growth. *J. Biol. Chem.* **281,** 37372–37380 (2006).

44. Papandreou, I., Cairns, R. A., Fontana, L., Lim, A. L. & Denko, N. C. HIF-1 mediates adaptation to hypoxia by actively downregulating mitochondrial oxygen consumption. *Cell Metab.* **3,** 187–197 (2006).

45. Clark, O., Yen, K. & Mellinghoff, I. K. Molecular Pathways: Isocitrate Dehydrogenase Mutations in Cancer. *Clin. Cancer Res.* **22,** 1837–1842 (2016).

46. Isaacs, J. S. *et al.* HIF overexpression correlates with biallelic loss of fumarate hydratase in renal cancer: Novel role of fumarate in regulation of HIF stability. *Cancer Cell* **8,** 143–153 (2005).

47. Gimenez-Roqueplo, A. P. *et al.* The R22X mutation of the SDHD gene in Hereditary Paraganglioma Abolishes the Enzymatic Activity of Complex II in the Mitochondrial Respiratory Chain and Activates the Hypoxia Pathway. *Am. J. Hum. Genet.* **69,** 1186–97 (2001).

48. Phan, T. G. & Bullen, A. Practical intravital two-photon microscopy for immunological research: faster, brighter, deeper. *Immunol. Cell Biol.* **88,** 438–444 (2010).

49. Stuker, F., Ripoll, J. & Rudin, M. Fluorescence Molecular Tomography: Principles and Potential for Pharmaceutical Research. *Pharmaceutics* **3,** 229–274 (2011).

50. Ntziachristos, V. Fluorescence Molecular Imaging. *Annu. Rev. Biomed. Eng.* **8,** 1–33 (2006).

51. Ford, S. J. *et al.* Structural and Functional Analysis of Intact Hair Follicles and Pilosebaceous Units by Volumetric Multispectral Optoacoustic Tomography. *J. Invest. Dermatol.* **136,** 753–761 (2016).

52. Chuah, S. Y. *et al.* Structural and functional 3D mapping of skin tumours with non-invasive multispectral optoacoustic tomography. *Ski. Res. Technol.* **0,** 1–6 (2016).

53. Fullerton, G. Basic concepts for nuclear magnetic resonance imaging. *Magn. Reson. Imaging* **I,** 39–53 (1982).

54. Abragam, A. & Goldman, M. Principles of dynamic nuclear polarisation. *Rep. Prog. Phys.* **41,** (1978).

55. Goldman, M. Spin Temperature and Nuclear Magnetic Resonance in Solids. *Oxford Univ. Press* (1970).

56. Ardenkjaer-Larsen, J. H. *et al.* Increase in signal-to-noise ratio of > 10,000 times in liquid-state NMR. *Proc. Natl. Acad. Sci. U. S. A.* **100,** 10158–63 (2003).

57. Clatworthy, M. R. *et al.* Magnetic resonance imaging with hyperpolarized [1,4-(13)C2]fumarate allows detection of early renal acute tubular necrosis. *Proc. Natl. Acad. Sci.* **109,** 13374–13379 (2012).

58. Day, S. E. *et al.* Detecting tumor response to treatment using hyperpolarized 13C magnetic resonance imaging and spectroscopy. *Nat. Med.* **13,** 1382–1387 (2007).

59. Albers, M. J. *et al.* Hyperpolarized 13C Lactate, Pyruvate, and Alanine: Noninvasive Biomarkers for Prostate Cancer Detection and Grading. *Cancer Res.* **68,** 8607–8615 (2008).

60. Nelson, S. J. *et al.* Metabolic Imaging of Patients with Prostate Cancer Using

Hyperpolarized [1-13C]Pyruvate. *Sci. Transl. Med.* **5,** (2013).

61. Lehmann, S. *et al.* Longitudinal and multimodal in vivo imaging of tumor hypoxia and its downstream molecular events. *PNAS* **106,** 14004–14009 (2009).

2. Development of a near-infrared reporter gene to study the transcriptional activity of HIF

1 Introduction

Hypoxia commonly arises in solid tumors as a result of a high oxygen (O_2) consumption by the proliferative cells, and of an inefficient O_2 delivery due to a poorly organized vascular structure. Tumor hypoxia and the consequent activation of HIF signaling participate in promoting cell survival, proliferation, and more importantly, invasion and metastasis formation. Hypoxia also negatively interferes with the outcome of radio- and chemotherapeutic treatments. Understanding the extent of tumor hypoxia by measuring the levels of O_2 or HIF expression is critical for optimizing treatment strategies in cancer patients, e.g. finding the adequate temporal window for maximizing the outcome of radiation therapy. The most direct way to measure oxygen concentration within a tumor is by inserting a polarographic needle electrode inside the tumor at different locations in order to obtain the oxygen partial pressure of the tissue[1]. Although this technique has provided significant results in various types of cancer[2], there are major drawbacks for routine use with patients or in pre-clinical research. It is invasive and cannot access all tumors, it cannot distinguish between tumor hypoxia and necrosis and lacks spatial resolution. To overcome those issues, numerous non-invasive solutions to homogeneously image tumor hypoxia, HIF expression and its localization have been designed. In PET imaging, ^{18}F-fluoromisonidazole (FMISO) has been developed as probe to capture hypoxic regions in both preclinical and clinical studies[3].

Nitroimidazole-based compounds are reduced by nitroreductases, a process that is reversible in the presence of oxygen. In hypoxic cell, reduced nitroimidazole groups are additionally reduced to reactive amino (NH_{2-}) groups, which bind to adjacent macromolecules, trapping the tracer within the cell. This imaging tool proved to be efficient in detecting hypoxic tumors, however it does not reflect all possible ranges of hypoxia as it becomes active only in severely hypoxic cells. In addition, information about the expression and activity of HIF cannot be inferred as HIF can be enhanced by pathways other than hypoxia. Recently, a novel PET imaging probe was developed to indirectly image HIF activity. Three ^{68}Ga-labeled sulfonamide derivatives were synthesized to target CA9, an enzyme expressed under the control of HIF. Pre-clinical results demonstrated a good binding affinity and selectivity towards CA9-expressing tumor cells, making those imaging agents eligible for further clinical development[4]. Limitations of PET are the short half-life of radioisotopes, which may not be compatible with the biological processes to study and which requires the proximity of a radiochemistry laboratory and a cyclotron, as well as intrinsic radiation exposure that precludes longitudinal studies. Therefore, imaging modalities using stable reporter molecules constitute attractive alternatives to PET. Optical imaging using fluorescent probes falls in this category. Exploiting the wavelength range suited for *in vivo* optical imaging, the simultaneous detection of multiple imaging agents with different excitation/emission characteristics becomes feasible. Imaging hypoxia and HIF expression can be tackled via two routes: by injecting an exogenous specific fluorescent probe, or by using fluorescent reporter genes. Exogenous imaging agents are very attractive as they offer the possibility to be translated into the clinics. Their *in vivo* behavior depends on their pharmacokinetics properties and reaching a good contrast between specific and non-specific signals is frequently difficult. In particular, it is difficult to target intracellular molecules such as HIF due to limited cell penetration. Several fluorescent probes have been designed for imaging HIF activity by targeting downstream gene products of HIF, such as CA9 for example, however the study of HIF activity has rather been extensively focusing on the use of fluorescent reporter genes. Reporter genes represent an invaluable tool to study gene expression irrespective of the subcellular location of the gene product. In that context, Danhier et al. [5] devised a dual reporter gene based on the expression of EGFP and of a luciferase gene fused with an oxygen-dependent degradation (ODD) domain. Both genes were placed under the control of five hypoxia responsive elements (HRE), and provided information about the evolution of HIF activity and hypoxia thanks to the short-lived oxygen-dependent

bioluminescence and the long-lived EGFP fluorescence. This elegant new reporter possesses however one drawback: the choice of the reporter protein. Luciferase necessitates the substrate D-luciferin in order to produce luminescence, hence the signal depends on probe delivery, which is an issue when targeting hypoxic, i.e. poorly vascularized tumor regions, leading to false readouts. Fluorescent proteins do in general not suffer from this limitation as they do not need an exogenous substrate (with the exception of some iRFPs that require biliverdin), so they typically need molecular oxygen for the formation of the chromophore structure though at low levels[6]. When using fluorescent proteins for *in vivo* applications, their spectral properties should be compatible with the spectral window (Chapter 1, Fig 5) with excitation and emission maxima in the range 600-850nm.

In this section, we describe the design and characterization of a new fluorescent reporter gene construct for studying the transcriptional activity of HIF, which is based on an infrared fluorescent protein sequence under the control of two HREs. By using an infrared fluorescent protein, we aimed at reducing signal contribution due to absorption, autofluorescence and scattering, thereby enabling superior tissue penetration. *In vitro* characterization of the reporter revealed a hypoxia-dependent induction of fluorescence, and the *in vivo* application of the reporter to various tumor models demonstrated its feasibility as a HIF activity readout. The use of this reporter can be combined with the injection of an exogenous probe, providing information on different aspects of the HIF signaling cascade, e.g. hypoxia levels and HIF transcriptional activity.

2 Material and Methods

Cells

Human DLD-1 colon adenocarcinoma and RKO colon carcinoma cells were obtained from the laboratory of Prof. Wilhelm Krek (ETH Zürich). Each cell line came as an isogenic pair. For the DLD-1 cells, one cell line contained an activating mutation on KRAS on one of its allele (DLD-1 $KRAS^{mut}$), whereas the other line had one of the KRAS allele null (DLD-1 $KRAS^{wt}$). Similarly to the DLD-1, one of the RKO cell line exhibited an activating mutation on one of the BRAF allele (RKO $BRAF^{mut}$), while its isogenic counterpart had one of the BRAF allele null (RKO $BRAF^{wt}$). Both DLD-1 cell lines were cultivated in RPMI medium supplemented with 10% Fetal Bovine Serum (FBS). The two RKO cell lines were cultivated in Dulbecco's Modified Eagle's Medium (DMEM) (all media came from Gibco, Carlsbad, USA) complemented with 10% FBS.

Lentiviral vector cloning

A new lentiviral plasmid pMuLE-H2SViRFP was created by recombining two entry vectors containing different reporter sequences into a final destination vector. The first entry vector contained a sequence consisting of an iRPF sequence under the control of two HREs and an SV40 promoter. The second plasmid was a kind gift from Prof. Ian Frew (University Medical Center Freiburg), and involved a GFP sequence under the control of a CMV promoter. The 2HRE-SV40-iRFP fragment was flanked by the recombination sites *attL1* and *attR5* and the CMV-GFP fragment by *attL5* and *attL2*.

For the recombinational cloning reaction, 10 fmoles of each entry vector were mixed with 20 fmoles of the destination vector, together with the enzyme LR Clonase II Plus (Invitrogen, Carlsbad, USA). The mix was incubated during 16 hours at 25° C to allow the two segments of interests in the entry vectors to be recombined within the destination vector in a site-specific recombination reaction (Fig 1). Following the recombination, 2µl of the mix were transformed into One Shot Mach1 T1 *E.Coli* (Invitrogen, Carlsbad, USA) and amplified for one hour at 37°C. The resulting bacterial medium was spread onto agar plates containing Ampicilin and incubated overnight at 37°C to select for the bacteria containing the destination vector. The surviving colonies were isolated and expanded by MaxiPrep (GenElute HP Maxiprep Kit, Sigma-Aldrich, St-Louis, USA).

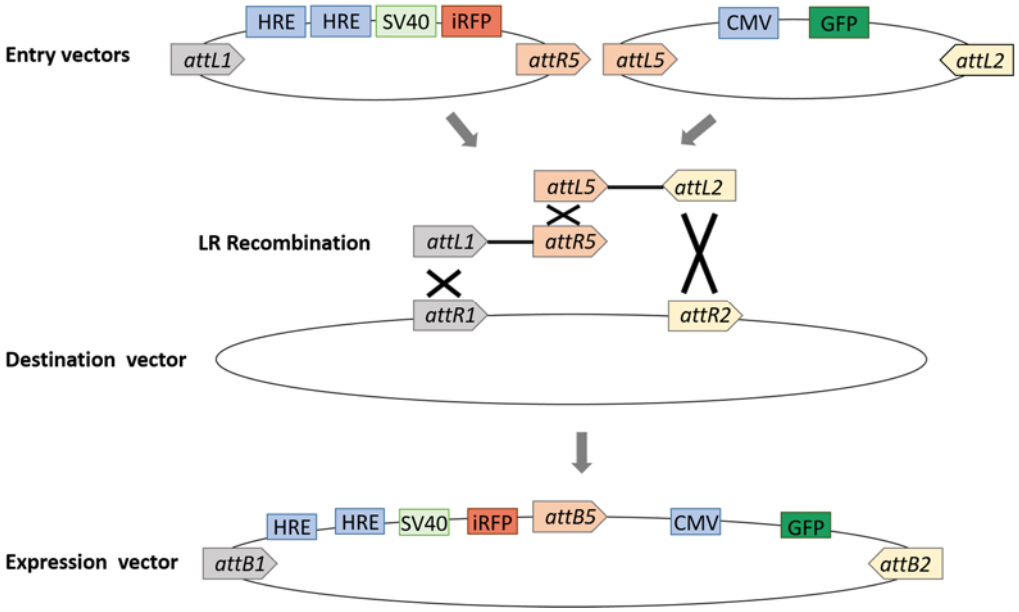

Figure 1 *Formation of a lentiviral expression vector by Multisite Recombination. The first entry vector contains an iRFP sequence under the control of two HRE sites and a SV40 promoter. This reporter gene is flanked by two recombination sites, namely attL1 and attR5. The second entry vector contains another reporter gene, GFP under the control of a CMV promoter, flanked by the recombination sites attL5 and attL2. Both entry vectors are recombined into a destination vector by site-specific recombination of the entry vectors and destination vector at their recombination sites in a reaction driven by the LR Clonase II. The final expression vector contains both reporter genes localized in sequential fashion between the recombination sites attB1, attB5 and attB2. Adapted from Petersen et al.*[7]

Viral particles preparation, cell transduction and clone selection

The viral particles used to transduce the DLD-1 and RKO cells were produced by HEK cells. In this prospect, HEK cells were transfected via calcium phosphate transfection with three different viral vector plasmids: a packaging plasmid psPAX2, an envelope plasmid pMD2G (Addgene, Cambridge, USA), and the reporter gene pMuLE-H2SViRFP. One day after transfection the HEK cells, culture medium was substituted with 10ml of fresh DMEM with 10% FBS. The cells were incubated for 8 hours, after which the culture medium containing viral particles was harvested, stored at 4°C and replaced by 10ml of fresh DMEM for an overnight incubation. The next day, the second harvest was pooled with the first one and centrifuged for 5 minutes at 500g. The supernatant was finally filtered through 0.45µm filters and stored at 4°C.

Transduction of DLD-1 $KRAS^{wt}$, DLD-1 $KRAS^{mut}$, RKO $BRAF^{wt}$, RKO $BRAF^{mut}$ started when the cell cultures reached 50% confluency. The culture medium was removed and substituted with

10ml of medium harvested from the HEK cells and containing the viral particles. To facilitate the binding of viral particles to the cell, 1µg of polybrene was added to each cell culture plate. All cell lines were allowed to transduce for 48 hours at 37°C. On the second day, the cells were split and selection of the successfully transduced cells started by adding puromycin (LabForce, Muttenz, Switzerland) in the medium at a concentration of 1µg/ml.

To select single-cell clones, all four cell lines underwent a minimal cellular dilution and were cultured on 10cm Petri dish to allow single-cell colonies to grow. For each cell line, an average of 10 colonies were picked-up and cultivated in individual plates, always under puromycin selection. Induction of iRFP signal in each clone was established under pseudo-hypoxia by treating them with 1mM of the prolyl-4-hydroxylase (PHD) inhibitor dimethyloxalylglycine (DMOG, Sigma Aldrich, St Louis, USA) over 24 hours. In the control condition, cells were treated with 1mM of dimethyl sulfoxide (DMSO, Sigma Aldrich, St Louis, USA). After treatment, the clones were harvested, counted, centrifuged and cell pellets of identical cell number were imaged using a 2D Maestro 500 imaging system (Cambridge Research & Instruments Inc., Hopkinton, USA). For each single-cell colony pellet, a ratio between the average fluorescent intensity of the DMOG stimulation and control condition was calculated. Cells inducing the strongest signal in pseudo-hypoxic conditions but also a decent ratio between the DMOG and control condition were selected for each of the four cell lines. These sets of cells fulfilling the aforementioned conditions were additionally studied for their cellular aspect and growth *in vitro* and *in vivo*. Upon these tests, the best clone for each cell lines was chosen.

Xenograft tumor models

DLD-1 $KRAS^{mut}$, DLD-1 $KRAS^{wt}$ and RKO $BRAF^{wt}$, RKO $BRAF^{mut}$ containing the pMuLE-H2SViRFP reporter gene were cultivated in RPMI with 10% FBS and DMEM with 10% FBS respectively until they reached 80% confluency. The cells were trypsinized and resuspended in a solution of 50% HBSS and 50% PBS (Gibco, Carlsbad, USA) to a concentration of $2.5 \cdot 10^7$cells/ml. $2.5 \cdot 10^6$ cells in 100µl were injected subcutaneously in the right flank of female Balb/c nude mice (Janvier Labs, Le Genest-Saint-Isle, France). Upon tumor formation, tumor size was monitored every two days by caliper measurements and the tumor volume was calculated according to

the formula $V = {}^{1}/_{2} \cdot (length \cdot width^2)$. Prior to each cell injection and imaging steps, the mice were gas-anaesthetized with 2.5% isoflurane in an oxygen-air mixture as a gas carrier. All steps were in accordance with the license number 185-2013 issued by the Cantonal Veterinary Office of Zurich.

***Ex vivo* imaging**

To characterize the longitudinal activity of HIF in pseudo-hypoxic conditions within the selected clones, iRFP intensity was measured during live cell imaging experiments. Cells were plated on 18mm coverslips (30'000 cells/coverslips) and allowed to grow up to a confluence of 50-60%. Next, the cells were given 1mM of DMOG, and for the control condition 1mM of DMSO was added to the culture media. Live cell imaging was performed on individual coverslips 8, 12, 24 and 48 hours after initial DMOG treatment. The coverslips were imaged with a brightfield microscope (Leica DMI 6000B, Wetzlar, Germany) and both GFP and iRFP were detected. Each time point was imaged in triplicate (3 different coverslips), and for each coverslips, 10 different frames were acquired. The iRFP signal was computed as the Corrected Total Cell Fluorescence (Chapter 3, Material and Methods).

***In vivo* planar fluorescence reflectance imaging**

Planar fluorescence reflectance imaging was carried out using a Maestro 500 imaging system (Cambridge Research & Instruments Inc., Hopkinton, USA). Spectral unmixing was applied to enhance the signal-to-background contrast for the fluorophore iRFP. In brief, 2D emission images were recorded at 27 different wavelengths in the case of iRFP (22 in the case of GFP) spanning a data cube ('lambda cube' or 'lambda stack') defined by two spatial and one spectral coordinate (intensity I(x,y,λ)). Reference spectra (spectral library) were defined for region(s)-of-interest (ROIs) displaying high concentration of the dye(s) as well as for ROIs attributed to background fluorescence. These spectra served as base function for the spectral deconvolution according to $I(x,y) = \sum_i I_i(\lambda) \cdot c_i(x,y)$ where I_i is the molar fluorescence intensity for the molecular species i and $c_i(x,y)$ its molar concentration at the location (x,y).

3 Results

Hypoxia and pharmacological PHD inhibition lead to increased iRFP fluorescence in transfected tumor cells *in vitro*

The successful viral transduction of the four colon cancer cell lines was confirmed by observing a cellular GFP signal after adding antibiotic selection to the cells culture media. Induction of iRFP fluorescence in the different clones was confirmed using the Maestro 500 system 24 hours after administration of DMOG leading to the stabilization of HIF-1α and induction of the HIF signaling cascade (Fig 2). For each cell line, the clones expressing a strong iRFP intensity under pharmacological treatment but also a good induction factor for iRFP compared to the control situation were tested for growth *in vivo*. Upon this last test, one clone was selected for each cell line for further studies.

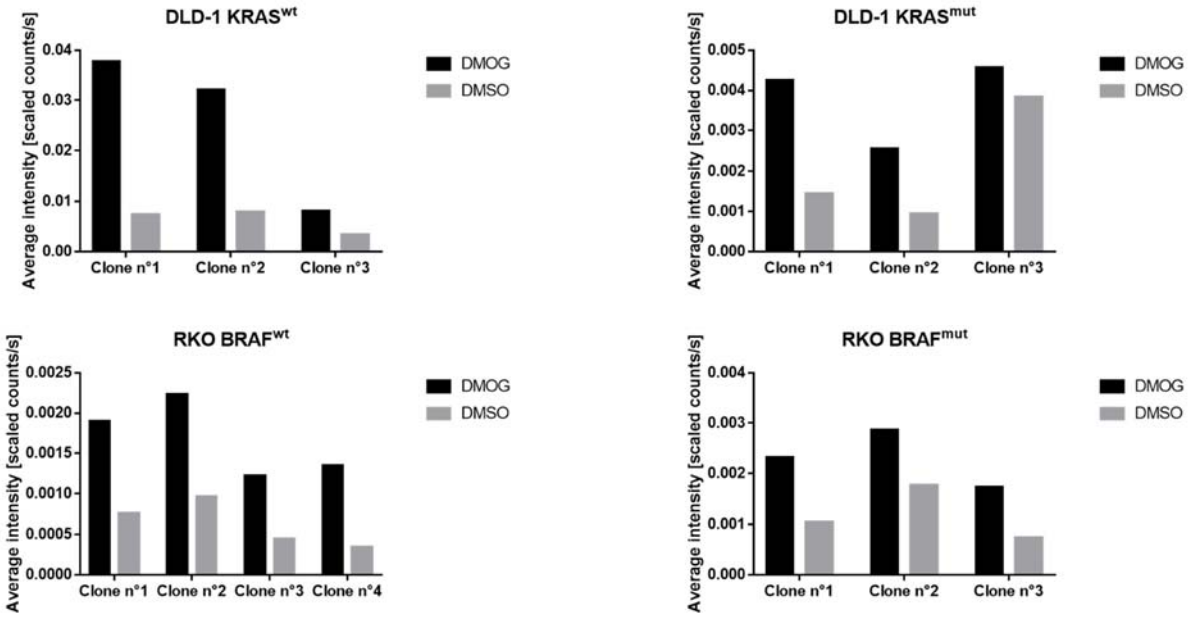

Figure 2 *iRFP induction after pharmacological treatment of the transduced clones with 1mM of DMOG for 24 hours. The average intensity induced in each clones was compared to the average intensity detected in the control clones treated with 1mM DMSO.*

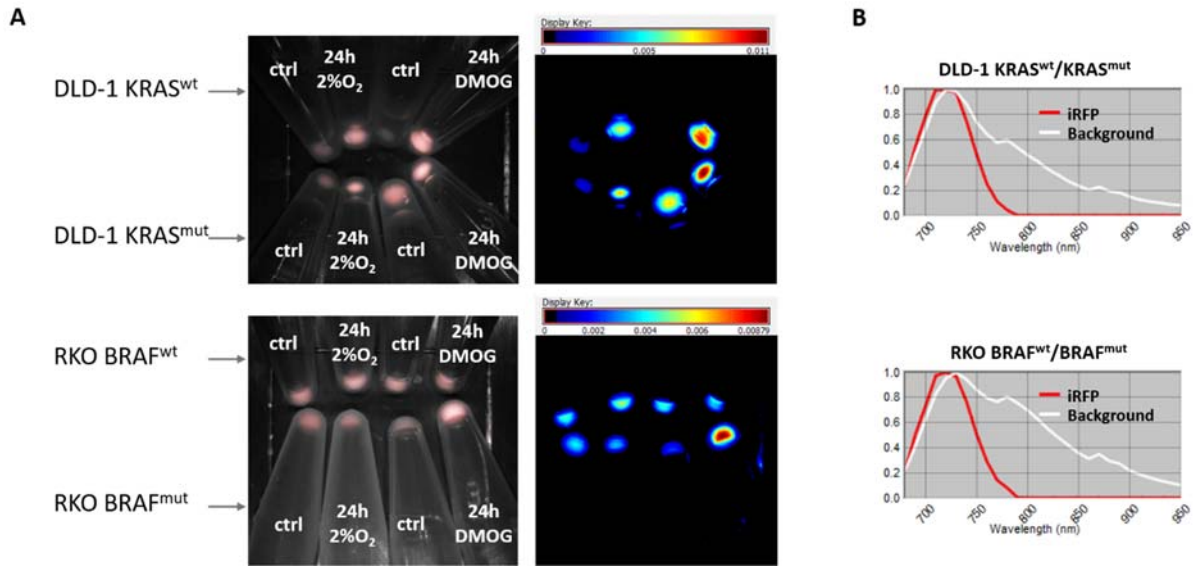

Figure 3 *Spectral unmixing of the selected clones for iRFP signal.* ***A*** *Fluorescence images obtained with a Maestro 500 2D imaging system of DLD-1 KRAS^{wt}, DLD-1 KRAS^{mut}, RKO BRAF^{wt} and RKO BRAF^{mut}cell pellets. The cells were treated with 1mM DMOG or placed in the hypoxia chamber (2% O_2) for 24 hours and then trypsinized, counted and centrifuged down in order to obtain cell pellets with equal amounts of cells. After spectral unmixing of the background and the cellular fluorescence (left), the spectral components attributed to iRFP were compared for their intensities on similar scales (right) to derive the level of reporter induction due to hypoxia and pharmacological PHD inhibition.* ***B*** *Background and iRFP spectra unmixed after Real Component Analysis (RCA) of the cube image acquired with the Maestro system for both DLD-1 and RKO isogenic pairs.*

We started by imaging cell pellets of the selected clones after 24 hours of hypoxia or pharmacological inhibition of PHD with the Maestro 500 imaging system to define a spectral library (Fig 3A). After spectral unmixing of the cell pellet images, the emission peak attributed to iRFP displayed as expected a maxima at 720nm, which confirmed the presence of the iRFP protein within the cells (Fig 3B). Next, the selected clones for each of the four cell lines were characterized *in vitro* for their longitudinal expression of iRFP under pharmacological inhibition of PHD. Both GFP and iRFP signals were measured with a brightfield microscope (Fig 4A) at different time points. In the DLD-1 KRAS^{wt} cells, a significant increase in fluorescence intensity was observed over a period of 48 hours of DMOG treatment compared to the control condition (yielding p=0.026*, p=0.0001*** and p<0.0001**** at 8, 24 and 48h respectively) (Fig 4B). At 12 hours of treatment statistical significance was not reached (p=0.096). For the DLD-1 KRAS^{mut} cells, the increase in fluorescence was significant at 24 and 48 hours compared to baseline (p<0.0001**** and p=0.0025** respectively). In addition to that, DLD-1 KRAS^{mut} fluorescent intensity was significantly higher than the DLD-1 KRAS^{wt} except at 12 hours after DMOG treatment where the higher signal observed in the mutant cell proves not to be

significant. Regarding the RKO cells, the RKO BRAF^{wt} cells displayed a significant increase in fluorescence at after 8 and 48 hours of DMOG treatment (p=0.012* and p=0.0038** respectively), and the RKO BRAF^{mut} showed a significant increase in fluorescence at 12, 24 and 48 hours of DMOG treatment (p<0.0001****, p=0.0003*** and p=0.0067** respectively). Similarly to the KRAS mutation in the DLD-1 cells, the mutated RKO cells presented a higher fluorescent signal than the RKO cells with wild-type BRAF which was significant after 8 and 24 hours of pseudo-hypoxia (p=0.0199* and p=0.0008***). Based on the results of the live cell imaging, induction factors for iRFP were computed for each cell line (Table 1).

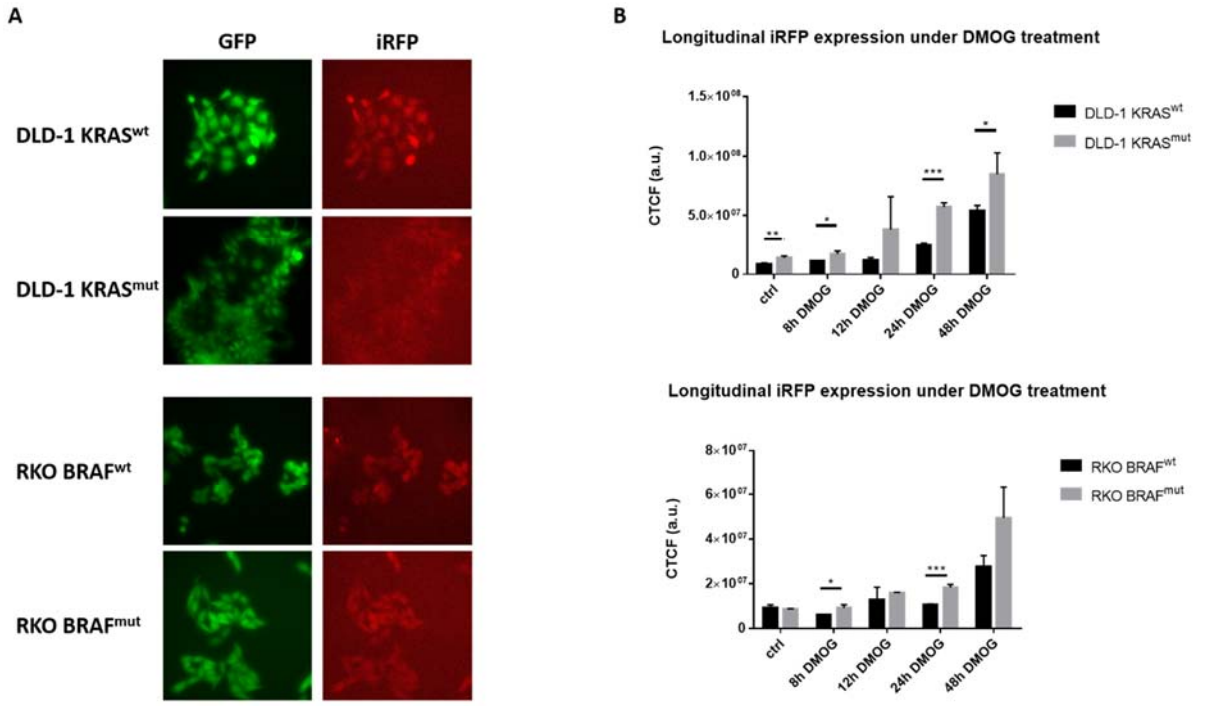

Figure 4 *Live cell imaging of DLD-1 KRAS^{wt}/KRAS^{mut} and RKO BRAF^{wt}/BRAF^{mut}.* ***A*** *GFP and iRFP expression in the transduced cells under brightfield microscope.* ***B*** *Corrected Total Cell Fluorescence (CTCF) of the four cell lines under longitudinal PHD inhibition treatment. Cells were seeded on coverslips and treated with 1mM DMOG for 8, 12, 24 and 48 hours. For the control experiment, all cells were given 1mM DMSO for 24 hours.*

Table 1 *Induction factor of iRFP fluorescent intensity in DLD-1 KRAS^{wt}, DLD-1 KRAS^{mut}, RKO BRAF^{wt}, and RKO BRAF^{mzt} live cell imaging 24 hours after treatment with 1mM DMOG or with 1mM DMSO as a control. Images were acquired with a brightfield Leica DMI 6000B. Intensity values are given as average intensity ±standard deviation (SD) (N=3).*

Tumor type	**I_{DMOG}/I_{DMSO}**
DLD-1 KRAS^{wt}	$2.86 \pm 1.66 \cdot 10^{-9}$
DLD-1 KRAS^{mut}	$4.13 \pm 4.55 \cdot 10^{-10}$
RKO BRAF^{wt}	$1.14 \pm 1.07 \cdot 10^{-8}$
RKO BRAF^{mut}	$2.12 \pm 1.42 \cdot 10^{-9}$

Detection of iRFP fluorescence in mouse subcutaneous tumor models in *in vivo* planar fluorescence imaging

All four HIF activity reporter cell lines were injected subcutaneously into the flanks of nude mice for *in vivo* studies. To assess the feasibility of monitoring the reporter gene expression longitudinally, intensity maps for each tumor type were measured at two different time points in the tumor development (Fig 5A). To enhance the signal-to-background ratio and to ensure comparability of data across the various tumor cell lines and mice, all images were unmixed using the same spectral library (Fig 5B). The spectrum extracted from the tumor region, with an emission maximum at 720nm, shows remarkable agreement with the iRFP spectrum obtained *in vitro* (Fig 3B) confirming the presence of iRFP within the tumor. The intensity map of each tumor type provides an indirect readout of the HIF-active subregions within the tumor mass. Furthermore, the analysis of the tumor mean fluorescence intensity normalized to the initial iRFP intensity showed a linear increase in iRFP before reaching a plateau (Fig 5C).

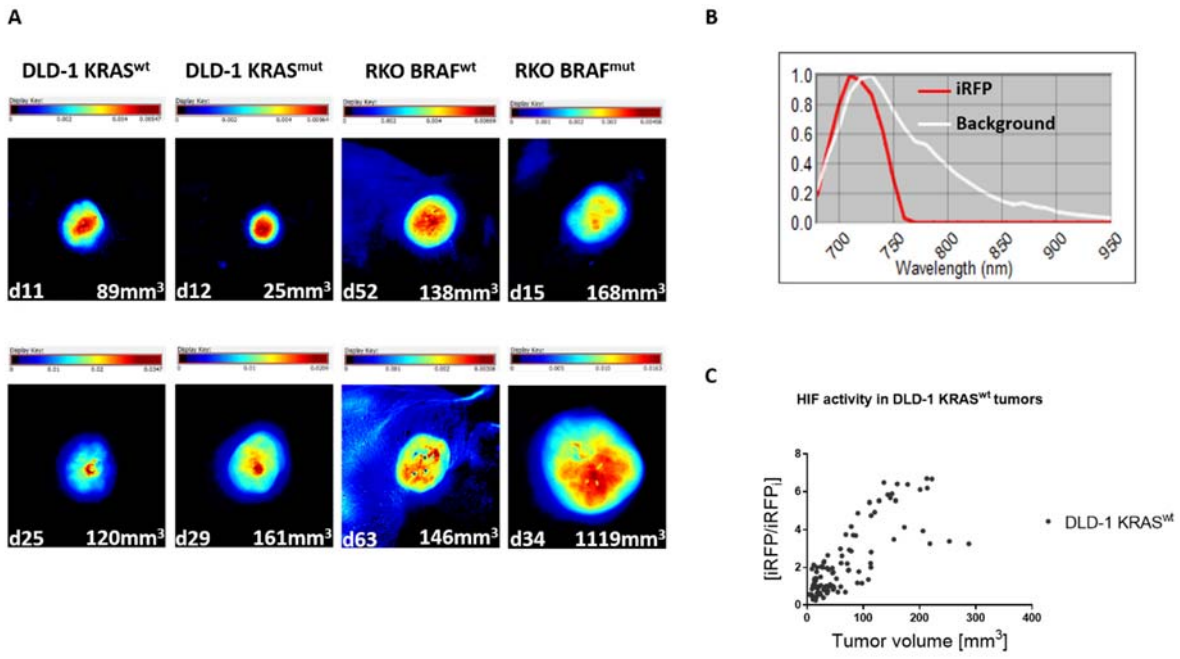

Figure 5 *iRFP intensity maps of DLD-1 KRAS^{wt}/KRAS^{mut}, RKO BRAF^{wt}/BRAF^{mut}tumors.* ***A*** *All four tumor types were analyzed at two different stages of the tumor dhevelopment by unmixing the acquired cubes with the same spectral library for each tumor type. For each unmixed image, the intensity maps for the iRFP component were drawn individually to get insight on the areas of the tumors expressing more or less iRFP. All images were acquired with the same exposure time (800ms).* ***B*** *Spectral library differentiating iRFP spectrum from background autofluorescence.* ***C*** *A representative longitudinal in vivo iRFP intensity normalized to the initial intensity with respect to the tumor volume (Caliper measurements) in DLD-1 KRAS^{wt}.*

4 Discussion

The use of reporter genes in biomedical research has proved to be an invaluable tool to investigate gene expression and gene function. However, for *in vivo* studies reporter genes are facing obstacles emerging from the physiological properties of the animal model or the tissues in which the reporter is used. The application of bioluminescence, the most commonly used reporter gene, in a tumor model is attractive due to the absence of background signal, but it may not provide fully accurate results; the erratic tumor vasculature could fail to deliver luciferin to the tumor cells expressing luciferase and the microenvironment might as well not provide the required cofactors for the enzymatic reaction. Fluorescence experiences even more severe limitations due to the light absorption and scattering by fat, water, deoxy- and oxyhemoglobin present in the tissues under study, as both the excited and emitted photon wave have to propagate through tissue. The spectral window optimal for *in vivo* imaging of tissues (600 to 850nm) restricts the use of GFP or red fluorescent proteins to studies of superficial tissues. Fluorescent proteins such as GFP are rather used in intravital imaging or two-photon microscopy[8]. Light penetration depth can be enhanced by shifting excitation and emission maxima of fluorophores towards the near-infrared optical window. In 2011, Filonov et al.[9] developed a new infrared protein, which provided increased brightness and photostability over IFP1.4[10], the most advanced infrared protein at that time. In addition, the new iRFP was noncytotoxic and the endogenous biliverdin concentration was sufficient to enhance its brightness in cells and animal models, while IFP1.4 required exogenous supply of biliverdin to fluoresce. Based on these interesting and promising results, iRFP was used to develop an iRFP transgenic mouse[11] to improve *in vivo* imaging. In this chapter, we are describing for the first time the formulation of a reporter gene for HIF activity based on the expression of iRFP for *in vivo* studies.

The lentiviral pMuLE-H2SViRFP reporter gene was constructed by combining two entry vectors containing two sequences of interest in a one-step Multisite Gateway recombination reaction. The versatility of this recombination technique resides in the fact that multiple sequences can be recombined within the destination vector in countless ways, constituting a powerful approach to quickly build vector libraries, for example to be used in gene expression studies[12]. In our case, we chose to combine a HIF activity-dependent iRFP sequence with a GFP sequence in order to obtain a control marker for the transduction efficiency of the lentiviral particles.

Given the GFP signal within the different cell cultures, transduction efficiency was estimated to lie between 80-90%, a result exceeding by far the 15-20% transfection efficiency achieved by chemical agents for the same HRE-iRFP sequence placed in a normal plasmid. These numbers confirm the power of lentiviral particles for an efficient and stable insertion of genetic material within eukaryotic cells.

Selection of single-cell clones was based on iRFP signal brightness induced under pharmacological PHD inhibition, induction factor and finally cell appearance and growth behavior *in vitro* and *in vivo*. For each tumor type, a balance was found between fluorescent intensity and cell survival. Some clones expressing a very bright signal upon DMOG administration did not form tumors following subcutaneous injection. In this regard, the clone chosen in the RKO $BRAF^{wt}$ case presented a lower iRFP intensity but proved to be the only clone growing *in vivo* among the pre-selected ones. The clones picked for DLD-1 $KRAS^{wt}$, DLD-1 $KRAS^{mut}$, and RKO $BRAF^{mut}$ displayed induction factors varying between 2.12 and 4.13 folds, sufficient for *in vivo* studies, as reported earlier using luciferase as HIF activity reporter[13].

HIF expression in cells under longitudinal DMOG treatment is fluctuating as a function of time (as it will be presented in Chapter 3). In both DLD-1 and RKO cells, maximum HIF expression was reached around 8-10 hours and 20-24 hours of DMOG treatment. With a maturation time of about 5.9 hours, iRFP expression following HIF activation should reach a maximum at approximately 12 and 24 hours of DMOG treatment. The fluorescent intensity in live cell imaging of DLD-1 $KRAS^{wt}$/$KRAS^{mut}$ matches this estimation, however in the case of the RKO $BRAF^{wt}$ the fluorescent intensity slightly decreased at 24 hours of DMOG treatment. This might be explained by the inadequate DMOG delivery to the cells present on the coverslips or fluorescence bleaching during image acquisition. The fluorescence intensities after varying periods of DMOG exposure revealed that i) PHD inhibition led to a significant increase in iRFP signals compared to the control situation, and ii) that mutant cells displayed a higher iRFP fluorescence intensity compared to their wild-type counterpart.

Imaging both *in vitro* and *in vivo* samples with the same 2D system demonstrated the value of spectral unmixing: fluorescent intensity information attributed to iRFP originated exclusively from the tumor ROI, eliminating signal contributions from molecules with different emission spectra, even if this comprises spectral contributions overlapping with the iRFP spectrum.

In vivo results obtained with the Maestro 2D planar imaging system provided limited information about the iRFP localization within the tumor. Typically, intensity distribution corresponded to a 2-dimensional point spread function about a center of gravity and rather reflected diffuse photon propagation in tissue than actual iRFP concentration profiles (Fig 5A). There are clinical evidence that tumors develop hypoxic regions heterogeneously distributed within the tumor mass[14], which makes the interpretation of the true origin for the fluorescent signal arduous. Nonetheless, studying iRFP expression in tumors longitudinally revealed a linear increase in intensity before reaching a plateau in both the DLD-1 and RKO tumor types. This behavior hints towards the fact that HIF is active during the initial development phase of the tumor, but that its activity is either reduced or masked by other effects as the tumor reaches a certain volume.

In conclusion, the new pMuLE-H2SViRFP lentiviral vector proved to be an efficient reporter gene for investigating HIF activity *in vivo*. Based on the results obtained with the DLD-1 and RKO transduced cells, the fluorescent contribution of the iRFP-expressing cells can be disentangled efficiently from autofluorescence and other fluorescent contributors within a tumor mass. In addition to that, the spectral properties of iRFP provide better access to deeper structures in molecular *in vivo* imaging. This far-red shift in fluorescence also allows for a combination with other fluorescent molecular probes. Besides iRFP, the presence of GFP within the vector could also be exploited in different, though superficial, experiment to discriminate tumor cells from other cell types, for example in an intravital imaging experiment with cells transduced with the pMuLE construct.

5 References

1. Gatenby, R. A. *et al.* Oxygen distribution in squamous cell carcinoma metastases and its relationship to outcome of radiation therapy. *Int. J. Radiat. Oncol. Biol. Phys.* **14,** 831–838 (1988).

2. Nordsmark, M., Bentzen, S. M. & Overgaard, J. Measurement of Human Tumour Oxygenation Status by a Polarographic Needle Electrode: An analysis of inter- and intratumour heterogeneity. *Acta Oncol.* **33,** 383–389 (1994).

3. Swanson, K. R. *et al.* Complementary but Distinct Roles for MRI and 18F-Fluoromisonidazole PET in the Assessment of Human Glioblastomas. *J. Nucl. Med.* **50,** 36–44 (2009).

4. Lau, J. *et al.* PET Imaging of Carbonic Anhydrase IX Expression of HT-29 Tumor Xenograft Mice with 68 Ga-Labeled Benzenesulfonamides. *Mol. Pharm.* **13,** 1137–1146 (2016).

5. Danhier, P. *et al.* Combining Optical Reporter Proteins with Different Half-lives to Detect Temporal Evolution of Hypoxia and Reoxygenation in Tumors. *Neoplasia* **17,** 871–881 (2015).

6. Remington, S. J. Fluorescent proteins: maturation, photochemistry and photophysics. *Curr. Opin. Struct. Biol.* **16,** 714–721 (2006).

7. Petersen, L. K. & Stowers, R. S. A Gateway Multisite recombination cloning toolkit. *PLoS One* **6,** (2011).

8. Hoffman, R. M. Application of GFP imaging in cancer. *Lab. Invest.* **95,** 432–52 (2015).

9. Filonov, G. S. *et al.* Bright and stable near-infrared fluorescent protein for in vivo imaging. *Nat Biotechnol* **29,** 757–761 (2011).

10. Shu, X. *et al.* Mammalian Expression of Infrared Fluorescent Proteins Engineered from a Bacterial Phytochrome. *Science (80-.).* **324,** 804–807 (2009).

11. Tran, M. T. N. *et al.* In Vivo image Analysis Using iRFP Transgenic Mice. *Exp. Anim.* **63,** 311–319 (2014).

12. Michael, I. P. *et al.* Highly efficient site-specific transgenesis in cancer cell lines. *Mol Cancer* **11,** 89 (2012).

13. Lehmann, S. *et al.* Longitudinal and multimodal in vivo imaging of tumor hypoxia and its downstream molecular events. *PNAS* **106,** 14004–14009 (2009).

14. Vaupel, P., Kelleher, D. K. & Höckel, M. Oxygen status of malignant tumors: pathogenesis of hypoxia and significance for tumor therapy. *Semin. Oncol.* **28,** 29–35 (2001).

3. *In vivo* study of HIF activity and pyruvate metabolism in colon carcinomas with a KRAS or BRAF mutation

Abstract

Hypoxia is a phenomenon arising in solid tumors with a disorganized and inefficient vasculature. As the amount of oxygen diminishes in the tumor regions out of the range of molecular diffusion, HIF-1α, a subunit of the Hypoxia Inducible Factor (HIF), is stabilized and dimerizes with the β subunit to form an active complex. HIF triggers the transcription of genes involved in angiogenesis, metastasis, cell survival and metabolism. In normoxic regions, HIF-1α is hydroxylated and degraded. It has been shown recently that in addition to a lack of oxygen, an altered level of metabolites and different oncogenes could also participate to the stabilization of HIF-1α and activate HIF. In this study, we aimed at understanding the influence of specific cancer-driving mutations on the HIF signaling and tumor metabolism. The human colon carcinoma cells DLD-1 and RKO exhibiting an active mutation on KRAS and BRAF respectively were used together with their corresponding wild-type cell lines. All cell lines were virally transfected with an infrared fluorescent protein (iRFP) reporter gene for HIF activity and implanted subcutaneously in the flank of Balb/c nude mice. Fluorescence intensity was measured longitudinally and used as an indirect readout for HIF signaling. Simultaneously, tumor-bearing mice were injected with a hyperpolarized solution of [1-^{13}C]-pyruvate to follow the conversion of [1-^{13}C]-pyruvate into [1-^{13}C]-lactate in tumors using ^{13}C-magnetic resonance spectroscopy (^{13}C-MRS). Results revealed an increased HIF activity in mutated tumors in early development phase (tumor volume < 100mm^3) due to hypoxia-independent factors. Metabolic measurements did not show any significant differences between mutated and wild-type tumors in both tumor types.

Catherine Germanier, Martin Schneider, Giorgos Batsios, Jael Xandry, Markus Rudin

1 Introduction

Tumors rely on a steady supply of oxygen (O_2) and nutrients for growing, which during the initial phase of development is warranted via molecular diffusion. As the cell mass outgrows the typical diffusion distance within tissue (200µm) tumor cells become increasingly exposed to metabolic stress and hypoxia. Shortage of O_2 induces signaling mediated by the Hypoxia Inducible Factor (HIF), a heterodimer transcription factor, the activation of which allows cells to adapt to hypoxic conditions. For tumor cells, HIF signaling is associated among others with tumor progression, angiogenesis and metabolic adaptation. Under normoxic conditions, the α subunit of HIF is hydroxylated by a prolyl-4-hydroxylase domain (PHD), the activity of which depends on the tissue oxygen level, and thereby marked for degradation by the 26S proteasome. Under hypoxic conditions, PHD activity is reduced; HIF-α is stabilized and dimerizes with the β subunit to form the transcriptionally active HIF complex. Yet, both temporal and spatial disconnect between tissue hypoxia and HIF mediated signaling have been reported[1], indicative of a HIF activity dependent regulatory feedback and of a hypoxia independent activation of the HIF complex. Moreover, recent studies on tumor metabolism established a link between altered levels of metabolites and HIF signaling. For example, in glioblastoma multiformae, a recurrent loss-of-function mutation of isocitrate dehydrogenase 1 (IDH1), a metabolic enzyme found in the tricarboxylic acid cycle (TCA), inhibits the conversion of isocitrate into α-ketoglutarate, a co-factor of the HIF-1α processing enzyme PHD. Low intracellular concentrations of α-ketoglutarate lead to inhibition of PHD and, hence, to the stabilization of the HIF-1α subunit and subsequent HIF transcriptional activity even in the presence of oxygen[2]. Analogous HIF activation has been reported for tumors expressing a loss-of-function mutation of the succinate dehydrogenase[3].

HIF signaling induces the transcription of a large array of genes including genes implicated in the upregulation of glycolysis. This way, HIF activity leads to regulation of key enzymes involved in (glucose) metabolism, while HIF-1α levels and thus HIF signaling are influenced by these metabolic adaptations due to altered metabolite levels such as α-ketoglutarate or succinate, hinting towards the presence of a feed-forward loop. The nature of metabolic reprogramming is cancer type-specific[4,5]. We therefore wondered to what extent metabolic rewiring and its implications on HIF signaling might be associated to cancer driving mutations. We focused on mutations of two modulators of the mitogen-activated protein kinase (MAPK) pathway, KRAS (G13D) and BRAF (V600E) in colorectal carcinomas. Colorectal cancers are the third deadliest cancer in 2016 in the United States[6] and among them about 45%[7] arise from the KRAS G13D mutation and 10%[8] from the BRAF V600E mutation. An *in vitro* study by Kikuchi et al.[9] showed that both KRAS G13D and BRAF V600E mutations in colon carcinoma cells enhance the hypoxic induction of HIF *in vitro.* In this study, we investigated the role of these two mutations on the induction of HIF *in vivo*, and whether HIF induction was linked to specific metabolic adaptations. By using colorectal tumor cells containing a modified version of a HIF activity reporter described earlier[1,10], we non-invasively examined the activity of HIF in subcutaneous colorectal tumors bearing a KRAS or BRAF driving mutation in a longitudinal manner. In addition, we explored the effect of the two mutations on the tumor metabolism *in vivo* by ^{13}C magnetic resonance spectroscopy (^{13}C-MRS) using hyperpolarized [1-^{13}C]-pyruvate as a substrate which plays an important gatekeeper role in channeling glucose either into the TCA cycle, towards conversion by lactate dehydrogenase (LDH), or towards protein synthesis via the aminotransferase (ALT). By combining fluorescent molecular imaging and ^{13}C-MRS, we found that HIF activity is significantly increased during the initial phase of tumor development in KRAS and BRAF mutated compared to wild-type tumors. In contrast, we found no different LDH activity between KRAS or BRAF mutated and the respective wild-type tumors.

2 Material and Methods

Cell lines and cell culture

Four human colon cancer cell lines exhibiting an activating mutation in the MAPK pathway were chosen for this work. The RKO derived F6-8 (BRAF mt/wt or RKO $BRAF^{mut}$) and the isogenic wild-type T29 (BRAF null/wt or RKO $BRAF^{wt}$) cell lines were cultivated in Dulbecco's Modified Eagle's Medium (DMEM) supplemented with 10% Fetal Bovine Serum (FBS) (Gibco, Carlsbad, USA). The BRAF mutant allele harbored a valine to glutamate mutation on the codon 600 (V600E), a mutation found in 90% of the BRAF mutations. The second set of cells, DLD-1 $KRAS^{mut}$ (KRAS wt/mut) and DLD-1 $KRAS^{wt}$ (KRAS wt/null) were cultivated in Roswell Park Memorial Institute medium (RPMI) with 10% FBS (all media from Gibco, Carlsbad, USA). The KRAS allele of the DLD-1 $KRAS^{mut}$ was mutated on codon 13 from glycine to aspartate (G13D), a mutation accounting for 20% of the KRAS mutations. All cell lines were a kind gift from Prof. Wilhelm Krek (ETH, Zürich).

Plasmid construction

The pMuLE-H2SViRFP plasmid used for this study was generated by recombining two entry vectors containing different sequences into a destination vector in a Multisite Gateway Recombination step (Invitrogen, Carlsbad, USA). In brief, an entry vector containing an infrared fluorescent protein (iRFP) sequence under the control of two Hypoxia Responsive Elements (HRE) and a SV40 promoter, and an entry vector containing a green fluorescent protein (GFP) sequence driven by a CMV promoter were recombined by homologous recombination of the sites flanking the sequences of interest in the entry vectors with the identical sites found on a destination vector. Both reporter sequences were incorporated in a sequential way and similarly oriented in a 5' to 3' fashion.

Generation of stably transduced cell lines

DLD-1 $KRAS^{wt}$/$KRAS^{mut}$ and RKO $BRAF^{wt}$/$BRAF^{mut}$ were cultivated in 10cm tissue culture dishes. At a confluency of 50%, 10ml of DMEM containing viral particles encapsulating the fluorescent reporter gene pMuLE-H2SViRFP were added to each plates with 1µg of polybrene and the cells were transduced for 48 hours. After transduction, the positive cells were selected with

puromycin at a concentration of 1µg per ml of medium. Single cell clones were picked from 10cm dishes with minimal cellular dilution and expanded in individual culture dishes. For each clones, we assessed the iRFP signal by treating them with the PHD inhibitor dimethyloxalylglycine (DMOG) at a concentration of 1mM for 24h and imaging the cell pellets with the 2D planar Maestro 500 imaging system (Cambridge Research & Instruments Inc., Hopkinton, USA). For each cell lines, the clones expressing a bright iRFP signal under pharmacological treatment and showing a strong induction factor for iRFP compared to the control condition were selected for further study.

Sprouting assay

Human umbilical vein endothelial cells (HUVECs) (Lonza, Switzerland) were cultivated in Endothelial Growth Medium (EGM^{TM}-2 BulletKit^{TM}, Lonza, Switzerland) supplemented with 2% FBS and vascular endothelial growth factor (VEGF). To form spheroids, HUVEC cells at a concentration of $2 \cdot 10^5$ cells/ml were mixed in EGM containing 10% of methylcellulose and plated in 25µl drops yielding 2000 cells per drops. Drops were incubated upside down to allow the formation of spheroids. The following day, spheroids were collected in EGM and embedded in a solution of 4mg/ml of rat tail collagen (Corning, Tewksbury, USA) buffered with NaOH 1N. The gels containing the spheroids were incubated in media obtained from cultures of DLD-1 KRAS^{wt}/KRAS^{mut} and RKO BRAF^{wt}/BRAF^{mut} after 72 hours of both normoxic (21% O_2) or hypoxic (1% O_2) condition for incubation. After 24 hours, gels were washed twice with PBS, fixed in 4% PFA and tips sprouting from the spheroids were imaged with a brightfield Leica microscope (Leica DMI 6000B, Wetzlar, Germany). A FIJI software (National Institute of Health) was used to analyze the resulting images and count the cell tips.

Xenograft tumor models

The four cell lines were cultivated up to 80% confluency and were then trypsinized and resuspended in a solution of 50% PBS and 50% of Hanks' Balanced Salt Solution (HBSS, Gibco, Carlsbad, USA) to a concentration of $2.5 \cdot 10^7$cells/ml. $2.5 \cdot 10^6$cells were injected subcutaneously in the right flank of 6-8 weeks old female Balb/c nude mice (N=10 for each cell line). Tumor size was monitored by caliper measurements every two days, allowing the

determination of the tumor volume using the formula $V = 1/2 \cdot (length \cdot width^2)$. The animals were sacrificed at the end of the experiment or prior to it if the tumor was exceeding a necrotic level or a tumor volume of 1500mm^3. Every step in the handling of the animals was approved by the Cantonal Veterinary Office of Zurich (license number 185-2013).

In vivo planar fluorescence reflectance imaging

The animals were anaesthetized with 2.5% isoflurane in an oxygen-air gas mixture prior to each imaging step. Longitudinal measurements of the iRFP expressing tumors were achieved with a 2D planar Maestro 500 imaging system. The mice were placed in the Maestro chamber and the iRFP and GFP signals were acquired by using a set of red (acquisition between 680 and 950nm in 10nm steps) and blue (acquisition between 500 and 720nnm, in 10nm steps) bandpass filters respectively. With each filter set an image is acquired at every wavelength step of the optical window covered by the filter, resulting in an image data "cube" defined by two spatial and one spectral coordinate (I(x,y,λ)). Using the Maestro 3.0.1.2 software a spectral library was built to differentiate the components of the fluorescent signal obtained in the images. During the study, all acquired images were unmixed with the same spectral library to detect the fluorescent contributions from the iRFP within the tumor and from the background and autofluorescence. A ROI was drawn around the tumor on the unmixed iRFP image and the iRFP intensity was calculated using the Maestro software. For consistency between the different studies, the exposure to image iRFP and GFP were kept constant, at 800ms and 20ms respectively.

Immunofluorescence

All mice were injected intravenously with pimonidazole (1.5mg/100ul, Hypoxyprobe-Kit, Hydroxyprobe, Burlington, USA) one hour before sacrificing them. Tumors extracted at an early stage of development were additionally injected with the nuclear marker Hoechst33342 (Sigma-Aldrich, St Louis, USA). The tumors were then extracted, embedded in optical cutting temperature (OCT) medium (Tissue-Tek®, Torrance, USA) and frozen on dry ice. 12µm tumor sections were fixed in paraformaldehyde 4% and washed in PBS. Sections were stained for the hypoxic marker pimonidazole (1:1000 rabbit anti-pimonidazole, Hypoxyprobe™-1 Omni

Kit, Hydroxyprobe, Burlington, USA), the hypoxia-inducible factor 1α (1:1000 rabbit anti-HIF-1, Novus Biologicals 100-479, Littleton, USA), the HIF downstream gene products carbonic anhydrase 9, CA9 (1:1000, rabbit anti-CA9, Abcam 15086) and glucose transporter 1, GLUT1 (1:1000 rabbit anti-GLUT1, Abcam 14683) and the endothelial cell marker CD31 (1:300 rabbit anti-CD31, Abcam 28364, Cambridge, UK). Whole tumor sections were imaged at a 20X magnification with a Pannoramic 250 slide scanner (3D-Histech, Budapest, Hungary).

In vivo imaging of lactate dehydrogenase (LDH) activity

A volume of 25.4µl of a stock solution of 0.5ml [1-^{13}C] pyruvic acid (Sigma Aldrich, St Louis, USA) containing 15mM trityl radical (tris(8-carboxyl-2,2,6,6-tetra(2-(1-hydroxyethyl))-benzo[1,2-d;4,5-d'] bis (1,3)dithiole-4-yl) methyl sodium salt, donation) and 1.5mM Gd(DOTA) (Dotarem®, Guerbet, Villepinte, France) was hyperpolarized for 1 hour using a homemade polarization system[11]. The sample was dissolved in 8ml of 50mM Tris-buffer and the pH was adjusted by adding 260µl of NaOH 1M to reach a final value of pH ~7.6.

For ^{13}C-MRS experiment using hyperpolarized [1-^{13}C] pyruvic acid, Balb/c nude mice were first anaesthetized with 2.5% isoflurane in air with 20% oxygen. A catheter was inserted into the tail vein and fixed for the duration of the experiment. During the measurements, the anaesthesia was reduced to 2% isoflurane. All experiments were performed on a Bruker Biospec 94/30 system (Bruker Biospin MRI, Ettlingen, Germany). Proton imaging was done with a quadrature volume resonant coil, and ^{13}C-MRS with a custom made 1.6cm diameter surface coil. Anatomical images were obtained with a Fast Spin Echo (RARE) sequence (TE/TR=8.102ms/1500ms; matrix size 256x256: FOV=40x40mm^2; slice thickness=0.7mm; excitation flip angle=90°) and used for tumor volume measurement and as reference for the shimming voxel and the slice positioning in the spectroscopic experiments. MRS experiments were carried out using a slice selective spectroscopy sequence triggered by the dissolution of the hyperpolarized sample (TE/TR=0.5712ms/3000ms; slice thickness=7.2mm; Gaussian shape excitation pulse with 0.1ms duration and 15° angle; bandwidth=2740 Hz; number of sampling points=4096).

Image processing

^{13}C-MRS spectra were processed using the jMRUI software (jMRUI 5.2 version). Spectral processing included zero and first order phase adjustment, baseline correction, and intensity evaluation. Intensity-time profiles were then analyzed using a Matlab program (R2016a, Mathworks), which considered the label exchange between [1-^{13}C]-pyruvate and [1-^{13}C]-lactate via the LDH reaction as well as the lifetime of the labeled states (longitudinal relaxation time T_1 for the hyperpolarization state of the two compounds)[12]. This allowed determining the ratio of maximum [1-^{13}C]-lactate to maximum [1-^{13}C]-pyruvate as well as of the rate constants of the LDH reaction.

Statistical analysis

Statistics for fluorescence images and DNP experiment results were analyzed using the software R 3.1.1 (The R foundation for Statistical Computing, Vienna, Austria). A linear mixed model analysis was performed with tumor type, tumor volume, fluorescence intensity or pyruvate kinetics, as well as the tumor type and tumor volume interaction, using lme4 package.

3 Results

Establishing a fluorescent reporter gene for HIF activity

To investigate the activity of HIF in DLD-1 KRAS^{wt}, DLD-1 KRAS^{mut}, RKO BRAF^{wt} and RKO BRAF^{mut} cells and tumors, the cell lines were transfected with viral particles encapsulating the fluorescent reporter gene pMuLE-H2SViRFP (Fig 1A) leading to expression of iRFP under the control of HREs. To assess the efficiency of the reporter, the selected cells were either treated with the PHD inhibitor dimethyloxalylglycine (DMOG) or placed in a 1% O_2 hypoxic chamber for 24 hours. First, the increased expression of HIF-1α under those conditions was confirmed by Western Blot (Fig 1B), and then HIF activity was assessed in live cell imaging of iRFP fluorescence (Fig 1C). All cell lines exhibited a significant increase in fluorescence under hypoxia and pseudo-hypoxia compared to the control conditions (Fig 1D). Interestingly the DLD-1 KRAS^{wt} and KRAS^{mut} expressed a stronger fluorescent signal under DMOG treatment compared to hypoxic conditions and the RKO BRAF^{wt} and BRAF^{mut} inversely expressed more fluorescence under hypoxic conditions compared to the DMOG treatment.

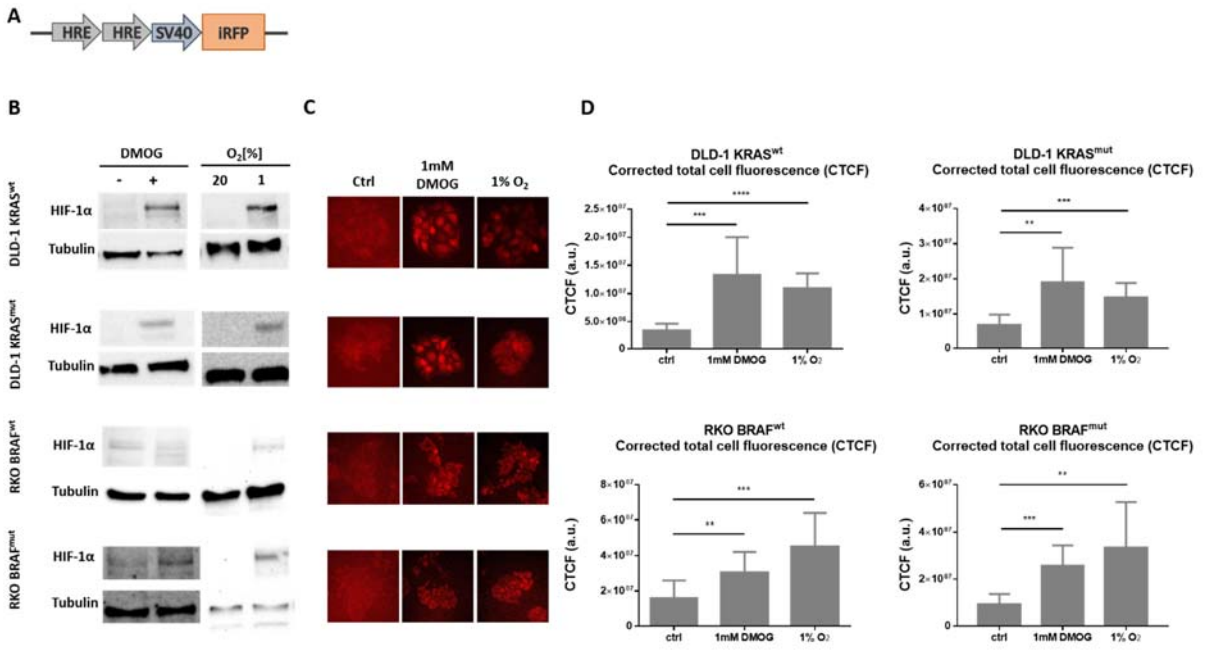

Figure 1 *HIF-1α and iRFP are upregulated in DLD-1 KRAS^{wt} and KRAS^{mut} as well as in RKO BRAF^{wt} and BRAF^{mut}.* ***A*** *Reporter construct pMuLE-H2SViRFP (HRE-iRFP segment)* ***B*** *Immunoblot for HIF-1α detection after 24 hours of 1mM DMOG treatment or 24 hours of hypoxia at 1% O_2 in DLD-1 and RKO cells after transduction with the fluorescent reporter plasmid.* ***C*** *Live cell imaging of the transduced DLD-1 and RKO cells 24 hours after 1mM DMOG treatment or hypoxia chamber 1% O_2.* ***D*** *Quantification of the corrected total cell fluorescence (CTCF) in live cell imaging experiment.*

KRAS- and BRAF-mutated tumors express a higher HIF activity *in vivo*

DLD-1 and RKO isogenic cells genetically modified to express iRFP as readout of HIF activity were injected subcutaneously in the thigh of Balb/c nude mice. As soon as the tumor became visible, 2D planar fluorescence reflectance imaging was performed on alternative days until termination of the study (Fig 3A). For each animal and measurements, the fluorescent intensities were normalized to the initial intensity and plotted against the tumor volume assessed via caliper measurements. iRFP intensity increased as the volume increased irrespective of the tumor type (Fig 3B), however for small tumors (volume < 100mm^3) the DLD-1 KRAS^{mut} and RKO BRAF^{mut} tumors displayed higher fluorescence intensities than DLD-1 KRAS^{wt} and RKO BRAF^{wt} tumors respectively. When comparing DLD-1 KRAS^{wt} and DLD-1 KRAS^{mut} tumors, both the tumor type ($p < 0.0013$***) and the interaction between tumor type and tumor volume ($p = 4.1 \cdot 10^{-10}$***) had a significant effect on the differences in HIF activity (Fig 3C, top). Similar effects were seen for the RKO pair regarding the tumor type ($p < 0.04$*) and the interaction between tumor type and tumor volume ($p = 5.1 \cdot 10^{-6}$***) (Fig 3C, bottom).

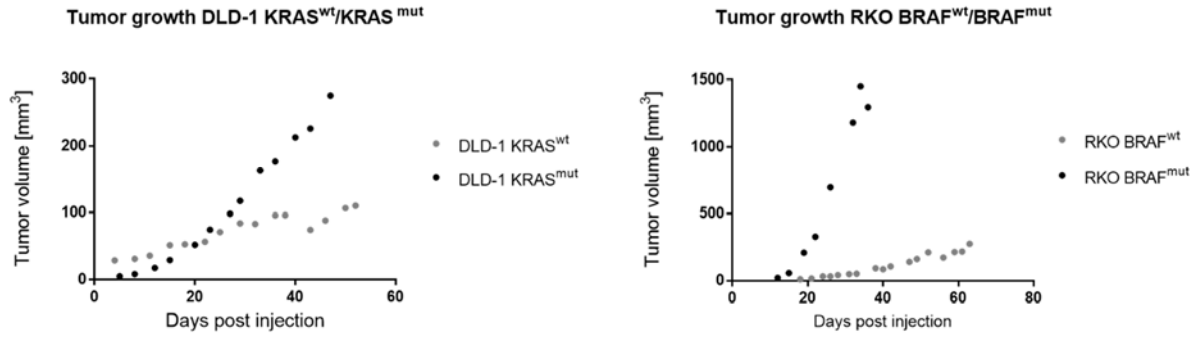

Figure 2 *Tumor growth curve for DLD-1 and RKO tumors in vivo. Tumor volumes were determined by caliper measurements of the width and length of the tumor and averages over the mice cohort were plotted against time after injection.*

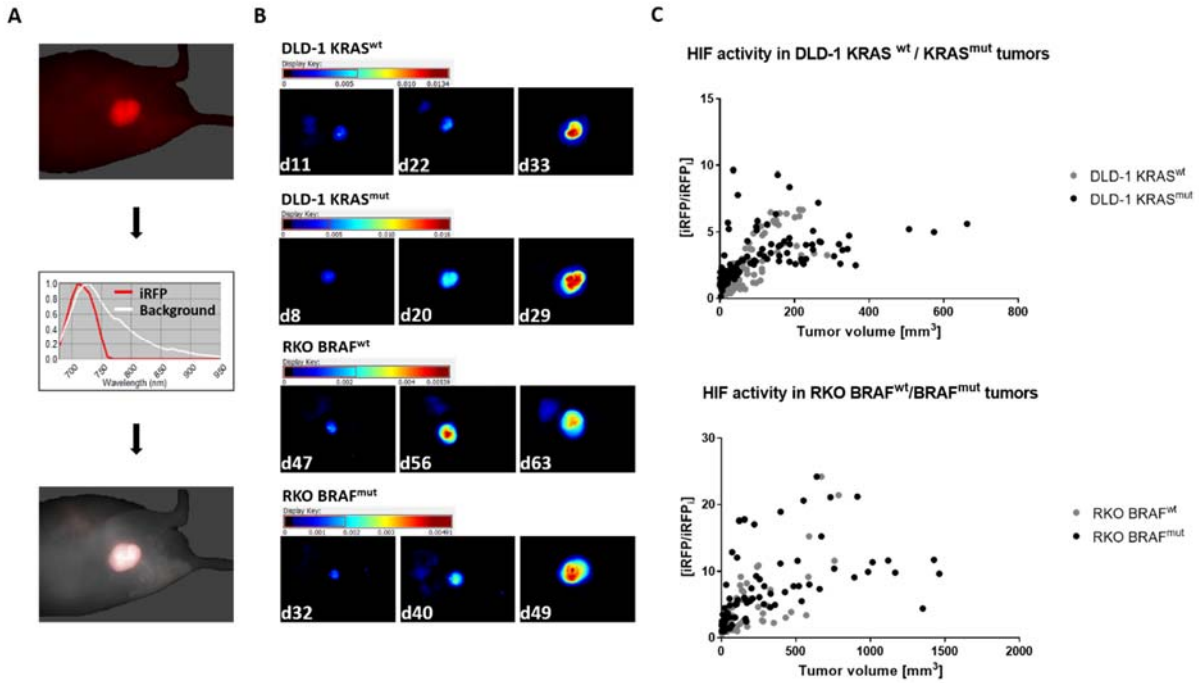

Figure 3 *In vivo imaging of iRFP expression reveals an increased HIF activity in KRAS and BRAF mutated tumors.* ***A Top:*** *Image showing the superposition of all wavelength-specific images acquired (projection of image cube along the spectral axis).* ***Middle:*** *Spectral library showing spectra of background (white) and iRFP (red).* ***Bottom:*** *Spectrally unmixed image showing spatial distribution of iRFP.* ***B*** *The intensities of the unmixed iRFP component of the image cube are compared at three time points for each cell line (right).* ***C*** *Normalized fluorescence intensities of DLD-1 and RKO tumors show a significant increase in HIF activity in the KRAS-mutated and BRAF-mutated cell lines compared to their wild-type counterparts.*

KRAS and BRAF activating mutations do not impact on the tumors pyruvate metabolism

LDH is one of the target genes of HIF. Therefore, it is plausible to assume that mutations having an effect on the activity of HIF might have also an effect on the conversion of pyruvate to lactate. We have monitored the fate of intravenously administered [1-^{13}C]-pyruvic acid in the same tumor-bearing mice that were used for fluorescence imaging. [1-^{13}C]-MRS measurements were initiated when the tumors reached a volume of about 20mm^3 and conducted on a weekly basis until termination of the study. Typically, resonances attributed to [1-^{13}C]-pyruvate, [1-^{13}C]-pyruvate(hydrate) and [1-^{13}C]-lactate could be observed, while the levels of [1-^{13}C]-alanine were too low to be reliably detected (Fig 4A). In all four tumor types, the lactate-to-pyruvate ratio and the LDH rate constant decrease as the tumor are growing. However, there were no significant differences in lactate-to-pyruvate ratio and LDH forward rate constant between wild-type and mutant DLD-1 ($p = 0.2677$ and $p = 0.09018$ respectively) and between wild-type and mutant RKO tumors ($p = 0.94$ and $p = 0.12$ respectively) (Fig 4B).

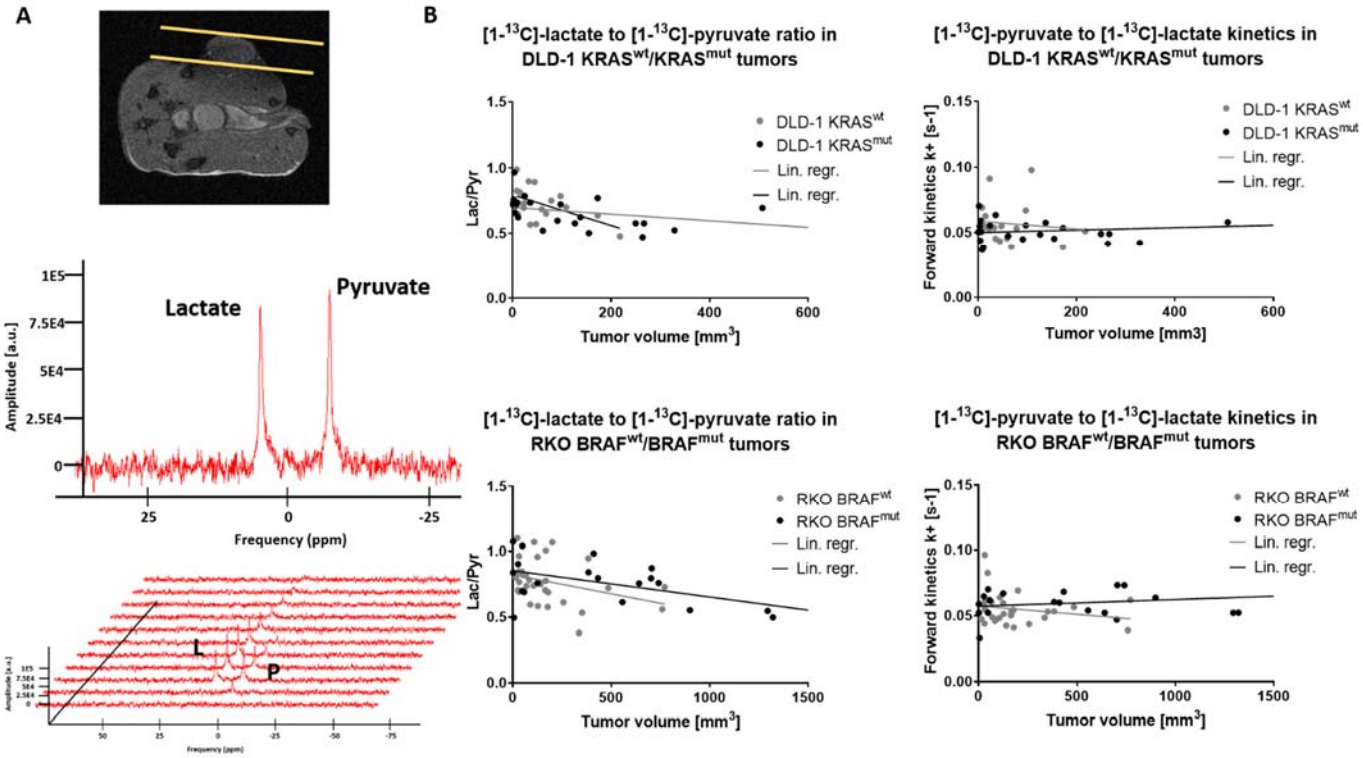

Figure 4 *In vivo pyruvate metabolism in DLD-1 KRAS^{wt} and KRAS^{mut}, RKO BRAF^{wt} and BRAF^{mut}tumors.* ***A*** *Slice-selection on a T2-RARE anatomical image for spectroscopy of DLD-1 and RKO tumors after injection of a hyperpolarized solution of [1-^{13}C] pyruvate (top). Lactate and pyruvate spectra are extracted (middle) and followed over time (bottom).* ***B*** *Quantification of the lactate-to-pyruvate ratio along with the kinetics of the pyruvate to lactate conversion show no significant difference between the mutated and non-mutated tumors.*

Ex vivo analysis reveals vascular differences between premature and mature tumors

In *in vivo* fluorescence imaging, we observed a significant difference in iRFP signal intensity between mutated and wild-type tumors in both the DLD-1 and RKO mice at an early stage of tumor development (tumor volume < 100mm^3). To validate the *in vivo* findings we evaluated various readouts of hypoxia and HIF signaling by histological analysis of tumor sections. We focused on the hypoxia marker pimonidazole, the HIF downstream product CA9, and the endothelial cell marker CD31 as indicator of tumor vascularization (Fig 5A). Quantification of the tumor stainings revealed higher levels of all three markers in the early phase of tumor development compared to the termination stage (Fig 5B). Interestingly, we did not observe any significant difference between the wild-type and mutated tumors, neither for DLD-1 nor RKO tumors, for any of the three markers during the early stage. While there was a trend towards increased CA9 and CD31 staining both with regard to the partial area stained and the stain intensity in line with the *in vivo* observations, this was not the case for RKO tumors.

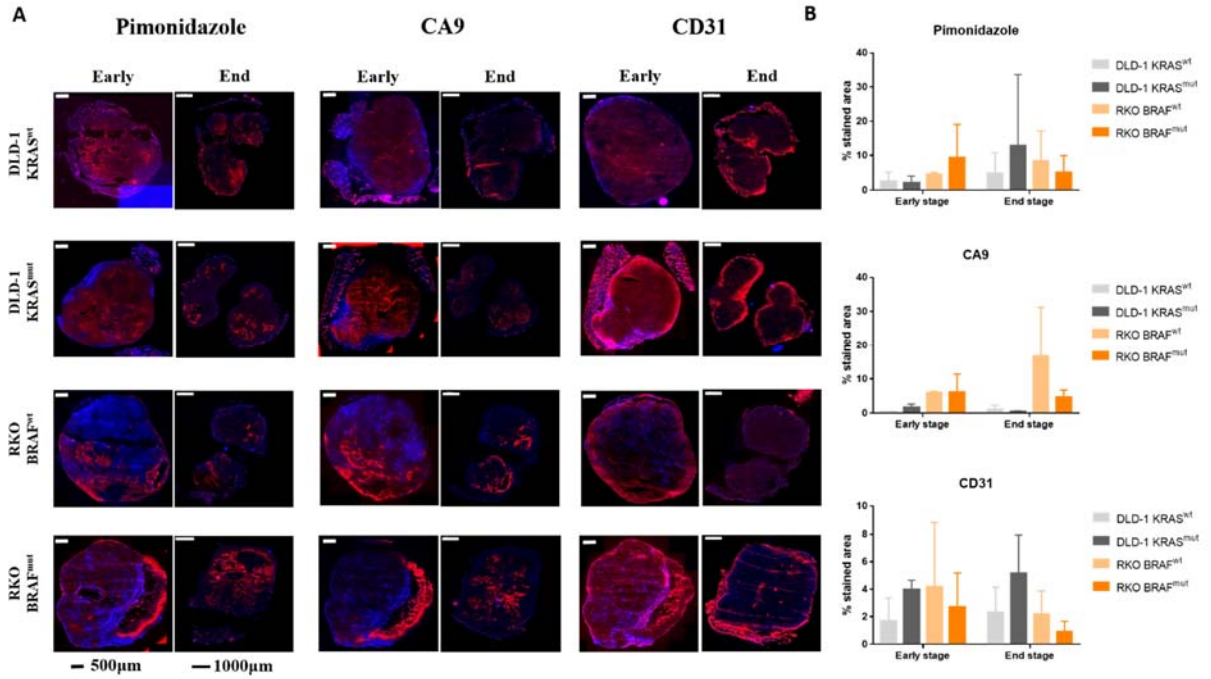

Figure 5 *Ex vivo immunofluorescence staining of the hypoxia marker pimonidazole, the HIF activity marker CA9 and the blood vessels marker CD31 at an early (tumor volume<100mm^3) and terminal stage of tumor development.* ***A*** *Immunofluorescence images of the whole tumor section stained for three different markers (red). Section of the same tumor is displayed for each tumor type. Scale bar is 500µm for the early stage tumors and 1000µm for the end stage tumors.* ***B*** *Quantification of the tumor staining by computing the ratio of stained area over the whole tumor section area.*

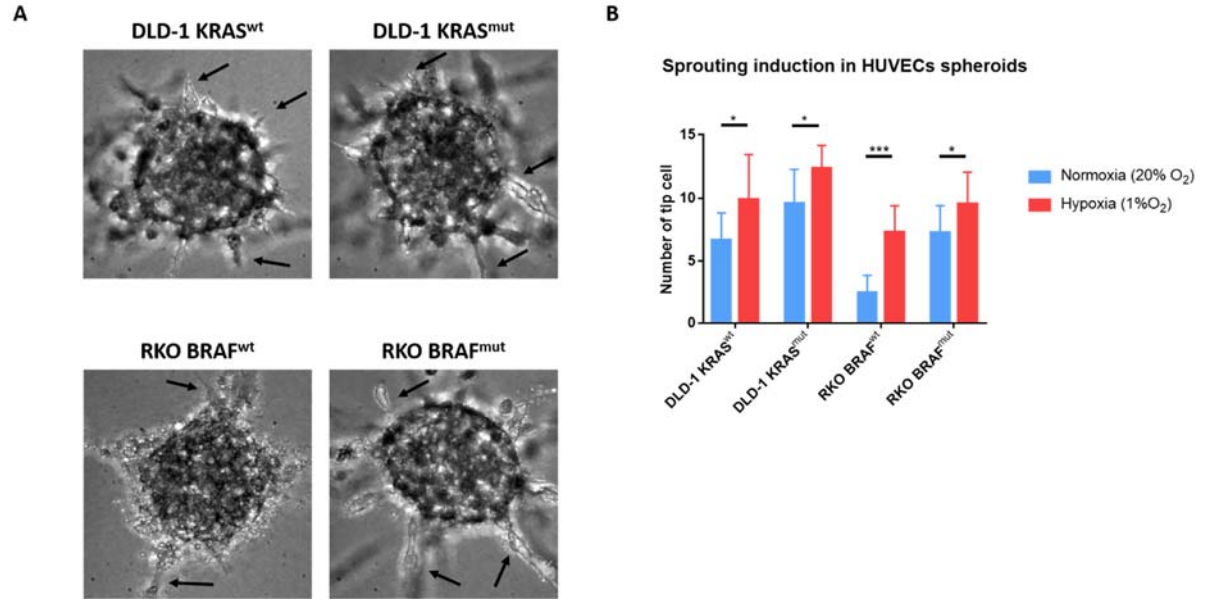

Figure 65 *Sprouting assay of Human Umbilical Vein Endothelial Cells (HUVECs) in culture medium of DLD-1 KRAS^{wt}, DLD-1 KRAS^{mut}, RKO BRAF^{wt}and RKO BRAF^{mut}.* ***A*** *HUVECs spheroids incubated 24 hours in condition media from the DLD-1 and RKO pairs in normoxic conditions.* ***B*** *Quantification of the sprouting of HUVECs (number of tip cells) induced by incubating the spheroids with the culture media of DLD-1 and RKO cells cultivated in both normoxic (21% O_2) and hypoxic conditions (1% O_2).*

Constitutive activation of KRAS and BRAF led to enhanced vascular sprouting of HUVECs spheroids

Figure 5 indicates increased CD31 staining in DLD-1 $KRAS^{mut}$ and to a lesser extent in RKO $BRAF^{mut}$ tumors. This indicates an enhanced secretion of proangiogenic factors promoting activation of endothelial cells and vascular sprouting. In order to corroborate this hypothesis, we evaluated the effect of factors secreted from tumor cells in a spheroid sprouting assay (Fig 6A). Spheroids made of HUVEC cells were treated with cell culture media harvested from DLD-1 $KRAS^{wt}$, DLD-1 $KRAS^{mut}$ and RKO $BRAF^{wt}$, RKO $BRAF^{mut}$ culture plates. All four media were prepared under both normoxic and hypoxic conditions. Media derived from KRAS mutant and BRAF mutant cell cultures induced significantly more sprouting from the spheroids than the corresponding wild-type cells when incubating the spheroids with normoxic media (DLD-1 $KRAS^{wt}$/DLD-1 $KRAS^{mut}$ p=0.0462*, RKO $BRAF^{wt}$/RKO $BRAF^{mut}$ p=0.0007***). Sprouting was enhanced under hypoxic conditions: for each of the cell lines, a significantly higher number of sprouting cells was found for gels cultivated in hypoxic media compared to the ones cultivated in normoxic media (DLD-1 $KRAS^{wt}_{normoxia.}$/DLD-1 $KRAS^{wt}_{Hypoxia}$ p=0.0228*, DLD-1 $KRAS^{mut}_{normoxia.}$/DLD-1 $KRAS^{mut}_{Hypoxia}$ p=0.0452*, RKO $BRAF^{wt}_{normoxia}$/RKO $BRAF^{wt}_{Hypoxia}$ p=0.0002***, RKO $BRAF^{wt}_{normoxia}$/RKO $BRAF^{wt}_{Hypoxia}$ p=0.0165*) (Fig 6B).

4 Discussion

In solid tumors, hypoxia develops as a result of the imbalance between oxygen delivery to and consumption by the proliferating cells, and has been found to constitute a critical factor for tumor progression and survival[13]. Clinical studies demonstrated a correlation between hypoxia and poor prognosis[14], highlighting the necessity for understanding the factors affecting tumor hypoxia and molecular mechanism associated. While HIF has been identified as key mediator of hypoxia-related signaling, it is meanwhile known that HIF signaling may be induced by factors independent of hypoxia, such as altered level of metabolites or oncogenes[2,5]. In this study, we evaluated the impact of the BRAF (V600E) and KRAS (G13D) cancer-driving mutations on the activity of HIF *in vivo* in colon carcinoma xenografts. Given

the link between HIF activity and glycolytic metabolic activity, we investigated whether these mutations affected intrinsic metabolism, in particular the flux of the LDH reaction.

Using a reporter gene assay, we could demonstrate that KRAS and BRAF mutated colon tumors displayed a significantly higher HIF activity than the corresponding wild-type control tumors. These findings go in line with results from an *in vitro* study by Kikuchi et al.[9], who showed that both KRAS and BRAF activating mutations can enhance the hypoxic induction of HIF-1α in colon carcinoma. Other studies by Richard et al.[15] and Sang et al.[16] also demonstrated the role of the MAPK pathway in upregulating the transcriptional activity of HIF via phosphorylation of HIF-1α by ERK1/2. As the mutations on BRAF and KRAS continuously drive the activation of the ERK1/2 kinases, this might explain the differences in HIF activity obtained *in vivo* in the mutated tumor models compared to the corresponding wild-type models.

Interestingly, differences in HIF activity between the KRAS/BRAF mutated and the wild-type tumors were more pronounced in the initial phase of tumor development, typically for tumors smaller than 100mm^3. Mutant tumors showed higher HIF activity-related iRFP fluorescence than wild-type tumors of similar size. Histological analysis of early tumors (50-100mm^3) revealed no difference in the extent of hypoxia between DLD-1 KRAS^{mut} and DLD-1 KRAS^{wt} tumors, while the level of the HIF product CA9 and the staining for CD31 appeared enhanced in mutant tumors. This indicates increased HIF signaling in DLD-1 KRAS^{mut} tumors, apparently not associated with a higher degree of hypoxia, but rather due to hypoxia-independent mechanisms. At later stages in tumor development, mutant and wild-type DLD-1 tumors show similar values for volume-normalized iRFP fluorescence intensity, which might hint at hypoxia being the dominating driver of HIF activity. This is also reflected by the histological analysis, which reveals an association between pimonidazole and CA9/CD31 stainings for DLD-1 tumors. RKO tumors show a similar behavior though the effects were smaller and typically less consistent. We conclude that during early stages of tumor development the increased level of HIF signaling observed in DLD-1 KRAS^{mut} (and to a lesser extent in RKO BRAF^{mut}) compared to the corresponding wild-type tumors is not the result of increased hypoxia but rather due to intrinsically higher levels of HIF-1α and associated HIF signaling in the mutant tumors. For larger tumors, hypoxia becomes the major driver of HIF activity.

Histology revealed higher levels of CD31 in mutant tumors indicative of enhanced angiogenic potential. This was confirmed when analyzing endothelial sprouting. HUVECs spheroids

exposed to medium derived from DLD-1 $KRAS^{mut}$ and RKO $BRAF^{mut}$ tumor cell cultures displayed an increased number of sprouts as compared to spheroids exposed to medium derived from cell cultures with wild-type cells. Various studies showed the impact of KRAS and BRAF mutation on driving tumor angiogenesis, supporting our findings. More interestingly, studies in thyroid carcinomas[17–19] showed that BRAF mutation was important in the early phase of the tumor development and in the predisposition of the neoplasia to dedifferentiation.

Given the link between HIF signaling and metabolism[2,3], constitutive activation of the oncogenes KRAS and BRAF might have an effect on metabolic activity. Regarding glucose metabolism, pyruvate acts as the gatekeeper of mitochondrial metabolism and is either directed towards the TCA or converted into lactate, thereby providing information about the primary use of glucose by colon carcinomas. Yun et al.[20] demonstrated that KRAS and BRAF mutated DLD-1 cells and RKO cells exhibit a Warburg phenotype, driving the pyruvate into lactate rather than into the TCA cycle. In line with this, we found a high pyruvate to lactate conversion. Interestingly, longitudinal monitoring of [1-^{13}C]-pyruvate metabolism in DLD-1 and RKO tumors did not reveal any significant difference between the genotypes, both with regard to lactate-to-pyruvate ratio and in LDH kinetics, not even during the early stage of tumor development, when HIF activity was enhanced in the mutant tumors. In all four tumors types pyruvate-to-lactate conversion decreased as a function of tumor size/time. The absence of significant differences between mutant and wild-type tumors in the initial phase might be explained by technical limitations and/or biological reasons. For example, Hutton et al.[21] using the same isogenic pairs as in our study did not find significant differences in the amount of protein associated with the metabolism in those tumor cells. In line with this, we could not detect any differences in the levels of the lactate dehydrogenase isozyme 5 (LDH5) on Western Blots of the four different cell lines (Supplementary Results, Fig 8), a puzzling result as the induction of LDH5 was shown to correlate with the accumulation of HIF in colorectal adenocarcinomas[22]. Apart from these tumor cell specific aspects, tumor heterogeneity may contribute to the lack of sensitivity in picking up alterations in metabolism due to KRAS and/or BRAF mutations. The tumor mass is composed of a variety of cells, of which only tumor cells comprise the mutation. Hence, any potential effect size would be reduced due to partial volume effects. On the other hand, we cannot exclude that spectra might be contaminated by contributions from adjacent healthy tissue, in particular for small tumors, thereby masking

potential differences originating from the tumor tissue. In this regard, spectroscopic imaging would provide better insight into the heterogeneity of tumor pyruvate metabolism, as shown in a recent study by Saito et al.[23] Finally, pyruvate may not be the molecule of choice to reveal differences in the metabolism of KRAS and BRAF mutated colon carcinomas. Hyperpolarized [1-^{13}C]-glutamate has recently been used as a biomarker in metabolic studies in gliomas[24] and this metabolite would represent an interesting molecule to study in KRAS and BRAF mutated colon carcinomas since there are evidence that those two mutations also impact on the reprogramming of glutamine[5,25].

In conclusion, in this study we have used an infrared fluorescent reporter gene assay (iRFP) to monitor the effects of cancer driving mutations KRAS and BRAF on HIF signaling. We have furthermore studied potential adaptation in the early steps of glucose metabolism by monitoring the fate of [1-^{13}C]-pyruvate using *in vivo* ^{13}C-MRS. We have found enhanced iRFP fluorescence in DLD-1 KRAS^{mut} and RKO BRAF^{mut} colon cancers as compared to the respective wild-type tumors in the early phase of tumor development indicative of KRAS/BRAF-induced HIF upregulation. In later tumor stages, no difference in HIF activity between mutated and wild-type tumors has been found, which may hint at hypoxia being the dominant driver of HIF signaling. HIF upregulation did not induce any detectable change in ^{13}C-pyruvate metabolism across the four tumor lines tested, in line with earlier results. Use of alternative substrates such as glutamate or assessment of the steady-state metabolic profile using ^{1}H-MRS or metabolic imaging might shine further light on metabolic adaptations associated with these cancer driving mutations.

5 References

1. Lehmann, S. *et al.* Longitudinal and multimodal in vivo imaging of tumor hypoxia and its downstream molecular events. *PNAS* **106,** 14004–14009 (2009).

2. Zhao, S. *et al.* Glioma-Derived Mutations in IDH1 Dominantly Inhibit IDH1 Catalytic Activity and Induce HIF-1a. *Science (80-.).* **324,** 261–265 (2009).

3. Selak, M. A. *et al.* Succinate links TCA cycle dysfunction to oncogenesis by inhibiting HIF-a prolyl hydroxylase. *Cancer Cell* **7,** 77–85 (2005).

4. Yuneva, M. O. *et al.* The Metabolic Profile of Tumors Depends on both the Responsible Genetic Lesion and Tissue Type. *Cell Metab.* **15,** 157–170 (2012).

5. Ratnikov, B. I., Scott, D. A., Osterman, A. L., Smith, J. W. & Ronai, Z. A. Metabolic rewiring in melanoma. *Oncogene* **36,** 147–157 (2017).

6. Siegel, R. L., Miller, K. D. & Jemal, A. Cancer statistics, 2016. *CA Cancer J Clin* **66,** 7–30 (2016).

7. Tan, C. & Du, X. KRAS mutation testing in metastatic colorectal cancer. *World J. Gastroenterol.* **18,** 5171–5180 (2012).

8. Barras, D. BRAF Mutation in Colorectal Cancer : An Update. **7,** 9–12 (2015).

9. Kikuchi, H., Pino, M. S., Zeng, M., Shirasawa, S. & Chung, D. C. Oncogenic KRAS and BRAF Differentially Regulate Hypoxia-Inducible Factor-1 and -2 in Colon Cancer. *Cancer Res.* **69,** 8499–8506 (2009).

10. Bürgi, S. *et al.* In vivo imaging of hypoxia-inducible factor regulation in a subcutaneous and orthotopic GL261 glioma tumor model using a reporter gene assay. *Mol. Imaging* **13,** (2014).

11. Krajewski, M. *et al.* A multisample dissolution dynamic nuclear polarization system for serial injections in small animals. *Magn. Reson. Med.* **910,** 904–910 (2016).

12. Batsios, G. Analysis of factors determining LDH activity in murine tumor models using hyperpolarized 13C MRS. *Diss. ETH. NO. 23519* (2016).

13. Vaupel, P. The Role of Hypoxia-Induced Factors in Tumor Progression. *Oncologist* **9,** 10–

17 (2004).

14. Vaupel, P. & Mayer, A. Hypoxia in cancer: Significance and impact on clinical outcome. *Cancer Metastasis Rev.* **26,** 225–239 (2007).

15. Richard, D. E., Berra, E., Gothié, E., Roux, D. & Pouysségur, J. p42/p44 Mitogen-activated Protein Kinases Phosphorylate Hypoxia-inducible Factor 1alpha (HIF-1alpha) and Enhance the Transcriptional Activity of HIF-1. *J. Biol. Chem.* **274,** 32631–32637 (1999).

16. Sang, N. *et al.* MAPK signaling up-regulates the activity of hypoxia-inducible factors by its effects on p300. *J. Biol. Chem.* **278,** 14013–14019 (2003).

17. Ciampi, R. & Nikiforov, Y. E. Minireview: RET/PTC Rrearrangements and BRAF Mutations in Thyroid Tumorigenesis. *Endocrinology* **148,** 936–941 (2007).

18. Li, Y., Nakamura, M. & Kakudo, K. Targeting of the BRAF gene in papillary thyroid carcinoma. *Oncol. Rep.* **22,** 223–230 (2009).

19. Paes, J. E. & Ringel, M. D. Dysregulation of the Phosphatidylinositol 3-Kinase Pathway in Thyroid Neoplasia. *Endocrinol. Metab. Clin. North Am.* **37,** 375–387 (2008).

20. Yun, J. *et al.* Glucose Deprivation Contributes to the Development of KRAS Pathway Mutations in Tumor Cells. *Science (80-.).* **325,** 1555–1559 (2009).

21. Hutton, J. E. *et al.* Oncogenic KRAS and BRAF Drive Metabolic Reprogramming in Colorectal Cancer. *Mol. Cell. Proteomics* **15,** 2924–2938 (2016).

22. Koukourakis, M. I., Giatromanolaki, A., Simopoulos, C., Polychronidis, A. & Sivridis, E. Lactate dehydrogenase 5 (LDH5) relates to up-regulated hypoxia inducible factor pathway and metastasis in colorectal cancer. *Clin. Exp. Metastasis* **22,** 25–30 (2005).

23. Saito, K. *et al.* 13C-MR Spectroscopic Imaging with Hyperpolarized [1-13C]pyruvate Detects Early Response to Radiotherapy in SCC Tumors and HT-29 Tumors. *Clin. Cancer Res.* **21,** 5073–5081 (2015).

24. Chaumeil, M. M. *et al.* Hyperpolarized [1-13C] glutamate: a metabolic imaging biomarker of IDH1 mutational status in glioma. *Cancer Res.* **74,** 4247–4257 (2015).

25. Son, J. *et al.* Glutamine supports pancreatic cancer growth through a KRAS-regulated metabolic pathway. *Nature* **496,** 101–5 (2013).

26. Potapova, T. a, Sivakumar, S., Flynn, J. N., Li, R. & Gorbsky, G. J. Mitotic progression becomes irreversible in prometaphase and collapses when Wee1 and Cdc25 are inhibited. *Mol. Biol. Cell* **22,** 1191–1206 (2011).

27. Zerilli, M. *et al.* BRAF(V600E) mutation influences hypoxia-inducible factor-1alpha expression levels in papillary thyroid cancer. *Mod. Pathol.* **23,** 1052–60 (2010).

28. Burrows, N., Babur, M., Resch, J., Williams, K. J. & Brabant, G. Hypoxia-inducible factor in thyroid carcinoma. *J. Thyroid Res.* **2011,** 762905 (2011).

29. Bottos, A. *et al.* Targeting oncogenic serine/threonine-protein kinase BRAF in cancer cells inhibits angiogenesis and abrogates hypoxia. *Proc. Natl. Acad. Sci. U. S. A.* **109,** E353-9 (2012).

30. Zeng, M. *et al.* Hypoxia Activates the K-Ras Proto-Oncogene to Stimulate Angiogenesis and Inhibit Apoptosis in Colon Cancer Cells. *PLoS One* **5,** e10966 (2010).

31. Zhang, X., Gaspard, J. P. & Chung, D. C. Regulation of Vascular Endothelial Growth Factor by the Wnt and K-ras Pathways in Colonic Neoplasia. *Cancer Res.* **61,** 6050–6054 (2001).

32. Chun, S. Y. *et al.* Oncogenic KRAS modulates mitochondrial metabolism in human colon cancer cells by inducing HIF-1a and HIF-2a target genes. *Mol. Cancer* **9,** 293 (2010).

33. Kerr, E. M., Gaude, E., Turrell, F. K., Frezza, C. & Martins, C. P. Mutant Kras copy number defines metabolic reprogramming and therapeutic susceptibilities. *Nature* **531,** 110–113 (2016).

6 Supplementary Material and Methods

Plasmid creation

To study the activity of the Hypoxia Inducible Factor (HIF) in the four colon cancer cell lines, a fluorescent reporter gene was established. A vector plasmid pMuLE-H2SViRFP was created by recombining an infrared fluorescent protein (iRFP690) flanked by two Hypoxia Responsive Elements (HRE) into an entry vector pENTR. This vector, together with another pENTR vector containing a GFP sequence, was recombined into a destination vector pDEST, generating the pMuLE-H2SViRFP.

Generation of viral particles and cell transduction

293T cells were cultivated in DMEM with 10% FBS in 15cm tissue culture dishes. At 80% confluency, the 293T cells were cotransfected with the vector plasmid pMuLE-H2SViRFP, the packaging plasmid psPAX2 and the envelope plasmid pMD2G (Addgene, Cambridge, USA). The next day the transfection medium was replaced by fresh DMEM with 10% FBS medium and the cells were incubated for 8h. After that period, the supernatant was collected and stored at 4 degrees. Fresh supplemented DMEM medium was added to the cells for 12 hours. When the second incubation was done, the supernatant was harvested, pooled with the first harvest, centrifugated at 500g for 5 minutes and filtered through 0.45µm filters.

Immunoblotting

The *in vitro* longitudinal expression of HIF was monitored under hypoxic and pseudo-hypoxic conditions. In pseudo-hypoxia, cell culture medium was supplemented with 1mM of the prolyl-4-hydroxylase (PHD) inhibitor dimethyloxalylglycine (DMOG) for 2 hours up to 24 hours. Hypoxic conditions were created by placing cell culture dishes in a hypoxic chamber (Binder, Tuttlingen, Germany) at 1% O_2 for 16, 24 and 48 hours. To prepare a cytoplasmic protein extract, the cells were washed twice in ice-cold PBS and lysed with high salt buffer containing 0.1% NP-40. The protein concentration was determined by Bradford assay (Biorad, Cressier, Switzerland). For the membrane-bound protein extraction, cells were washed in ice-cold PBS and lysed with RIPA buffer. The amount of protein was calculated by adding 2µl of solution to the nanodrop spectrophotometer (ND-1000) and determining the sample absorbance. The

protein expression was analyzed with immunoblot by loading the lysates on a 10% SDS PAGE gel. The antibodies used for detection were: polyclonal anti-HIF-1α (NB 100-479, Novus Biologicals), polyclonal anti-CA9 (Ab15086, Abcam), polyclonal anti-LDH (Ab9002, Abcam), and polyclonal anti-GLUT1 (Ab14683, Abcam). All gels were loaded with 5µg of proteins except for CA9 gels which were loaded with 30µg of proteins.

Live cell imaging

iRFP expression in live cells: 30'000 cells were plated on 18-mm coverslips. At 70-80% confluency cells were placed in pseudo-hypoxic conditions for 24 hours and in hypoxic conditions for 24 and 48 hours. After each incubation period, the coverslips were placed in a Ludin chamber (Life Imaging Services) and immersed in Opti-MEM medium (Gibco, Life Technologies). The cells were imaged with an inverted Leica microscope (Leica DMI 6000B). The resulting images were analyzed in ImageJ by computing the corrected total cell fluorescence (CTCF) for each cell culture condition[26]. We used the strong GFP expression of the cells to discriminate the cellular area from the background. Applying the cellular and background areas defined with in the GFP channel to the iRFP images allowed us to compute the integrated density and area of the cells as well as the mean intensity of the background. Eventually the CTCF was given by the formula $CTCF = cell\ integrated\ density - (area\ of\ selected\ cells \cdot background\ mean\ fluorescence)$

7 Supplementary results

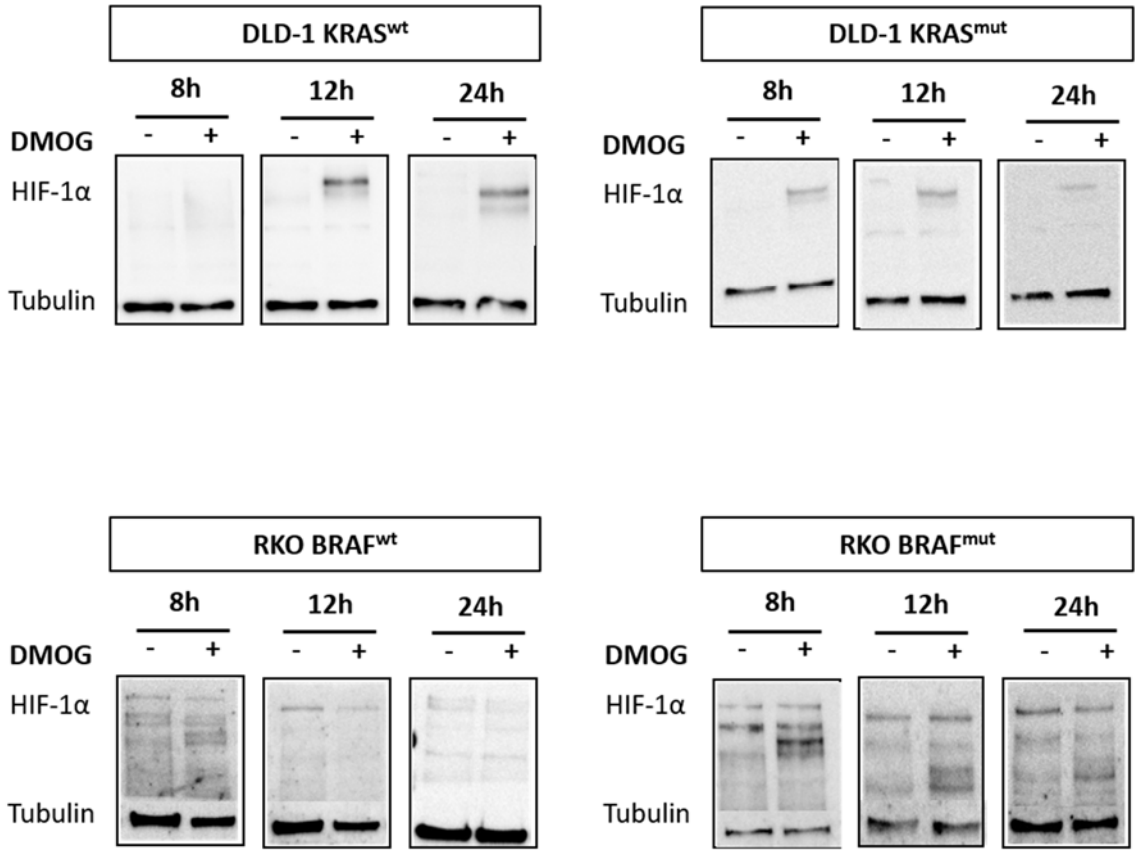

Figure 76 *Detection of HIF-1α in DLD-1 and RKO cells under longitudinal pharmacological inhibition of PHD with 1mM DMOG. The expression of HIF-1α follows a cycle, with an increased expression after 12 and 24 hours of DMOG treatment.*

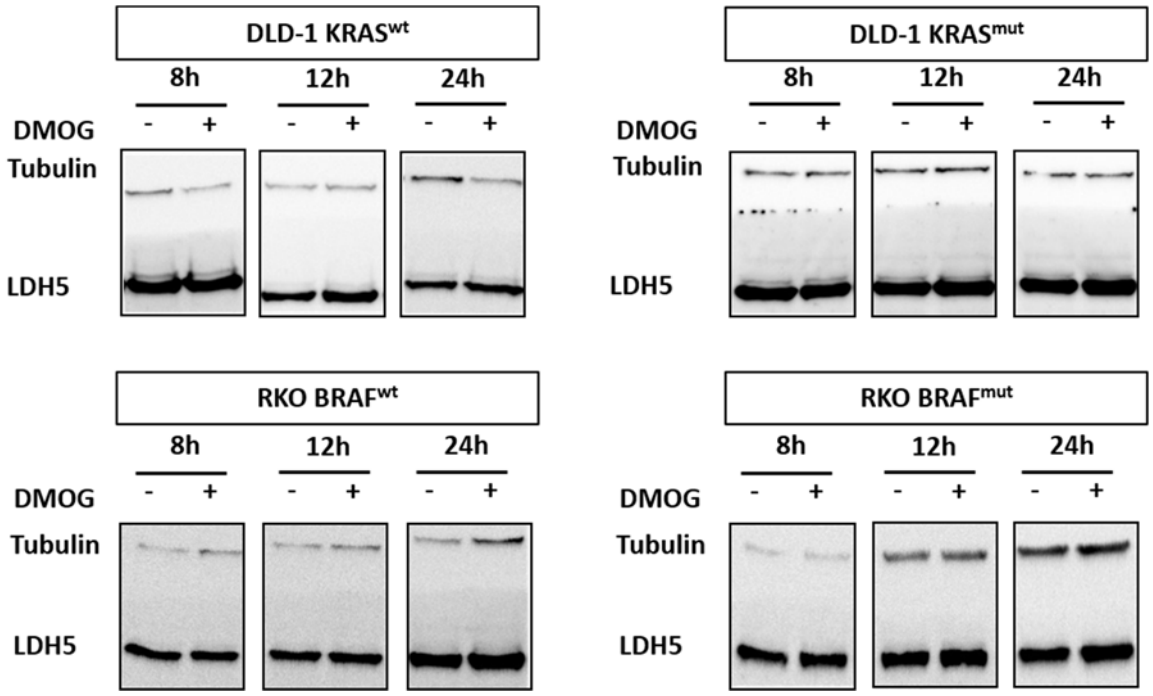

Figure 8 *Detection of Lactate dehydrogenase 5 (LDH5) in DLD-1 and RKO cell lines. The four cell lines were treated longitudinally with the PHD inhibitor DMOG (1mM). For each cell line, no differences were observed between LDH5 expression in treated and non-treated cellular extracts at the three time points evaluated.*

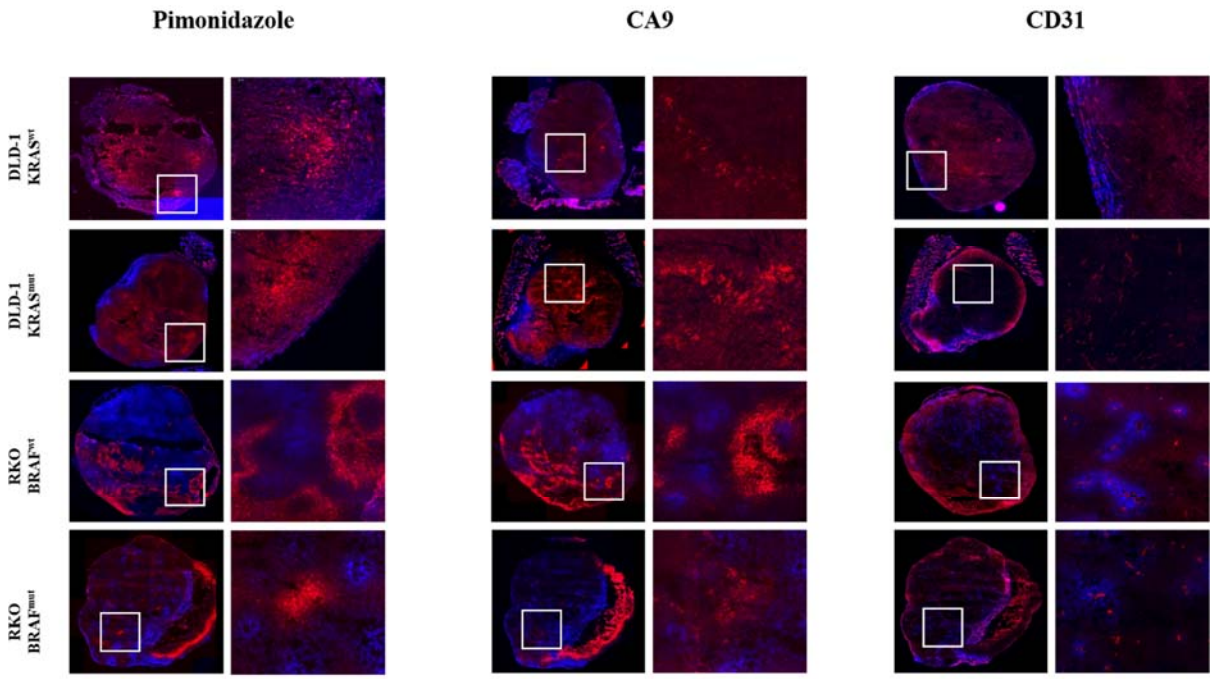

Figure 97 *Ex vivo staining of DLD-1 and RKO tumors extracted before reaching a volume of 100mm^3. Tumors from all four cell lines were stained for the hypoxia marker pimonidazole, the downstream gene of HIF carbonic anhydrase 9 (CA9) and the endothelial cell marker CD31 for tumor blood vessels. The whole tumor sections were scanned at a 20X magnification.*

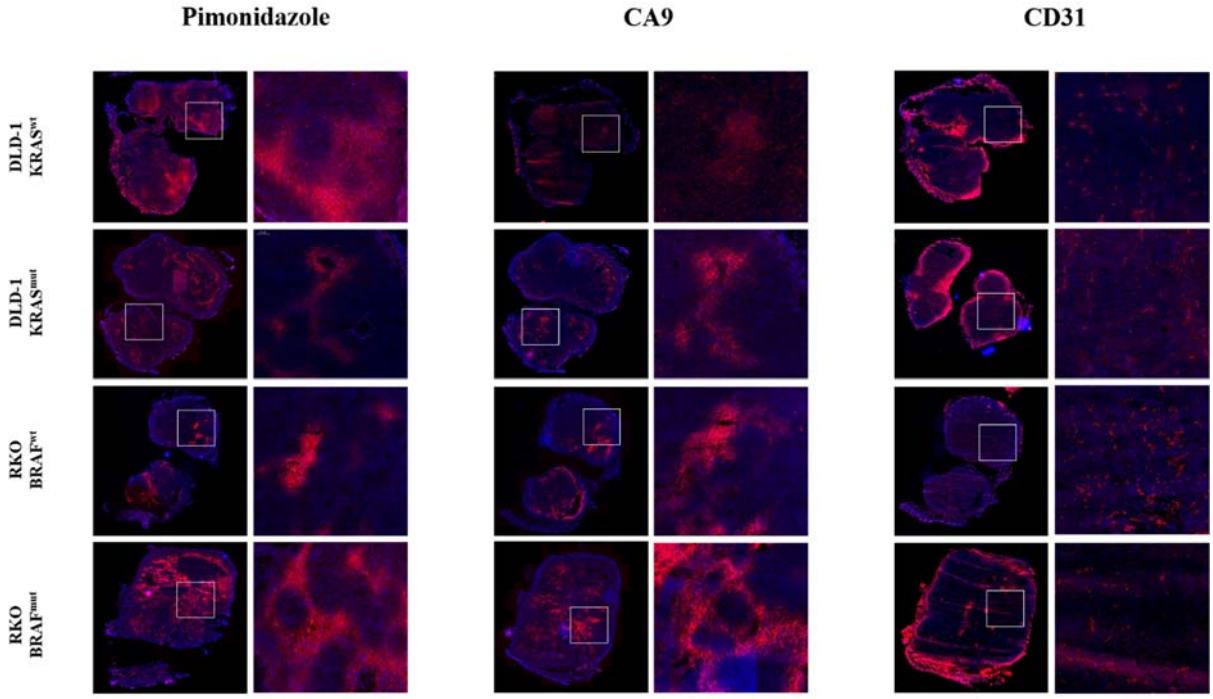

Figure 108 *Ex vivo staining of DLD-1 and RKO tumors extracted at the end of the study. Tumors from all four cell lines were stained for the hypoxia marker pimonidazole, the downstream gene of HIF carbonic anhydrase 9 (CA9) and the endothelial cell marker CD31 for tumor blood vessels. The whole tumor sections were scanned at a 20X magnification.*

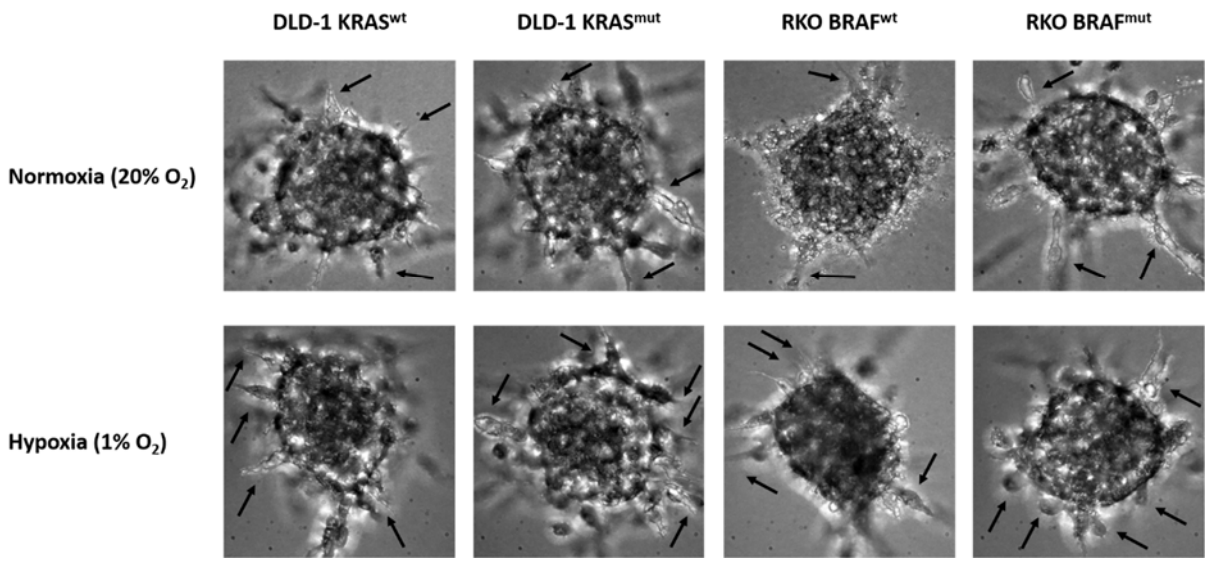

Figure 9 *Sprouting assay with HUVECs spheroids and condition media from DLD-1 and RKO cell lines. Spheroids were embedded in Rat Tail collagen gels (Rat Tail collagen 4mg/ml) and incubated with condition media for 24 hours. The condition media were obtained from DLD-1 KRAS^{wt}, DLD-1 KRAS^{mut}, RKO BRAF^{wt}and RKO BRAF^{mut} cultivated for 72 hours either in normoxic conditions (20% O_2) or hypoxic conditions (1% O_2).*

4. General discussion and outlook

1 General discussion

Studies about cancer metabolism were initiated more than 100 years ago with Otto Warburg and his finding that, in the presence of oxygen, proliferating tumor cells preferentially ferment glucose into lactate rather than oxidizing it into the TCA cycle[1], a characteristic called the Warburg effect. Speculations about the reasons for such a peculiar cellular behavior lead to the hypothesis that the mitochondrion in cancer cell was malfunctioning and/or completely shut down. Researchers eventually refuted this theory and demonstrated the proper functioning of mitochondria in most tumor types[2]. This example reflects how the field of cancer metabolism has evolved and how we now have a clearer idea of its different characteristics. However, there are still many unknowns, and the scientific community is still puzzled regarding the Warburg effect: why such an inefficient way of producing energy? More extensive research unraveled different metabolic behaviors and their link to various oncogenic pathways bringing molecular biologists and oncologists to recognize that tumors reprogram their metabolism and that this step constitutes one of their hallmarks[3].

The central dogma in metabolic rewiring by the tumor cells connects HIF and metabolism. It is now well established that under hypoxic conditions, tumor cells activate HIF, which modulates the cellular adaptation to low levels of O_2 and affects the expression of various metabolic enzymes. However, other cellular events contribute to the regulation of HIF signaling as well, as reflected by the mismatch of HIF-active and hypoxic areas observed in tumors[4], or the activation of HIF under normoxic conditions[5,6]. A more complete picture takes into account oncogenes and other elements of the tumor microenvironment as triggers for HIF signaling. The complex interplay between HIF activity and metabolism is revealed by the fact that the expression levels of several key enzymes and transporters involved in glucose metabolism are regulated by HIF, while the HIF activity on the other hand critically depends on the availability of products of the respective enzymatic reactions, i.e. metabolites such as α-ketoglutarate.

In this work, we focused on the study of HIF activity and pyruvate metabolism in the context of two specific cancer-driving mutations. Based on different studies observing the activation

of HIF as a consequence of a mutation in metabolic enzymes[7], we hypothesized that a tumor with a specific genetic make-up, in our case an activating mutation on KRAS or BRAF, would be linked to a specific metabolic fingerprint. Different bodies of evidence demonstrated that this mechanistic view of one-to-one correspondence of genetic and metabolic fingerprint does not hold true. One should rather regard the tumor metabolism as being heterogeneous[8], both within the tumor mass and between tumors with similar initial oncogenic mutations. From the primary driving mutation, a tumor is going to develop by acquiring additional oncogenic mutations[9], each influencing the metabolism in a different way. Similarly, heterogeneity of tumor cells within a single tumor is highly depending on the tumor microenvironment, which has been shown to be a determinant of the preferred metabolism[10]. A hypoxic cell will trigger different metabolic routes than a normoxic one to survive. Therefore, it is not possible to think about a tumor type possessing a single specific metabolic fingerprint. The complexity of tumor metabolism can be further illustrated by the fact that different tumor type harboring oncogenic mutation in similar pathways will follow completely different metabolic routes. For example, BRAF mutated melanomas have been shown to be addicted to glutamine[11], whereas Ras-mutated lung carcinomas were relying on glucose to fuel the TCA cycle and displayed little changes in glutamine metabolism[12]. In addition to that, the tumor masses not only comprise tumor cells: fibroblasts, and various immune cells are also present. Hence, “tumor metabolism” does not apply to the sole metabolic activity of tumor cells, but rather reflects the weighted contributions of all cellular players.

A major factor shaping tumor heterogeneity is HIF, as it contributes to the development of tumor aggressiveness, metastasis, stemness and angiogenesis[13]. One might eventually say that “the clonal diversity and heterogeneity in the microenvironment will lead to heterogeneous HIF expression and thus metabolic heterogeneity”. In light of the complexity of the tumor metabolism and of the different factors acting on it, it becomes obvious that the multimodal/multiparametric imaging strategies targeting different molecular events should be used to elucidate a possible link between the different biological processes. Such a synergy can be illustrated by PET-MRI combination and the potential simultaneous use of ^{13}C- and ^{18}F-labeled compounds to investigate glycolytic fluxes within a tumor[14]. The injection of ^{18}F-FDG would provide information about the glucose delivery to the tumor site, its transport into the cell and phosphorylation by hexokinase. On the other hand, injecting at the same time a solution of ^{13}C-pyruvate provides information about the last steps of the glycolysis within a

tumor, the conversion of pyruvate into lactate or eventually acetyl-CoA. This dual injection might be of interest for example for assessing increased or reduced mitochondrial function, which cannot be assessed with ^{18}F-FDG alone. In this work, we used such a dual imaging strategy to investigate to what extent cancer driving mutations affect the metabolic fate of pyruvate and the activity of HIF.

^{1}H-spectroscopy allows measuring the steady-state levels of endogenous metabolites occurring at millimolar concentration. The strength of the method is spectral resolution, i.e. several metabolites can be measured simultaneously, though long acquisition times are typically required, preventing kinetics measurements. This can be achieved by inserting labeled substrates. ^{13}C-MRS is of particular interest in this regard, as the natural abundance of the isotope is 1.1%; hence, background signals due to endogenous compounds will be low. Introduction of an isotopically enriched substrate allows monitoring its fate in great detail[15]. Recording ^{13}C-MRS spectra in a time-resolved manner yields information on metabolic fluxes and reaction kinetics, though temporal resolution is in general low due to the low gyromagnetic ratio of the ^{13}C nucleus. The gain in sensitivity provided by hyperpolarizing the spin state of metabolites using DNP rendered ^{13}C-MRS a powerful technique to investigate selected metabolic processes in tumors *in* vivo, and the approach holds promise to provide clinically useful biomarkers. The majority of studies published to date use [1-^{13}C]-pyruvate as substrate, which is attractive due to its MRS properties (the lifetime of the hyperpolarized state under *in vivo* conditions is long enough to study the processes of interest), and due to its gatekeeper role in metabolism (analyzing its metabolic products allows differentiating whether pyruvate is predominantly channeled through the TCA cycle or predominantly processed with LDH and/or ALT). Yet, in principle, any nuclear spin can be hyperpolarized. When focusing on ^{13}C-MRS, quaternary carbons should be isotopically enriched as any directly bound hydrogen nuclei would lead to a fast decay of the hyperpolarized state. In this regard, glutamine would be an attractive candidate as Lobo et al.[16] have shown that inhibiting glutaminase could slow down tumor cell growth. The option to hyperpolarize [5-^{13}C]-glutamine and [1-^{13}C]-glutamine has been investigated, both molecules showing different advantages. [5-^{13}C]-glutamine has a shorter T_1 than [1-^{13}C]-glutamine, however the chemical shifts obtained from [5-^{13}C]-glutamine and [5-^{13}C]-glutamate are bigger than the ones obtained with [1-^{13}C]-glutamine and [1-^{13}C]-glutamate, allowing a better distinction and

quantification of the peaks[17,18]. Nonetheless, [1-13C]-glutamate proved to be a useful source to follow its subsequent metabolism in the TCA cycle[19].

HIF, similarly to PI3K, Myc or Ras, participates to the modulation of the tumor metabolism to adapt to harsh conditions. In this work, we used a fluorescent reporter gene to investigate the longitudinal expression of HIF in colon carcinoma *in vivo*. The new viral construct produced to transduce the different cell lines proved to be a robust tool and can be adapted to any tumor cell line to follow the stabilization and activation of HIF. *In vivo* measurements were performed on alternative days from the initial tumor budding to the termination point. However, hypoxia is a very dynamic process[20] and the frequency at which HIF activity was determined may not fully reflect those changes, but rather a general hypoxic state which is built up as the tumor develops. As we have seen that KRAS- and BRAF-mutated tumors exhibit pronounced differences in HIF expression in the early phase of tumor development, it would have been interesting to investigate such expression patterns within a shorter temporal window, i.e. a couple of hours. Palmer et al.[21] have demonstrated the feasibility of imaging hypoxia in a temporal window of about 2 hours by optical imaging in mice using a dorsal window chamber. This technique also enables the more accurate localization of HIF-active subregions of the tumor and helps understanding how the activity of HIF evolve within those areas. However, in our case the maturation time of the iRFP protein (half-time ~2.8 hours) would not allow to resolve such dynamic events.

While the studies regarding the HIF signaling and pyruvate metabolism presented in this thesis yielded interesting results, they also revealed several limitations and problems. The use of the iRFP reporter has obvious advantages (absorption and emission spectrum) for *in vivo* imaging compared to bioluminescence or other red fluorescent proteins, however, due to its relative novelty several technical hurdles exist. First, there is no antibody against iRFP that might be used for measuring iRFP in Western Blots of cellular extracts under hypoxic conditions and correlating its expression with the HIF stabilization or the expression of other HIF downstream products, essential steps for assay validation. Such an antibody would have also been of great use in *ex vivo* imaging of the stained tumor sections. Since we were interested in the more general localization of hypoxic areas and HIF-expressing tumor subregions, we scanned whole tumor sections with a specific scanner whose longest wavelength was 633nm. Unfortunately, this was not sufficient to excite and detect the iRFP molecules expressed on the section, and

important information such as iRFP colocalization with the hypoxia marker pimonidazole or with the downstream gene of HIF CA9 could not be obtained. In this perspective, an antibody for iRPF would have been necessary to tag iRFP with a secondary antibody excited at a lower wavelength. In addition to conditional iRFP expression, GFP was constitutively produced by the virally transduced tumor cells. The expression of GFP was necessary to follow the cell transduction efficiency and facilitate the cell selection process by tagging the positively transduced cells. Nonetheless, the presence of GFP diminished the amount of information provided in *ex vivo* imaging by preventing the staining of a molecular marker of interest in that channel and the dual identification of related proteins, such as HIF and CA9 or pimonidazole and CA9.

The spectroscopic part of this project was also facing limitations. DNP represents a very useful technique to enhance the sensitivity towards ^{13}C-labeled metabolites *in vivo*, and several of them such as [1,4-$^{13}C_2$]-fumarate, ^{13}C-labeled bicarbonate or ^{13}C-labeled urea[22–24], have shown to provide suitable polarization and lifetime for *in vivo* studies. Nevertheless, not every metabolite of interest fulfills these requirements, limiting the range of adequate molecules for *in vivo* MRS. [1-^{13}C]-pyruvate is one of the best-established compound in the field of DNP and metabolism, and has been successfully translated into the clinics, yet it will not provide information about other metabolic pathways within tumors. This way, additional work needs to be done to establish new reliable compounds to investigate new metabolic routes. Furthermore, the process of DNP requires a specific equipment, i.e. a polarizer close enough to the MR scanner for the hyperpolarized compound to be dissolved and injected into the animal model in a time frame determined by the lifetime of the label. A possible solution to these technical constraints has been investigated by Ji et al.[25]. By separating the polarizing agent and the ^{13}C spins in a micro-particulate architecture, they were able to delay the transfer of polarization from the radical towards the metabolite of interest. Typically the lifetime $T_1(^{13}C)$ of the hyperpolarized micro-particulate samples studies lay between 5 and 37 hours. These results indicate that it might be possible to store a hyperpolarized compound, thereby enabling its transport for off-site use without losing too much of the polarization. The final preparation for the experiment then occurs off-site. Lastly, the [1-^{13}C]-pyruvate concentration (~40mM) used during DNP experiments relatively high compare to the normal intracellular pyruvate level (~0.2mM) and may shift the metabolism. The K_m constant for the pyruvate to

lactate conversion lying between 0.7 and 0.9mM[26,27], we might be measuring fully saturated enzymatic systems.

2 Outlook

Fluorescent optical imaging and ^{13}C-MRS are the two main imaging techniques used in this work. Both have been established *in vivo* in colon carcinomas harboring a KRAS or BRAF activating mutation. Nevertheless, there is room for improvement of both techniques. HIF activity was assessed by detecting iRFP with a 2D planar imaging system, which prevented fathering information on its 3D distribution within the tumor and also did not follow for accurate quantification. In the future, it would be interesting to make use of a newly-developed hybrid FMT/MRI system in our laboratory to get 3D reconstruction of the fluorophore concentration within the tumor mass. This can be achieved by utilizing prior anatomical information obtained with MRI images for 3D reconstruction of FMT data. Given the heterogeneous nature of tumors, such information would be important for better quantification and correlation with other readouts associated with HIF signaling. To fully exploit this potential, also the levels of [1-^{13}C]-pyruvate and [1-^{13}C]-lactate should be recorded in a spatially resolved manner using ^{13}C-MR spectroscopic imaging[28]. This would then allow assessing regionally specific enzyme activities and relate them to local HIF activity.

The analysis of the iRFP signals revealed that the KRAS and BRAF mutation were enhancing the HIF activity during early tumor stages, possibly providing those tumors with developmental advantages with respect to the wild-type ones by stimulating the tumor vasculature. To test this hypothesis, it would be interesting to treat all four tumor models with an anti-angiogenic therapy such as Avastin[29] and follow their effects on the tumor growth. A more pronounced shrinkage of tumor volume should be observed in the mutated tumors regarding their increased vasculature compared to the corresponding wild-type tumors. At the same time, HIF activity would be measured to monitor any possible changes in response to the treatment.

The logical step following the establishment of imaging techniques is to apply them to answer targeted biological questions by modulating the different parameters measured. The next step

in this project would be to link HIF activity and the tumor pyruvate metabolism in colon carcinoma harboring a KRAS or BRAF mutation. By modulating both processes and using the fluorescent reporter gene for HIF activity and metabolic spectroscopy as readouts, the impact of HIF on the metabolism and vice versa could be disentangled. The fact that colon carcinomas also rely on glutamine as a precursor for the synthesis of macromolecules (proteins, lipids, nucleic acids), would direct us to investigate the glutamine metabolism rather than pyruvate in DLD-1 and RKO cell lines. Demonstrating the possible glutamine dependency of the mutated cell lines would provide relevant information on a treatment regime to adopt for those particular tumor types. The first step should be to determine the glutamine uptake in DLD-1 and RKO tumors (both mutated and wild type) by ^{1}H-MRS of glutamine and glutamate. Proton spectroscopy results would yield a prior glimpse on the possible differences in glutamine intake between mutated and wild-type tumors. To follow on this outcome, treating the different cell lines *in vitro* and *in vivo* with a glutaminase inhibitor such as CB-839[30] could then provide information on the impact of metabolism on HIF and on the tumor relationship towards a specific metabolic pathway. Inhibition of glutaminase would lead to a reduction of glutamate levels. First, by following the activity of HIF in both treated and control cells and tumors we would gain insight on the influence of a loss of glutamate on the activity of HIF. It is hypothesized that a decrease in glutamate fueling of the TCA cycle translates into a decrease of the levels of α-ketoglutarate, which subsequently would inhibit PHD and lead to a stabilization of HIF. Secondly, comparing the tumor development under treatment would provide some clues about the dependence of the tumors on glutamine metabolism, and whether this affects mutated cells more than the wild-type ones, as suggested by Son et al. in metabolic studies of pancreatic cancer[31]. To test the possible impact of HIF on glutamine metabolism, ^{1}H-MRS glutamine experiments should be repeated with DLD-1 and RKO tumors in which HIF is pharmacologically inhibited by the RNA antagonist EZN-2968[32]. The results obtained under treatment should be compared to the initial ^{1}H spectroscopy studies to understand whether the inhibition of HIF impacts on the glutamine metabolism, and if so, in which way it affects it. Simultaneously, the efficiency of EZN-2968 can be evaluated optically by monitoring the longitudinal iRFP intensity within the tumors. Taken together, results from the HIF reporter gene and ^{1}H-MRS measurements could contribute to the better understanding and managing of the HIF-metabolism relationship and help adapting treatments for patients exhibiting similar KRAS or BRAF mutations.

Finally, the last parameter to modulate is the MAPK pathway. The Ras-Raf-Mek-Erk contains many levels at which inhibition can be achieved. However, drugs targeting the upstream effector Ras have proved to be so far inefficient[33] and focus is rather drawn on inhibiting the downstream Raf, Mek and Erk[34]. Various pharmaceutical agents have been clinically approved to target the different MAPK effectors and among them, two would be of interest for an *in vivo* study: a BRAF inhibitor and a Mek inhibitor. Treating colon carcinomas with a BRAF inhibitor would be interesting to understand first, whether the effect of the drug varies between a cell line with a constitutively active BRAF (RKO $BRAF^{mut}$) and the control cell line (RKO $BRAF^{wt}$), and second whether similar effects are achieved on a cell line with a MAPK pathway overactivated by another effector as BRAF (DLD-1 $KRAS^{mut}$). Then, using a Mek inhibitor represents a logical choice as Mek plays a central role in the MAPK pathway and is activated both by Ras and Raf effectors. The first agent to be use would be Encorafenib (LGX-818), a BRAF inhibitor in Phase 3 clinical trials showing interesting activity in melanomas (BRAF V600E) and which has also been investigated in clinical trial on colorectal cancer in combination with PI3K or EGFR inhibitors. The second agent of interest would be Selumetinib (AZD6244), a Mek inhibitor showing promising efficacy as a monotherapy in cancer with a deregulated MAPK pathway[35]. Both drugs should be administered to the four cell lines that we established in this work, and *in vivo* growth should be monitored. In addition, HIF activity should be monitored during the whole treatment regime to determine whether its activity is affected and can be correlated to the MAPK activity.

Based on the outcome of the different inhibition studies it would be potentially interesting to combine different therapies. If an interplay can be established between HIF activity and glutamine metabolism or between the KRAS/BRAF mutation and HIF activity or glutamine metabolism, then both parameters in the interaction paradigm should be targeted with inhibitory compounds. As it has been showed in the different MAPK inhibition studies, the outcome of a treatment can vary greatly between different tumor models as some resistance feed-back loops are developed by the treated tumors. Intervening on two molecular targets represents an optimal way to decrease tumor growth and potentially eradicate the development of cancer. Additionally, the intra- and intertumoral heterogeneity of tumors regarding the metabolism or the oncogenes activated require a clear understanding of it in order to adapt the treatment. Pharmacological modulations of specific metabolic routes or

oncogenic pathways will help us to better grasp those heterogeneities and provide a more personalized therapy to patients with identified mutations.

3 References

1. Warburg, B. Y. O., Wind, F. & Negelein, E. The Metabolism of Tumors in the Body. *J. Gen. Physiol.* (1926).

2. Zu, X. L. & Guppy, M. Cancer metabolism: Facts, fantasy, and fiction. *Biochem. Biophys. Res. Commun.* **313,** 459–465 (2004).

3. Hanahan, D. & Weinberg, R. A. Hallmarks of cancer: The Next Generation. *Cell* **144,** 646–674 (2011).

4. Lehmann, S. *et al.* Longitudinal and multimodal in vivo imaging of tumor hypoxia and its downstream molecular events. *PNAS* **106,** 14004–14009 (2009).

5. Zeng, L. *et al.* Aberrant IDH3α expression promotes malignant tumor growth by inducing HIF-1-mediated metabolic reprogramming and angiogenesis. *Oncogene* **34,** 1–9 (2014).

6. Isaacs, J. S. *et al.* HIF overexpression correlates with biallelic loss of fumarate hydratase in renal cancer: Novel role of fumarate in regulation of HIF stability. *Cancer Cell* **8,** 143–153 (2005).

7. Prensner, J. R. & Chinnaiyan, A. M. Metabolism unhinged: IDH mutations in cancer. *Nat. Med.* **17,** 291–293 (2011).

8. Carmona-Fontaine, C. *et al.* Metabolic origins of spatial organization in the tumor microenvironment. *Proc. Natl. Acad. Sci.* **114,** 201700600 (2017).

9. Vogelstein, B. *et al.* Genetic Alterations during Colorectal-Tumor Development. *N. Engl. J. Med.* **319,** 525–532 (1988).

10. Anastasiou, D. Tumour microenvironment factors shaping the cancer metabolism landscape. *Br. J. Cancer* **116,** 277–286 (2016).

11. Ratnikov, B. I., Scott, D. A., Osterman, A. L., Smith, J. W. & Ronai, Z. A. Metabolic rewiring in melanoma. *Oncogene* **36,** 147–157 (2017).

12. Davidson, S. M. *et al.* Environment Impacts the Metabolic Dependencies of Ras-Driven Non-Small Cell Lung Cancer. *Cell Metab.* **23,** 517–528 (2016).

13. LaGory, E. L. & Giaccia, A. J. The ever-expanding role of HIF in tumour and stromal biology. *Nat. Cell Biol.* **18,** 356–65 (2016).

14. Menzel, M. I. *et al.* Multimodal Assessment of In Vivo Metabolism with Hyperpolarized [1-13C]MR Spectroscopy and 18F-FDG PET Imaging in Hepatocellular Carcinoma Tumor-Bearing rats. *J Nucl Med* **54,** 1113–1119 (2013).

15. Wijnen, J. P. *et al.* In vivo 13C magnetic resonance spectroscopy of a human brain tumor after application of 13C-1-enriched glucose. *Magn. Reson. Imaging* **28,** 690–697 (2010).

16. Lobo, C. *et al.* Inhibition of glutaminase expression by antisense mRNA decreases growth and tumourigenicity of tumour cells. *Biochem. J.* **348,** 257–261 (2000).

17. Cabella, C. *et al.* In vivo and in vitro liver cancer metabolism observed with hyperpolarized [5-13C]glutamine. *J. Magn. Reson.* **232,** 45–52 (2013).

18. Gallagher, F. A., Kettunen, M. I., Day, S. E., Lerche, M. & Brindle, K. M. 13C MR spectroscopy measurements of glutaminase activity in human hepatocellular carcinoma cells using hyperpolarized 13C-labeled glutamine. *Magn. Reson. Med.* **60,** 253–257 (2008).

19. Gallagher, F. a *et al.* Detection of tumor glutamate metabolism in vivo using (13)C magnetic resonance spectroscopy and hyperpolarized [1-(13)C]glutamate. *Magn. Reson. Med.* **66,** 18–23 (2011).

20. Dewhirst, M. W. Relationships between cycling hypoxia, HIF-1, angiogenesis and oxidative stress. *Radiat. Res.* **172,** 653–65 (2009).

21. Palmer, G. M. *et al.* In vivo optical molecular imaging and analysis in mice using dorsal window chamber models applied to hypoxia, vasculature and fluorescent reporters. *Nat. Protoc.* **6,** 1355–1366 (2012).

22. Clatworthy, M. R. *et al.* Magnetic resonance imaging with hyperpolarized [1,4-(13)C2]fumarate allows detection of early renal acute tubular necrosis. *Proc. Natl. Acad. Sci.* **109,** 13374–13379 (2012).

23. Gallagher, F. A. *et al.* Magnetic resonance imaging of pH in vivo using hyperpolarized 13C-labelled bicarbonate. *Nature* **453,** 940–943 (2008).

24. Wilson, D. M. *et al.* Multi-compound polarization by DNP allows simultaneous assessment of multiple enzymatic activities in vivo. *J. Magn. Reson.* **205,** 141–147 (2010).

25. Ji, X. *et al.* Transportable hyperpolarized metabolites. *Nat. Commun.* **8,** 13975 (2017).

26. Witney, T. H., Kettunen, M. I. & Brindle, K. M. Kinetic modeling of hyperpolarized 13C label exchange between pyruvate and lactate in tumor cells. *J. Biol. Chem.* **286,** 24572–24580 (2011).

27. Carpenter, L. & Halestrap, a P. The kinetics, substrate and inhibitor specificity of the lactate transporter of Ehrlich-Lettre tumour cells studied with the intracellular pH indicator BCECF. *Biochem. J.* **304 (Pt 3,** 751–760 (1994).

28. Albers, M. J. *et al.* Hyperpolarized 13C Lactate, Pyruvate, and Alanine: Noninvasive Biomarkers for Prostate Cancer Detection and Grading. *Cancer Res.* **68,** 8607–8615 (2008).

29. Marshall, J. The Role of Bevacizumab as First-line Therapy for Colon Cancer. *Semin. Oncol.* **32,** 43–47 (2005).

30. Gross, M. I. *et al.* Antitumor Activity of the Glutaminase Inhibitor CB-839 in Triple-Negative Breast Cancer. *Mol. Cancer Ther.* **13,** 890–901 (2014).

31. Son, J. *et al.* Glutamine supports pancreatic cancer growth through a KRAS-regulated metabolic pathway. *Nature* **496,** 101–5 (2013).

32. Greenberger, L. M. *et al.* A RNA antagonist of hypoxia-inducible factor-1a , EZN-2968, inhibits tumor cell growth. *Mol. Cancer Ther.* **7,** 3598–3608 (2008).

33. Ostrem, J. M. L. & Shokat, K. M. Direct small-molecule inhibitors of KRAS: from structural insights to mechanism-based design. *Nat. Publ. Gr.* **15,** 771–785 (2016).

34. Uehling, D. E. & Harris, P. A. Recent progress on MAP kinase pathway inhibitors. *Bioorg. Med. Chem. Lett.* **25,** 4047–4056 (2015).

35. Zhao, Y. & Adjei, A. A. The clinical development of MEK inhibitors. *Nat. Rev. Clin. Oncol.* **11,** 385–400 (2014).

Appendix A

In vivo iRFP detection in DLD-1 $KRAS^{wt}$ and $KRAS^{mut}$ tumors using fluorescent molecular tomography (FMT) – A proof of feasibility

1 Methods

Fluorescence Molecular Tomography (FMT)

Fluorescent Molecular Tomography (FMT) experiments were carried out using a home-built system[1,2]. In brief, the system is equipped with several diode lasers operating at different wavelengths (B&W Tek, Newark, USA) connected to a fiber switch (Piezo Systems Jena, Jena, Germany). For the actual study a laser source at a wavelength of 690nm a laser equipped with acousto-optic tunable filter (Supercontinuum laser WhiteLase SC480, Fianium UK) has been used. The laser beam was deflected using a scan head equipped with two galvanometric mirrors (ScanLab, Pucheim, Germany) to excite a grid of 10 by 10 matrix of source points on the mouse surface above the tumor. Two sets of measurements were performed using the same mesh: measurement at the excitation wavelength for which the reflected signal was collected using a 680nm bandpass filter and a measurement at the emission wavelength using a 720nm bandpass filter. For signal detection a 16bit charge-coupled device (CCD) camera (ANDOR Corporation, Belfast, UK) has been used. Reconstruction home-built Matlab program was used for the reconstruction of the fluorophore (iRFP) distribution within the object in three dimensions[3]. The reconstructed images were analyzed with Amide, a medical image analysis tool. Volume-of-interest (VOIs) were drawn around the tumor boundary and mean intensity and standard deviation were computed in Amide for each VOIs.

2 Results

Detection of iRFP fluorescence in *in vivo* FMT

DLD-1 KRAS^{wt} and DLD-1 KRAS^{mut} colon models were evaluated using FMT. Both tumor types were measured longitudinally and for each time point, a 3D reconstruction of the iRFP distribution within the tumors was carried out (Fig 1A). Based on the transverse view, the depth of the center of gravity of the detected fluorescent signal was estimated at a depth of 2.5mm±0.1mm for the DLD-1 KRAS^{mut} tumor, and 0.7±0.1mm deep for the DLD-1 KRAS^{wt} tumors. The fluorescence intensity distribution was homogenous with a concentric decline from the center of gravity. The quantification of the mean tumor fluorescent intensity over the VOI revealed an increase in signal up to 10 folds in the DLD-1 KRAS^{wt} tumors, and up to 5 folds in the DLD-1 KRAS^{mut} tumors with respect to the initial signal (Fig 1B). A statistical analysis based on a mixed linear model showed that the tumor type had no effect on the iRFP intensity (p=0.239). However, the interaction between tumor volume and tumor type had a significant effect on the differences in iRFP intensities (p=$6.294 \cdot 10^{-2}$***). Nevertheless, those results go in the opposite direction from the results obtained with the same cells in repeated planar imaging studies. Here the DLD-1 KRAS^{wt} tumors in combination with their volume seem to have a greater expression of HIF and therefore iRFP, whereas the repeated measures with the 2D Maestro system showed the exact opposite.

In some other tumors, the maximum fluorescence intensity was not centrally located and diverted from the center. This can be explained, in some examples, by the necrotic surface which contributed to the fluorescent signal. Planar imaging could not fully establish the precise localization of iRFP and was of use only for quantification of the global tumor fluorescence. To remedy to this problem, fluorescence data were reconstructed in 3D. In fact, some tumors displayed very inhomogeneous patterns of intensities both on the transverse plane and in depth. This rendered the quantification of the average tumor fluorescence very difficult and inaccurate as precise VOIs were then difficult to draw. In some cases, the reconstructed fluorescence intensity was confined to superficial regions, less than millimeter deep, which did not match with the geometry of the tumor, indicating problems with 3D reconstruction. Obviously, the simple model for 3D reconstruction, a 3D slab, missed essential features characterizing the fluorescence experiment, i.e. the irregular surface and the

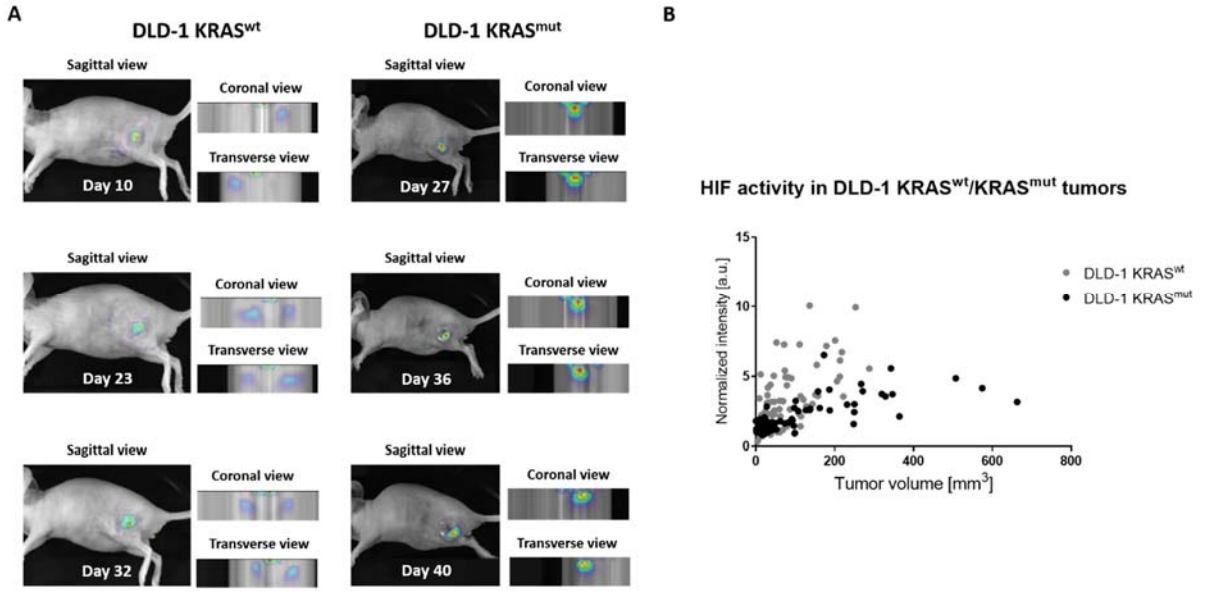

Figure 1 *FMT reconstruction of iRFP distribution in DLD-1 KRAS^{wt}/KRAS^{mut} tumors.* ***A*** *Transverse, sagittal and coronal view of the iRFP fluorescent signal within DLD-1 tumors at three different stages of tumor development. Tumors were excited with a 690nm laser on a grid of 10x10 point sources, first to collect an image stack at the excitation wavelength using a 690nm bandpass filter, and then to collect the corresponding image stack at the fluorescence maximum of iRFP using a 720nm bandpass filter. The ratio of two image data sets (emission intensity/excitation intensity) was used for 3D reconstruction of the tumor-associated iRFP fluorescence using a Matlab program developed in-house. The reconstructed fluorescence intensity maps were used as input for the Amide software to obtain a view of the fluorescent signal in the three anatomical planes and to draw VOIs to compute the mean fluorescence intensity of each tumor. The top plane of the coronal and sagittal view represents the surface of the animal exposed to laser excitation.* ***B*** *After FMT measurements and Matlab reconstruction, the evolution of the tumor VOIs mean fluorescent intensity was normalized to the initial mean intensity and plotted as a function of the tumor volume in DLD-1 KRAS^{wt} and DLD-1 KRAS^{mut} tumors.*

heterogeneity within the tissue. In addition, 3D reconstruction may be hampered by low signal-to-noise values as the reporter construct was not constitutively expressed but induced under hypoxic conditions. This highlight the need for improved reconstruction algorithms considering prior information about the sample geometry and composition. To be fully quantitative, FMT measurements should be undertaken with better priors, for example with a hybrid FMT system providing Magnetic Resonance Imaging images of the small-animal anatomy, and should not be combined with additional fluorescent measurements in order to preserve to iRFP brightness. In a recent study, Lai et al.[4] using a hybrid FMT/CT system showed that the 3D fluorophore distribution in subcutaneous and orthotopic lung adenocarcinoma constitutively expressing iRFP could be accurately detected and reconstructed.

3 References

1. Stuker, F. Hybrid Imaging : Combining Fluorescence Molecular Tomography with Magnetic Resonance Imaging. *Diss. ETH No. 19664* (2011).

2. Stuker, F. *et al.* Hybrid Small Animal Imaging System Combining Magnetic Resonance Imaging With Fluorescence Tomography Using Single Photon Avalanche Diode Detectors. *IEEE Trans. Med. Imaging* **30,** 1265–1273 (2011).

3. Stuker, F., Ripoll, J. & Rudin, M. Fluorescence Molecular Tomography: Principles and Potential for Pharmaceutical Research. *Pharmaceutics* **3,** 229–274 (2011).

4. Lai, C. W. *et al.* Using Dual Fluorescence Reporting Genes to Establish an In Vivo Imaging Model of Orthotopic Lung Adenocarcinoma in Mice. *Mol. Imaging Biol.* **18,** 849–859 (2016).

5. Acknowledgment

I would like to first thank the members of my committee. Prof. Wilhelm Krek for providing me the raw material to start my work, i.e. the DLD-1 and RKO cell lines, and for his inputs and objective comments during our committee meeting. Then, I would like to thank Prof. Ian Frew, to allow me to work in his laboratory to get familiar with viral transduction and to also provide me essential material, i.e. the plasmids that allowed me to transform my cells and go on with my project. Finally, I am thanking my supervisor, Prof. Markus Rudin, for offering me the opportunity to work on this challenging project and to enter the world of imaging. I could really profit from his expertise and his availability whenever I was stuck on my project. Besides work, it was also always a pleasure to talk with him about the news, politics, his latest hike and the wonder of nature, to listen to his history lessons, and best of all, to have him as an audience for me to make fun of the “bourbines”! Merci!

When I started my PhD, I knew a few biological techniques in theory, Ruth Keist showed me the practice. I would like to thank her for sharing with me her incredible knowledge, for teaching me all the techniques I needed to know in a very precise way, for answering all my questions and for her inputs every time things were not going according to the plan! After her, Jael Xandry took over and was an invaluable help when it came to repeating Western Blots, to jump in cell culture for me when experiments in Hönggerberg were taking too much time and to take the time to tackle some issues I had put aside for sake of time (CA9…).

Martin Schneider developed the HRE-iRFP construct which I used in my cells in last instance! He created a very powerful tool for *in vivo* optical imaging, and gave me the biggest push forward in the entire project. For this, I am thanking him a million times.

The metabolic part of this project could not have been done without the help of Giorgos Batsios. I would like to thank him for his time, his critical vision, and for sharing a sweet tooth with me! Sugar always made long lab evenings better. A big thank you to Grzegorz Kwiatkowski aka Greg for jumping in the project at the end, I could not have finished it without him.

A few people took part to this adventure for short periods of time and helped me going forward. I would like to thank Divya Vats for introducing me to *in vivo* imaging techniques and the work with mice, Joachim Albers and Tomàs Hejhal for their help with the viral

transduction, Patrick Wespi and Jonas Steinhauser for the emergency help with DNP experiments, Alexander Kalyanov and Giovanni Pellegrini for their inputs in our collaborative work.

I was told once by a professor and friend that the work atmosphere is never given, one has to work on it. In this regard, I think that at the AIC we did a pretty good job as I always enjoyed coming in the morning, even on Western Blot days! For this, I would like to thank first the Irchel crew, Ramanil Perera, Jael Xandry, Manoj Desai and Martin Schneider for the fun we had, the fruitful discussions, and their support in every steps of my PhD. The Hönggerberg team, past and present, was also an incredible reason to enjoy coming uphill for work or beers and BBQ! Katerina Dikaiou, Aline Seuwen, Aileen Schröter were there when I started and became great friends. Then came the cool guys of AIC, Georges Hankov, David Bühlmann, Giovanna Ielacqua, Markus Vaas, Zhiva Skachokova, who made my stay in the lab incredibly pleasant and funny. I thank them all for their craziness!

Outside the lab I was well surrounded by my wonderful friends, and thank to them also I made it through. Nadia Rosenberg was my bubble where I could be silly, speak French and let out my worries and doubts about research and life. Yannick and Alice were always there to provide me with a non-scientific environment, to show me what life is outside the lab, and more importantly, to feed me!

Finally, I would like to thank my parents, Elisabeth and Dominique, for giving me the opportunity to study, to trust me and to support me in the different choices I made in my life. They gave me independence, love, and a great home to come back to. I would not be the person I am today without them, and I feel truly blessed. My brother François and my sister Céline were supporting me with their funny pictures and messages, they listened to me when I needed to talk about the difficulties I was facing, and their external vision regarding my work were always very useful to overcome some obstacles! A special “merci” goes additionally to Céline for adding my amazing brother-in-law Jordi and wonderful niece Laia into the picture! I would like to thank the rest of my family for their interest and curiosity about my research, and in particular my grandmother Gisèle! With her imagination, she moved with me in all the steps I took during my studies, and was truly enthusiastic to discover things with me! I am so happy to have her by my side!